الجمهورية الجزائرية الديمقراطية الشعبية

People's Democratic Republic of Algeria

وزارة التعليم العالي والبحث العلمي

Ministry of Higher Education and Scientific Research

Kasdi Merbah University Ouargla
College of Mathematics and Matters Sciences
Chemistry Department
Reference:

جامعة قاصدي مرباح ورقلة
كلية الرياضيات وعلوم المادة
قسم الكيمياء
المرجع

Thesis presented with a view to obtaining

of the diploma of

Doctorate in LMD

Specialty: Environmental chemistry

Theme :

Synthetic and natural particles for the treatment of polluted water Synthesis, identification and application

Presented by **Nour elhouda BABAAMI**

Publicly supported on 22/02/2024

Before the jury composed of:

NEDJIMI Mohammed said	**Professor**	**President**	**University of Ouargla**
ZENKHRI Louiza	**Professor**	**Rapporteur**	**University of Ouargla**
BOUDJEMAA Souheyla	**Professor**	**Rapporteur**	**University of Ouargla**
ZERROUKI Hayet	**Professor**	**Examiner**	**University of Ouargla**
MEKLID Abdelhek	**Professor**	**Examiner**	**University of Biskra**
MIMOUNI Mourad	**Professor**	**Examiner**	**University of El-Oued**

الجمهورية الجزائرية الديمقراطية الشعبية

People's Democratic Republic of Algeria

وزارة التعليم العالي والبحث العلمي

Ministry of Higher Education and Scientific Research

Kasdi Merbah University Ouargla
College of Mathematics and Matters Sciences
Chemistry Department
Reference:

جامعة قاصدي مرباح ورقلة
كلية الرياضيات وعلوم المادة
قسم الكيمياء
المرجع

Thesis presented with a view to obtaining

of the diploma of

Doctorate in LMD

Specialty: Environmental chemistry

Theme :

Synthetic and natural particles for the treatment of polluted water Synthesis, identification and application

Presented by **Nour elhouda BABAAMI**

Publicly supported on 22/02/2024

Before the jury composed of:

NEDJIMI Mohammed said	**Professor**	**President**	**University of Ouargla**
ZENKHRI Louiza	**Professor**	**Rapporteur**	**University of Ouargla**
BOUDJEMAA Souheyla	**Professor**	**Rapporteur**	**University of Ouargla**
ZERROUKI Hayet	**Professor**	**Examiner**	**University of Ouargla**
MEKLID Abdelhek	**Professor**	**Examiner**	**University of Biskra**
MIMOUNI Mourad	**Professor**	**Examiner**	**University of El-Oued**

Dedication

I dedicate this work to the soul of my beloved mother and to my beloved father who have always supported me. This thesis is the result of your efforts and encouragement.

To my dear husband and partner in this journey. Thank you for your love and unwavering support throughout this journey. You have always been there to encourage me, even when I wanted to give up. I couldn 't have done this without you.

To my dear family, my beloved brothers, sisters, and nephews. You are the pillar that supports my life. You are the source of my strength and inspiration, and I thank God every day for having you in my life.

To my wonderful husband 's family, I am very grateful to be in the circle of your love.

To my dear professor and supervisor who believed in me, even when I didn 't believe in myself. This work would not have been completed without your efforts and guidance.

And finally, to my dear friends, thank you for your continued support and honesty. You add a special color to my life, and I am grateful for every moment I have spent with you.

With all my love and gratitude,

Nour Elhouda

Acknowledgement

First of all, I thank God, the Almighty, for giving me the health, courage and will to complete this work.

The research journey of last four years has been full of challenges for me and I would like to express my sincere gratitude to numerous individuals for their contribution and assistance from inception to culmination of my journey.

This work was carried out within the Laboratory of Research valorisation and promotion of Saharan resources VPRSat the Faculty of Mathematics and Matter Sciences of the University KasdiMerbah-Ouargla, in collaboration with both of the Laboratory of Catalysis and Synthesis in Organic ChemistryLCSCO, Faculty of Sciences, University of Tlemcen, Algeria and Centre for Scientific and Technical Research in Physico-Chemical Analysis CRAPC-Ouargla and laboratory of the ONA of the Ouargla WWTPs,under the direction of Mrs Louiza ZENKHRI Professor at KasdiMerbahOuargla UniversityandMrs Souheyla BOUDJEMA Professor at KasdiMerbahOuargla University.

First and foremost, I am most indebted to my principal supervisor, Professor Louiza ZENKHRI, who initially helped me merge my specialty, environmental chemistry, with specialty, materials chemistry, to result in this wonderful work. I am grateful to her for his timely academic guidance and positive criticism which helped me improve my analytical, research, scientific-writing and presentation skills. I am also thankful to her and also my co-supervisor Professor Souheyla BOUDJEMA for their painstaking effort in reviewing my thesis. The compilation of this thesis would have not been possible without their valuable suggestions and comments. I would like to thank you for your encouragement and inspiration throughout this project that helped me finish my study without any hurdles.

I express my gratitude to members of the discussion committeewho kindly agreed to judge this work

I thank Mr Mohamed Lakhdar BELFAR professor and director of the laboratory VPRS, for welcoming me in his team and for all the help provided during my stays, and all the laboratoir members for creating a warm working atmosphere during these years.

My gratitude goes to Director of CRAPC Laboratory Mr BELKHALFA Hakim for providing access to his laboratory and allocate a place for me to conduct my research experiments, as well as to use the equipment available in the laboratory, I would also like to

thank you for providing me with the chemicals needed for this process, and all the members of CRAPC Laboratory with whom I worked during my research study In particular: Mrs BAY Halima, Mrs RAMDANI Soumia, TIDJANI Iman and MOUKHTARA Islam.

I wish to express my sincere gratitude to the Director of Higher Normal School of Ouargla Mr BEN BRAHIM Faouzi for his kind welcome and his generous decision to grant me access to the school's laboratories. , allowing me to work alongside the esteemed faculty. My special appreciation goes to Professor ELABED Ibrahim, Mr. BIN ARIMA Abdel Hakim, and Ms. BIN ZAHI Khadija for their exceptional guidance and assistance.

I would like to express my sincere gratitude to the Director of the Sanitation Disinfection Office in Ouargla, Mr. CHATOUH, and all those working there for the warm welcome you extended to me within your company, especially Ms. BOUDIA Nadia. They placed their equipment at my disposal with complete confidence. I am veryhonored to have had the opportunity to conduct training with you in the field of wastewater purification. I learned a lot during this training. Thank you for the time you gave me and your valuable information.

I would like to thanks all my professors at the University of Ouargla for their advice and guidance, especially Professor SARAOUI Mabrouk for his support.

I Also owe a debt of gratitude to to my classmates Gania BENAZIA, Hibatarrahmen YAZZI, Noura MABROKI, Manal BASSA who always stood by when I needed their and made my course an adventure as fruitful as fun, Thank you for these good times and our infinite laughter.

I am very appreciative of the support I received from my colleagues from Tlemcen university Mounir MEKIDICHE, Bouchra MEKIDICHE, Your collaboration with us has greatly benefited us.

I would like to show my gratitude to number of professional and scientific individuals who have facilitated completion of this work: NEGADI sofiane, ELHADH ABDELKADER Hanan and FT-IR from CSCO laboratory in Tlemcen, which provided me with the physicochemical analysis using a variety of methods, I would like to thank GADJA Omar from the Geology of desert laboratory of KasdiMerbah University for his availability and kindness and for following part of my thesis path by helping to accomplish the RDX measurements of samples with great gentleness.

I would like to express my sincere gratitude to Mr HADJI Mohammad Yassin in the realization of granulometricanalysis from LEC Géosciences laboratory

I would like to express my sincere gratitude to Mrs BOUGHABA Latifa for your invaluable help in the realization of optical microscopy analyses in the Phoniculture laboratory of the University of Ouargla.

I thank the pedagogical laboratory workers, KATEB Zouhair, GHENIMI Anisa, and BEDIAF Hanan for their help.

I would also like to thank Mabrouki Tarek for his help in collecting the clay.

Dad, I am very proud to be your daughter, it is a great opportunity to have you in my life, you have always seen in me a studious student.

Finally, I would like to thank my husband, SID Nouh , for his love, patience and understanding. Without whose support I would have struggled to find the inspiration and motivation needed to complete my research.

Abstract

According to the Ministry of Higher Education and Scientific study of Algeria, the axis "Environment and Sustainable Development" and "Water Resources" are among the priority fields for scientific study. Considering the significance of the subsequent sub-axes: "Environmental conservation policies," "Waste water treatment and recovery," and "Water treatment technology." This thesis discusses directions and the use of contemporary technology to remove pollutants from water and recover depolluting materials for this purpose. It does this within the context of a PHD memorandum from the "PRFU" project.

Because of their special qualities, which include high specific surface area, adjustable pore activity, and catalytic activity, chemical compound and certain natural substances hold great promise for the treatment of contaminated water. These qualities make them perfect for eliminating a variety of water pollutants, including nitrates and organic pollutants.

The synthesis, identification, and application of crystalline structures in the treatment of contaminated water for chemicals and/or other natural compounds are included in this thesis. Along with outlining the socioeconomic advantages of using chemical compounds for water purification, it also gives a general review of the many methods—such as adsorption and photocatalysis that can be used to treat contaminated water.

The results of the experiment demonstrated that, in general, the synthesized particles had significant elimination efficiencies and were successful in eliminating red Congo from contaminated water. They also had micro and mezo row diameters. The outcomes also show that it is practicable to eliminate contaminants from water and offer proof of their efficacy in practical settings.

Three chemical compounds {$[Fe_2(OH)_2(C_4O_4)_2H_2O).2H_2O]$ (FS), $[NH_4[Cd(C_2O_4)2H_2O]$ (CD) and $Cu((C_4H_6O_5)_2(C_8H_9NO)_2$ (CMA)} were developed, their crystallographic structure was identified and catalytic activity for degradation of poluants (FS) and (CD) was studied. (FS) demonstrated excellent efficacy and cheap cost in eliminating red Congo pollutants from artificially contaminated water, leading us to explore this molecule as a viable option for commercialization. $NH_4[Cd(C_2O_4)2H_2O]$ also showed poor ability to remove nitrates and red Congo from contaminated water. While natural clay materials are very effective in removing the coloring of the proportion of mud in the Hejira area (Oued N'sa) and clay in the El-Mghaeir area.

Keywords: Synthetic particles, natural particles, water treatment, organic pollutants, Congo red, nitrates, adsorption, photocatalysis, photodegradation.

الملخص

يعتبر محور "البيئة والتنمية المستدامة" ومحور "موارد المياه" من بين المحاور ذات الاولوية في البحث العلمي حسب آخر تحديث لوزارة التعليم العالي والبحث العلمي في الجزائر. وبالنظر الى اهمية المحاور الفرعيةالتالية : "تكنولوجيا معالجة المياه" ،"معالجة مياه الصرف الصحي واستعادتها" و"تحليل تكلفة الثلوث وازالة الثلوث" ومن بين هذه المحاور وفي اطار مذكرة تخرج ضمن مشروع « PRFU » فإن مضمون هذه الاطروحة يعالج مشكلة ثلوث المياه وتطبيق التكنولوجيات الحديثة في ازالة الملوثات وتثمين مزيلات الثلوث المستعملة لهذا الغرض.

تعتبرالمركبات الكيميائية وبعض المواد الطبيعية مواداواعدةلمعالجةالمياهالملوثة، وهذا لاكتسابها خصائصفريدة،مثلمساحةالسطحالعالية،وقابليةالتعديل،والنشاطالتحفيزي، مايجعلهامثاليةلإزالةمجموعةواسعةمنالملوثاتمنالماء مثل الملوثاتالعضويةوالنترات.تشملهذهالأطروحةتصنيعوتحديد البنى البلوريةلموادا كيميائيةو\أخرى طبيعيةوتطبيقها في مجال معالجة المياه الملوثة. كمايقدمنظرةعامةعلى بعضالطرقالمختلفةالتييمكنمنخلالهااستخداماالمركبات الكيميائيةلمعالجةالمياهالملوثة،بمافيذلكالامتزازوالتحفيزالضوئي، مع تسليط الضوء على المنفعة الاجتماعية/الاقتصادية لتنقية الماء بهذه المواد.

أظهرتالنتائجأنالجسيماتكانت من المرتبة ميكرو وميزووكانتفعالةفيإزالةالكونغو الاحمرمنالمياهالملوثة،معكفاءاتإزالةتصلإلىحد كبير بشكل عام.كماتوضحالنتائج المتحصل عليهاإمكانية ازالة مجموعة واسعة من الملوثات من الماءويوفردليلاًعلىفعاليتهافيتطبيقاتالعالمالحقيقي.

أسفرت النتائج على تصنيع ثلاث مركبات كيميائية $[Fe_2(OH)_2(C_4O_4)2H_2O).2H_2O]$ (FS), $[NH_4[Cd(C_2O_4)2H_2O]$ (CD)$Cu(C_4H_6O_5)_2(C_8H_9NO)_2]$(CMA),[مع التوصيف الكامل لها وتوصيف مادة طينية طبيعية. أعطى المركب $Fe_2(OH)_2(C_4O_4)2H_2O)_2.2H_2O$كفاءة عالية في ازالة ملوث الكونغو الأحمر من المياه الصناعية الاصطناعية، بتكلفة قليلة مما يسمح لنا باعتبار هذا المركب واعد للتسويق الاقتصادي. كما أظهر المركب $NH_4[Cd(C_2O_4)2H_2O]$قدرة ضعيفة في ازالة النترات وقدرةازالة معتبرة في للكونغو الاحمر من المياه الصناعية الاصطناعية. في حين تعتبر المواد الطينية الطبيعية مواد جد فعالة في كل من ازالة الملونبالنسبة لطين منطقة الحجيرة (واد نساء)، وتحسين كفاءة مياه الصرف الصحيبالنسبة لطين منطقة المغير .

الكلماتالرئيسية: الجسيماتالاصطناعية،والجسيماتالطبيعية،ومعالجةالمياه،الملوثاتالعضوية،الكونغو الاحمر, النترات,والامتزاز،والتحفيزالضوئي،والتحلل الضوئي.

Resumé

Les axes "Environnement et Développement Durable" et "Ressources en eau" figurent parmi les domaines prioritaires de la recherche scientifique telle que mise à jour par le Ministère de l'Enseignement Supérieur et de la Recherche Scientifique d'Algérie. Compte tenu de l'importance des sous-axes suivants : "Technologie des traitements des eaux", "traitement des eaux usees et valorisation", "Politiques de mréservation de l'environnement".En se réferant à axes, et dans le cadre d'un PHD mémorandum issu du projet "PRFU", le contenue de cette thèse abordent le problème de la pollution de l'eau et l'application des technologies modernes pour éliminer les polluants et valoriser les matériaux depolluants à cet effet.

Les composés chimiques et certaines substances naturelles sont des substances prometteuses pour le traitement de l'eau contaminée, grace à leurs propriétés uniques, telles que la surface spécifique élevée, l'activité réglable des pores et l'activité catalytique, ce qui les rend idéales pour éliminer un large gamme de polluants de l'eau tels que les polluants organiques et les nitrates.

Cette thèse comprend la synthése et l'identification de structures cristallines et l'application dans le traitement de eaux contaminé pour les substances chimiques et / ou d'autres substances naturelles. On presente également un aperçu des différentes façons dont les composés chimiques peuvent être utilisés pour traiter l'eau contaminée, y compris l'adsorption et la photocathalyse, tout en soulignant les avantages socio-économiques de purifier l'eau avec ces substances.

Les résultats ont montré que les particules synthétisé avaient des tailles du rang micro et mezzo et étaient efficaces pour éliminer le Congo rouge de l'eau contaminée, avec des efficacités d'élimination importante en général. Les résultats obtenus demontre également la possibilité d'éliminer des polluants de l'eau et fournissent des preuves de leur efficacité dans des applications réelles.

Trois composés chimiques {[$Fe_2(OH)_2(C_4O_4)2H_2O).2H_2O$] (FS), [$NH_4[Cd(C_2O_4)2H_2O$] (CD)et $Cu((C_4H_6O_5)_2(C_8H_9NO)_2$ (CMA)} ont été élaboré,leur structure cristallografique a été identifier et l'activité catalytique pour la dégradation des poluants de (FS) et (CD) a été étudier. (FS)a donné une efficacité élevée pour éliminer le polluant Congo rouge de l'eau artificiellement pollué et avec un faible coût, ce qui nous permet de considérer ce composé prometteur pour la commercialisation économique. (CD) avait une faible capacité d'élimination des nitrates mais une capacité moyenne d'élimination du rouge Congo. D'un autre côté, la détérioration du rouge Congo et les taches des eaux usées de l'ONA de Ouargla sont toutes deux grandement facilitées par les matériaux argileux naturels.

Mots-clés : particules synthétiques, particules naturelles, traitement des eaux, polluants organiques, rouge Congo, adsorption, nitrates, photocatalyse, Photo-dégradation.

Figure List

Figure	Designation	Page
Figure.I.1	Congo red structure.	**10**
Figure.I.2	Schematic of the co-precipitation method.	**13**
Figure.I.3	Tetrahedral unit of clay minerals.	**15**
Figure.I.4	Octahedral unit of clay minerals.	**15**
Figure.I.5	The structure of kaolinite	**16**
Figure.I.6	The structure of smectite	**16**
Figure.I.7	The structure of chlorite	**17**
Figure.I.8	Analog Structure of UIO-67.	**23**
Figure.I.9	scheme of adsorbintion of congo red using Fe_3O_4@ZTB-1	**24**
Figure.I.10	Schematic of the preparation of surface-modified Fe_3O_4@BTCA.	**24**
Figure.I.11	Schematic diagram of the adsorption of Congo red dye by Fe_3O_4BTCA through H-bonding carboxyl anions.	**24**
Figure.I.12	Possible mechanism of CR adsorption by $([Mn_3(L1)_2(L2)_2(H_2O)_8]\cdot 4H_2O)n$	**25**
Figure.I.13	removel of Congo red by H_3BTC.	**25**
Figure.I.14	$LiNbO_3$trigonal strecture	**26**
Figure.I.15	A scheme showing the method of removing nitrates from water using a photocatalyst$LiNbO_3$	**26**
Figure.I.16	synthesis stages of aluminum oxide nanoparticles (Al_2O_3NPs)/Moringaoleifera gum activated carbon (MOGAC)-based nanocomposites	**27**
Figure.I.17	suggestion of mechanisms to removal of nitrate ion by Al_2O_3/MOGAC nanocomposites	**27**
Figure.I.18	Schematic of the correlation of nitrate over Pd-Cu/CNT-TiO_2 catalysts in the presence of H_2 and CO_2	**28**
Figure.I.19	Link method between a compound TG-g-P(MMA)/B and Congo red	**30**
Figure.II.1	The location of the clay(CM) sample by Google Earth.	**41**
Figure.II.2	The location of theclay(CH) sample by Google Earth.	**42**
Figure.III.1	Infrared spectrum of the prepared compound	**51**
Figure.III.2	SEM image of the compound CD	**52**
Figure.III.3	EDS spectrum for CD sample	**53**
Figure.III.4	X-ray spectrum of the prepared sample (red) and trace of acetanilide (black)	**54**
Figure.III.5	histogram of the qualitative composition of the sample	**55**
Figure.III.6	WH plots	**56**
Figure.III.7	Asymmetric Molecular Structure	**57**
Figure.III.8	Molecular unit of the prepared compound	**57**
Figure.III.9	Primary network structure	**58**
Figure.III.10	Projection of the primary cell along the axes a, b, c	**59**
Figure.III.11	Representation of the hydrogen bonds formed at the level of the crystal structure of the compound	**59**
Figure.III.12	Isothermeadsoption BET Plot	**60**

Figure.III.13	isotherme pressure composition	**60**
Figure.III.14	X-rays diffractometers of initial product (green) , after being washing with ethanol to dissolve acetanilid, (bleu), calistresidu (red).	**63**
Figure.III.15	Representation showing the pore channels befor and after losing water and amonium cation	**63**
Figure.III.16	Photocatalytic degradation of Congo red under visible light irradiation using $NH_4[Cd(C_2O_4)_2].2H_2O$	**65**
Figure.III.17	The kineticsof coloran CR adsorption	**66**
Figure.III.18	CR degradation efficiency in the presence of (CD1) catalyst in the various Advanced Oxidation Processes	**66**
Figure.III.19	A schematic representation of CR deterioration over a $NH_4[Cd(C_2O_4)_2].2H_2O$ photocatalyst when exposed to UV light.	**67**
Figure.IV.1	SEM image of the compound	**73**
Figure.IV.2	Powder X-ray diffraction pattern, the red of the title compoud and the green of [fluorenyllithium .2 ethylenediamine] database	**74**
Figure.IV.3	primitive cell conception	**78**
Figure.IV.4	cristalline lattice conception	**79**
Figure.V.1	Surface morphology of FS compound by SEM analyses	**83**
Figure.V.2	EDX spectrum of FS compound	**84**
Figure.V.3	The infrared product spectra	**84**
Figure.V.4	Phasis identification using X-ray's diffraction.	**85**
Figure.V.5	asymetric unit.	**86**
Figure.V.6	molecular unit	**86**
Figure.V.7	lattice presentation	**86**
Figure.V.8	H bounds presentation	**87**
Figure.V.9	plot BET of FS	**88**
Figure.V.10	adsorption plot	**92**
Figure.V.11	Comparaison of the two cat FS5 et FS12.	**93**
Figure.V.12	photos of adsorption reactions of FS1/2 and FS5.	**94**
Figure.V.13	XRD patterns of FS	**94**
Figure.V.14	XRDpatterns of the catalysts FS, FS before reaction, FS after reaction	**95**
Figure.V.15	Patterns of the catalysts FS1, FS2, FS1/ before adsorption, FS1/2 after adsorption.	**96**
Figure.VI.1	Location of ONA by google earth	**101**
Figure.VI.2	PH changes of wastewater treated with chemically activated clay	**104**
Figure.VI.3	Temperature changes of wastewater treated with chemically activated clay	**104**
Figure.VI.4	Electrical conductivity values changes of wastewater treated with chemically activated clay	**105**
Figure.VI.5	Turbidity values changes of wastewater treated with chemically activated clay	**106**
Figure.VI.6	Changes in the value of suspended matter (TSS) of wastewater treated with chemically activated clay	**107**
Figure.VI.7	Changes in the value of the biochemical demand for oxygen (BOD_5)	**108**

	of wastewater treated with chemically activated clay	
Figure.VI.8	Changes in the value of the chemical demand for oxygen (COD) of wastewater treated with chemically activated clay	**109**
Figure.VI.9	Changes of physical properties (pH, T, EC) of wastewater treated with chemically and thermally activated clay	**110**
Figure.VI.10	Efficiency of sulfuric acid and heat activated clay in removing organic pollutants.	**110**
Figure.VII.1	The Google Earth-captured location of the sample collection region	**115**
Figure.VII.2	The clay sample	**115**
Figure.VII.3	Vibratory sieve shakers (Retsch. AS 200).	**117**
Figure.VII.4	Experimental setup used in clay purification.	**117**
Figure.VII.5	The shaking process.	**118**
Figure.VII.6	A picture of the clay before and after 24 h.	**118**
Figure.VII.7	Scanning electron microscopic images of clay materials.	**119**
Figure.VII.8	FTIR spectrum of clay sample	**120**
Figure.VII.9	Xrays patter of the clay	**121**
Figure.VII.10	Quantitative analysis of the clay	**123**
Figure.VII.11	Asymetric unit	**124**
Figure.VII.12	The molecule	**124**
Figure.VII.13	Arrangement in kornerupine lattice	**124**
Figure.VII.14	The kineticsof coloran CR adsorption	**125**
Figure.VII.15	CR degradation byfenton,photocatalysisand photofenton.	**126**

Table Liste

Table	Designation	Page
Table.II.1	The natural and chemical materials used.	**40**
Table.III.1	The quantitative and qualitative composition of the CD sample recorded by the EDS device	**52**
Table.III.2	Specific details of phase identification	**53**
Table.III.3	The two phases involved in the chemical composition of the sample under analysis	**55**
Table.III.4	X-ray indexing results for the sample and compound of the scientific publication	**55**
Table.III.5	Grains' particle size (D) and strain (e).	**56**
Table.III.6	Characteristic results of Brunauer-Emmett-Teller analysis	**60**
Table.III.7	Values given to the program for design appropriate experiments	**61**
Table.III.8	The experiments conducted.	**61**
Table.III.9	Operating conditions of different parameters.	**64**
Table.IV.1	Quantitative and qualitative composition of the sample by the EDS device	**73**
Table.IV.2	Comparison between the two compounds precursor	**74**
Table.IV.3	Lattice parmeters found for the synthetised product	**75**
Table.IV.4	fluorenyllithium .2 ethylenediamine] caracteristics	**76**
Table.IV.5	Similarity between Maleic acid and ethylenediamine	**76**
Table.IV.6	Similarity between flurenyl and acetanilid	**77**
Table.V.1	Results of quantitative and qualitative analysis of the FS sample	**84**
Table.V.2	lattice parameters	**85**
Table.V.3	COD Determinaton	**86**
Table.V.4	The BET meusure characteristic of FS	**88**
Table.V.5	Experimental conditions for the Red Congo degradation process	**91**
Table.V.6	Experimental conditions for the Red Congo adsorption process	**92**
Table.VII.1	Conditions for preparing clay	**115**
Table.VII.2	Granulometric analysis of the sample results	**115**
Table.VII.3	Quantitative results of clay EDX	**119**
Table.VII.4	Qualitative analysis results of the clay	**122**
Table.VII.5	Cell parameters of the clay phases	**122**
Table.VII.6	Crystallite size and lattice strain	**122**

Table.VII.7 Abundances of the different phases in the clay sample **123**

summary

Dedication
Acknowledgement
Abstract
Figure list
Tables list
General introduction 1

CHAPTER ONE
GENERALITIES ABOUT SOFT CHEMISTRY, MATERIALS AND CLAY MINERALS

I.1.The pollution 7
I.1.1. Water Pollution 7
I.1.1.1. Water pollution with nitrates 9
I.1.1.2. Water pollution with Congo red (CR) 9
I.2. Organic-inorganic hybrid materials 11
I.2.1. Methods of synthesis materials using soft chemistry 11
I.2.1.1. Solid track 11
I.2.1.2. Mechanical activation 12
I.2.1.3. Mechanosynthesis (high energy grinding) 12
I.2.1.4. The polymerizable complex method 12
I.2.1.5. Hydro(solvo)thermal syntheses 12
I.2.1.6.Sol-gel synthesis 13
I.2.1.7.Co-precipitation 13
I.3. Clay and Clay minerals 14
I.3.1. Clay 14
I.3.2.Clay minerals 14
I.3.3. The building blocks of clay 15
I.3.3.1. Tetrahedral structural unit 15
I.3.3.2. Octahedral structural unit 15
I.3.4. Types of clay 15
I.3.4.1. Type 1:1 or T-O type 16
I.3.4.2. Type 2:1 or T-O-T 16
I.3.4.3. Type 2:1:1 or T-O-T-O 17
I.3.5. Physical and chemical properties of clay minerals 17
I.3.5.1. Cation–exchange capacity 17
I.3.5.2. Swelling capacity 18
I.3.5.3. Surface charge properties 18
I.3.5.4.Adsorptive properties 18
I.3.5.5.Specific surface area (SSA) 19
I.3.5.6.Plasticity 19
I.3.5.7.Dispersion/flocculation 19
I.3.6.Modifying (activating) clay 19
I.3.6.1. Methods for modifying clay minerals 20
a. Thermal activation 20

b. Chemical activation 20
I.4.Methods for removing Pollutants from water 20
I.4.1. Photocatalysis 20
I.4.2. Photocatalysts 21
a. Fenton process 21
b. Photo- Fenton process 21
I.4.3. Adsorption 22
Bibliographic reference 31

Chapter TWO: MATERIALS AND METHODS

Introduction 40
II.1. Chemical product (precursors) 40
II.2. Natural product 41
II.3. Wastewater 42
II.3.1. synthetic wastewater 42
II.3.2.Hurbain wastewater 42
II.4. Physico-chemical measurements. 43
II.4.1.Fourier Transform Infrared Spectroscopy(FTIR): 43
II.4.1.1.Sample preparation 43
II.4.2.Visible (UV-Vis) 43
II.4.3.Scanning Electron Microscope 44
II.4.3.1.Sample preparation 44
II.4.4.The BET method 45
II.4.5.Structural identification of powders by x-ray techniques 45
II.4.6.Particle size analysis 45
II.4.7. Multi-parameter device 46
II.4.8. Turbidity Meter 46
II.5. Informatic support 46
II.5.1.FullProf Suite 46
II.5.2.HighScore Plus and QualX 46
II.5.3.Mercury 3.8 46
II.5.4.ImageJ software 47
II.5.5.Origin 47
II.6. Database 47
II.6.1. COD powder diffraction file database 47
II.6.2. ICSD (Inorganic crystal structure database) 47
II.7.Crystallographic Data File (Cif) 48

CHAPTER THREE : $NH_4[Cd(C_2O_4)2H_2O]$

Investigation of $NH_4[Cd(C_2O_4)2H_2O]$ in Nitrite removal from synthtic wastewater

Introduction 50

III.1. Synthesis of $NH_4[Cd(C_2O_4)_2].2H_2O$ (CD) 50
III.2. Identification of $NH_4[Cd(C_2O_4)_2].2H_2O$ 50
III.2.1. InfraRed Spectroscopie analysis 50
III.2.2. Elemental analysis 52
III.2.3. Results of crystal structure analyze by X-ray diffraction 53
III.2.3.1. Qualitative Analysis Results 53
III.2.3.2. Quantitative Analysis Results 54
III.2.3.3. Indexing of the X-ray spectrum 55
III.2.3.4. Cristallite size and lattice strain (Williamson-Hall method) 56
III.3. Description of the Crystal Structure 57
III.3.1. Asymmetric Molecular Unit 57
III.3.2. Molecule (Molecular Unit) 57
III.3.3. primary cell's 58
III.3.4.The role of hydrogen bonds in the cohesion of the compound 59
III.4. BET interpretation 59
III.5. Removing nitrates from synthetic wastewater 61
III.5.1. Preparation of the contaminated medium 61
III.5.2. Result 62
III.6. Removing Congo red from synthetic wastewater 64
III.6.1. Adsorption 64
III.6.2. Fenton's process 64
III.6.3. Photocatalysis 65
III.6.4. photo-Fenton 65
III.6.5. Result 65
Conclusion 68
Reference 69

CHAPTER FOUR : $Cu((C_4H_6O_5)_2(C_8H_9NO)_2$
Synthesis, caracterization and design of a new isomorphous of [fluorenyllithium .2 ethylenediamine]

Introduction 72
IV.1. Synthesis of $Cu((C_4H_6O_5)_2(C_8H_9NO)_2$ 72
IV.2. $Cu((C_4H_6O_5)_2(C_8H_9NO)_2$ identification 72
IV.2.1. Elemental analysis 72
IV.2.2. Cristal structure analysis result 73
IV.2.3. Lattice indexation 75
IV.2.4. Structure description 76
IV.2.5. Molecule conception 78

Conclusion 79
Reference 80

CHAPTER FIVE : $[Fe_2(OH)_2(C_4O_4)2H_2O]_2.2H_2O$
DIHYDROXY SQUARATE COMPOUNDS FOR WATER DEPOLLUTION

Introduction 82
V.1. Synthesis of $Fe_2(OH)_2(C_4O_4)2H_2O).2H_2O$ 83
V.2. Physico-chemical characterization of $[Fe_2(OH)_2(C_4O_4)2H_2O]_2.2H_2O$ 83
V.2.1. Elementary analysis 83
V.2.2. Spectroscopy InfraRed analysis 84
V.2.3. X-ray powder diffraction study 85
V.2.3.1. Qualitative analysis 85
V.2.3.2. Structure description 86
V.2.3.3. H bounds 87
V.2.3.4. Water and OH 87
V.2.4. BET analysis of FS structure 87
V.3. Degradation of Congo red 90
V.3.1. Adsorption 90
V.3.2. Fenton's process 90
V.3.3. Photocatalysis 90
V.3.4. photo- Fenton 91
V.4. result 91
V.4.1. Congo red degradation 91
V.4.1.1. Fenton's process 91
V.4.1.2. Photocatalysis 92
Conclution 96
Reference 98

CHAPTER SIX : CLAY (CM)
(Illite , Kaolinite, SiO_2) CLAY

Introduction 100
VI.1. Clay (CM) sample preparation 100
VI.2.Wastewater 100
VI.3. Activation of clay 101
VI.3.1. Chemical activation 101
a. Activation with hydrochloric acid (HCl) 101
b. Activation with sulfuric acid (H2SO4) 102
VI.3.2. Thermal activation 102
VI.4. Processing step for wastewater treatment 103
VI.4.1. The effect of chemical activation 103
VI.4.1.1. The effect of the chemical activation of clay on the change of the value of the pH for –wastewater 103
VI.4.1.2. The effect of the chemical activation of clay on the change of the value of the Temperature for wastewater 104
VI.4.1.3. The effect of the chemical activation of clay on the change of the value of the EC for wastewater 105
VI.4.1.4. The effect of the chemical activation of clay on the change of the 105

value of the turbidity for wastewater
VI.4.1.5. The effect of the chemical activation of clay on the change of the value of the suspended material (TSS) from wastewater 106
VI.4.1.6. The effect of the chemical activation of clay on the change of the value of the biochemical demand for oxygen (BOD_5) from wastewater 107
VI.4.1.7. The effect of the chemical activation of clay on the change of the value of the chemical demand for oxygen (COD) from wastewater 108
VI.4.2. The effect of thermal activation 109
VI.4.2.1. Effect of activated clay with sulfuric acid and heat on the efficiency of changing physical properties (pH, T, EC) 109
VI.4.2.2. Efficiency of sulfuric acid and heat activated clay in removing organic pollutants. 110
Conclusion 110
Reference 111

CHAPTER SEVEN : CLAY (CH)
Kornerupine Clay

Introduction 113
VII.1. Samples 113
VII.2. Simple preparation 114
VII.2.1. Granulometry analysis 114
VII.2.2. Grain separation 115
VII.3. Sample characterization 117
VII.3.1. Clay microstructure using SEM-EDX 117
VII.3.2.Clay identification using FT-IR 119
VI.3.3. X-Rays Analysis 120
VII.3.3.1. Crystallite size and lattice strain 121
VII.3.3.2. Qualitative analysis results 121
VII.4.Crystal structure description 122
VII.5.Remove of congo red dye by clay 124
VII.5.1.Adsorption 124
VII.5.2.Fenton 124
VII.5.3.Photodegradation 124
VII.5.4.Photo-Fenton 125
Socio-economic study
Conclution general 127
Annexe

General introduction

Environmental pollution is one of the biggest global challenges facing humankind and the planet [1]. Its consequences are far-reaching, contributing to numerous diseases, pandemics, and deaths, while disrupting the delicate balance of our ecosystems. This escalating crisis stems primarily from human activities associated with urbanization, industrialization, mining, resource exploration, and unsustainable practices in natural resource utilization. Despite international attention to the issue, the severe long-term effects of pollution continue to be felt all over the world [2].

Pollution can take many different forms, including air, soil, and water pollution brought on by the presence of hazardous organic and inorganic substances or by changes in the ratios of certain fundamental elements in the environment from their natural states. Because water plays such a significant part in daily life and is a necessary component of many industries, it is crucial to note that water pollution is one of the most significant pollution issues. Due to the fact that the pollution issue has become more severe in recent years, numerous governments worldwide have instigated the establishment of organizations to manage the sources of pollution and safeguard the environment [3-5].

Adsorption on clay sediments is one of the most significant methods that have been used to address this issue [6], along with some physicochemical methods including coagulation [7], fusion, and reverse osmosis, adsorption on activated carbon, or magnesium oxide and clay [8].

Due to its low cost, straight forward design, and convenience of use, adsorption is a well-known and successful technique that has been extensively investigated as an alternative to other waste removal methods. Moreover, adsorption produces no hazardous materials during the process. Because they are readily available locally and may be chemically or thermally manipulated, clay minerals have gained popularity as inexpensive adsorbents in recent years [9].

In the other hand, materials technology presents promising prospects for mitigating pollution through the development of efficient methods for producing porous and nanoporous materials.[10-12] These materials offer significant advantages over conventional porous materials such as activated carbon and zeolites, making them highly competitive for environmental remediation applications [13].

This thesis is a part of the work of the University Research and Training project (PRFU) {Projet de Recherche et de Formation Universitaire} which began in 2021entiteled

"Development and physico-chemical characterization of nanomaterials for the treatment of polluted water". This thesis is considered as the first fruit of this project.

In this work, we focused on two of the most challenging pollutants in the world: Congo red, an organic dye that pollutes water bodies due to the discharge of untreated wastewater from textile factories and nitrate, an ionic pollutant that is found in groundwater due to the infiltration of agricultural fertilizers. To eliminate or at least reduce these pollutants, we chose two treatment methods: the first using hybrid materials synthesized by co-precipitation mehode in soft chemistry process, namely $NH_4[Cd(C_2O_4)2H_2O]$ (CD), $Cu((C_4H_6O_5)_2$ $(C_8H_9NO)_2$ (CMA), and $Fe_2(OH)_{2(}C_4O_4)_2.2H_2O$ (FS), and the second using untreated natural clay from Wad El-Nessa (Ouargla) region. And in other hand we treated urban wastewater in Ouargla using clay from El-M'Gheir after it was chemically and thermally treated.

The objective of this study is to evaluate the effectiveness and cost of the degradation of red Congo by hybrid chemical complexes and natural clay. This thesis provide new solutions for water pollution and improve the performance of traditional techniques by removing some organic pollutants from water, such as those found in urban wastewater (Congo red), and ionic pollutants (nitrate), using organic-inorganic hybrid materials synthesized by co-precipitation method in soft chemistry process at room temperature. These materials are based on metals (cadmium, copper, and iron), acids (squaric acid and malic acid), amides (acetanilide, ammonium oxalate), in addition to two types of natural clay, one of which was chemically and thermally treated, while the other was used as it was obtained from nature.These materials were characterized usingFourier-transform infrared spectroscopy (FTIR), X-ray diffraction (XRD), scanning electron microscopy (SEM/EDS), and surface area analysis (BET) method. Cristalline structures identification were found using HighScore Plus softward, WhileMercury softward was utilized in structures visualization and FullProf programs in aterns indexation. The titles comounds efficiency in removing pollutants from water was then tested using photo-Fenton and photo-Fenton photocatalysis methods.

This manuscript, which begins with this introduction, is divided into two parts. The first part consists of two chapters, the first of which deals with some definitions, followed by a bibliographic study and the background of the study. The second chapter is dedicated to describing the different synthesis methods, the method of filtering the clay, and the presentation of the techniques for characterizing the prepared materials and the clay, as well as the tools used.

The second part discusses the results in five chapters. Chapter three presents the results of the synthesis of the compound CD which is a new member in $NH_4[Ti(C_2O_4)2H_2O]$ family and the results of its effectiveness test in removing nitrate and Congo red from water. Chapter four deals with the results of the synthesis of the compound CMA an isomorphous of [fluorenyllithium-2ethylenediamine]. Chapter five deals with the compound FS, which was characterized and tested for its effectiveness in removing Congo red. The sixth chapter gives the results of the removal of organic matter from urban wastewater in Ouargla using M'Gheir clay after chemical and thermal activation and chapter seven presents the results of the characterization of the Wadi Nissa clay and the test of its effectiveness in removing Congo red from water. Finally, we conclude with a general conclusion.

Reference

[1] *Grand challenges in environmental sciences.National Research Council (U.S.). Committee on Grand Challenges in Environmental Sciences.* *2001*

[2] Khasanova, S.; Alieva, E.; Shemilkhanova, A. Environmental Pollution: Types, Causes and Consequences. *BIO Web Conf.***2023**, *63*, 07014. https://doi.org/10.1051/bioconf/20236307014.

[3] Christmann, P.; Taylor, G.; Taylor, G. Globalization and the Environment: Strategies for International Voluntary Environmental Initiatives. *The Academy of Management Executive (1993-2005)***2002**, *16* (3), 121–136.

[4] Berry, M. A.; Rondinelli, D. A. Proactive Corporate Environmental Management: A New Industrial Revolution. *AMP***1998**, *12* (2), 38–50. https://doi.org/10.5465/ame.1998.650515.

[5] *Asian Energy and Environmental Policy: Promoting Growth While Preserving the Environment by ZhongXiang Zhang :: SSRN*. https://papers.ssrn.com/sol3/papers.cfm?abstract_id=1094209 (accessed 2023-12-17).

[6] Uddin, M. K. A Review on the Adsorption of Heavy Metals by Clay Minerals, with Special Focus on the Past Decade. *Chemical Engineering Journal***2017**, *308*, 438–462. https://doi.org/10.1016/j.cej.2016.09.029.

[7] Jiang, J.-Q.; Zeng, Z.; Pearce, P. Preparation and Use of Modified Clay Coagulants for Wastewater Treatment. *Water, Air, & Soil Pollution***2004**, *158* (1), 53–65. https://doi.org/10.1023/B:WATE.0000044833.75579.8b.

[8] Mavros, P.; Daniilidou, A.C.; Lazaridis, N.K.; L. Stergiou. Color removal from aqueous solutions. Part I. Flotation. **1994**. Environ. Technol., 15(7): 601-616.

[9] Murra, H. H. Current Industrial Applications of Clays. *Clay Science***2006**, *12* (Supplement2), 106–112. https://doi.org/10.11362/jcssjclayscience1960.12.Supplement2_106.

[10] *Samanta P ; Desai A V ; Let S ; Ghosh S K.Advanced Porous Materials for Sensing, Capture and Detoxification of Organic Pollutants toward Water Remediation | ACS Sustainable Chemistry & Engineering*. https://pubs.acs.org/doi/abs/10.1021/acssuschemeng.9b00155 (accessed 2024-01-02).

[11] *Xiaolu L , Gaurav V, Zhongshan C , Baowei H, Qifei H, Hui Y, Shengqian M, Xiangke W. Metal-organic framework nanocrystal-derived hollow porous materials: Synthetic strategies and emerging applications - ScienceDirect*. https://*DOI: 10.1016/j.xinn.2022.100281*

[12] Elgarahy, A. M.; Elwakeel, K. Z.; Akhdhar, A.; Hamza, M. F. Recent Advances in Greenly Synthesized Nanoengineered Materials for Water/Wastewater Remediation: An Overview. *Nanotechnol. Environ. Eng.***2021**, *6* (1), 9. https://doi.org/10.1007/s41204-021-00104-5.

Part One

BIBLIOGRAPHIC STUDY AND BACKGROUND TO THE STUDY

Chapter One

GENERALITIES ABOUT SOFT CHEMISTRY, MATERIALS AND CLAY MINERALS

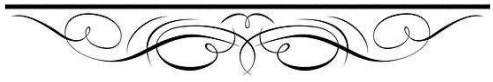

I.1.The pollution

The term 'pollution' refers to the presence of a substance within the environment whose chemical composition or quantity impedes the natural functioning of ecological processes and generates undesirable effects on both the environment and human health[1]. Pollutants are substances, existing in diverse forms like liquids, solids, or gases, which degrade the environment. This occurs when their concentration surpasses the natural level, which can be attributed to human actions or natural events [2].

There are different types of pollution, but the three main types are: air, water and soil pollution. Given water's paramount importance as the basis of all living systems, this thesis will specifically address the various sources and types of water pollution, their detrimental impacts on ecosystems and human health, and potential solutions to mitigate this global crisis.

I.1.1.Water Pollution

Water pollution, defined as any alteration in water's chemical, physical, or biological characteristics that negatively impacts the environment and human health, poses a significant threat. Water's universal solvent property makes it a prime carrier of contaminants. According to UNESCO, one liter of wastewater can contaminate eight liters of freshwater [3].Water pollution originates from various sources, including industrial activities like degassing at sea, paper mill discharges, and oil spills; agricultural practices involving fertilizers and pesticides; and automobile emissions containing unburnt fuels and oil [4-6].

The World Health Organization (WHO) reports that 80% of diseases are waterborne, with drinking water in many countries failing to meet WHO standards. Up to 3.1% of deaths are attributed to unhygienic and poor-quality water. WHO and UNICEF estimate that water pollution causes 2.2 million deaths annually, primarily among children under five [7-9].The severity of water pollution is assessed based on the type and concentration of pollutants present, as well as the proximity of water bodies to urban areas. Inadequate treatment of drinking water and wastewater can lead to direct human exposure to pollutants, resulting in the spread of infectious diseases like cholera. Moreover, fecal contamination of water sources can cause illnesses such as hepatitis.Certain chemicals, including heavy metals like cadmium and lead, and dioxins, can enter the human body through the food chain, particularly through the consumption of contaminated seafood, pou

ltry, and meat. These chemicals can cause a range of health issues, including reproductive problems and cancer[10].

Globally, an estimated 80% of municipal and industrial wastewater is released into the environment without treatment, posing a significant threat to ecosystems and human health. This issue is particularly prevalent in less developed countries where wastewater treatment and sanitation infrastructure are inadequate [11].Water pollution stems primarily from industrialization, agricultural activities, natural factors, and insufficient water supply and sewage treatment facilities. Industries, including distilleries, tanneries, pulp and paper mills, textile factories, food processing plants, iron and steel mills, and nuclear power plants, are major contributors to water pollution.Industrial processes release various toxic chemicals, organic and inorganic substances, toxic solvents, and volatile organic compounds. If these wastes are discharged into aquatic ecosystems without proper treatment, they cause water pollution[12].

Agricultural activities contaminate water with nitrates, phosphorus, pesticides, soil sediments, salts, and pathogens. The use of untreated or partially treated wastewater for irrigation in water-scarce regions of developing countries, including China and India, poses environmental and health risks due to the presence of pollutants in the sewage.In some developing regions, long-term wastewater irrigation to meet agricultural water demands has led to severe agricultural land and food contamination. A study in India's Musi River region revealed a higher incidence of illness in villages using wastewater irrigation compared to those using clean water. Natural factors also contribute to water pollution. For instance, in the Chinese Loess Plateau, trace element concentrations in water exceed global averages due to natural weathering and manufacturing processes. Poor river water quality is associated with high sodium and salinity levels[13].

Inadequate water supply and sewage treatment facilities significantly impact drinking water quality, especially in developing countries. China's rapid economic growth, industrialization, and urbanization, coupled with underinvestment in basic water supply and treatment infrastructure, have led to water pollution, increased incidence of infectious and parasitic diseases, and elevated exposure to industrial chemicals, heavy metals, and algal toxins[14].

I.1.1.1.Water pollution with nitrates

Over the past few decades, the global spotlight has turned towards nitrate water pollution, leading the World Health Organization (WHO) to establish a maximum allowable concentration of 10 mg/L for nitrate-nitrogen ($NO3^{-}$-N) in drinking water[15].High nitrate concentrations in the marine environment cause serious impacts, including eutrophication, toxic algal blooms, and hypoxia[16,17].Also, high concentration of nitrate in drinking water increases the risk of diseases and health effects such as methemoglobinemia, diabetes, spontaneous abortion, thyroid disease, and stomach cancer [18].

In North Africa's arid and semi-arid regions, groundwater resources, though limited in size, serve as the primary source of water for essential needs such as drinking, agriculture, and industry. Algeria, facing a long-standing potable water shortage, has witnessed excessive groundwater exploitation[19-22].

In southern Algeria, where the economy heavily relies on petroleum and agriculture, meeting the daily water demand for the city of Ouargla, estimated at 9,000 l/s [23], has led to increased groundwater extraction. This has resulted in a decline in groundwater quality, attributed to the dissolution of evaporate layers and interactions between superimposed aquifers.

A study by (Kharroubi. M and al.2022) analyzing 64 groundwater well samples in the Ouargla region revealed nitrate concentrations ranging from 0 to 78 mg/L, with an average of 25.6 mg/L. Notably, 12.5% of samples exceeded the World Health Organization's (WHO) maximum allowable limit for nitrate in drinking water (2011) [24].Wells with high nitrate concentrations were found in agricultural areas of Ain Moussa, likely due to excessive fertilizer use, and urban areas of Ouargla, Naqoussa, and Ain El Bayda, potentially linked to domestic sewage leakage. These findings confirm that the water quality in these areas does not meet WHO standards for drinking and irrigation water[25].

I.1.1.2. Water pollution with Congo red (CR)

The world faces another environmental challenge .it is pollution from synthetic dyes. Synthetic dyes, used extensively in industries such as textiles, rubber, paper, plastic, cosmetics, etc.These dyes can be classified in three categories:anionic, cationic and non-ionic[26]. the textile industry, account for 65-75% of all dye production.Most it are made up of azo, anthraquinone dyes[27].

The improper disposal of industrial wastewater containing synthetic dyes into rivers and lakes has caused significant problems. In addition to affecting the aesthetic quality of water, synthetic dyes can reduce light transmittance, photosynthesis, and water quality. Furthermore, high concentrations of synthetic dyes can harm aquatic ecosystems and human health.

Synthetic dyes can cause acute or chronic respiratory (e.g., asthma), urinary tract, and lung cancer, as well as adverse effects on red blood cells, skin allergies (e.g., eczema, urticaria), and even carcinogenic, teratogenic, and mutagenic effects.

Due to their color and toxicity even at low concentrations, synthetic dyes pose one of the biggest environmental problems today, highlighting the urgent need to remove them from wastewater[28,29].

Congo red(1-naphthalenesulfonic acid, 3,3′-(4,4′-biphenylenebis (azo)) bis (4-amino-) disodium salt) (CR) is a benzidine-based anionic diazo dye with a high water solubility and stability, making it difficult to remove from wastewater. It is produced by coupling tetrazotized benzidine with two molecules of naphthionic acid and is used in the textile, printing, dyeing, paper, and plastic industries. it containing a specific chemical group called azo binding, a double nitrogen-nitrogen bond in its molecular structure –N=N– (Figure I.1)[30]. The bright red color of the dye is due to its absorption of specific wavelengths of light. Some studies have suggested that red Congo has toxic effects leading to its decline in various applications[31], characteristics of Congo red photocatalytically destroyed[32].

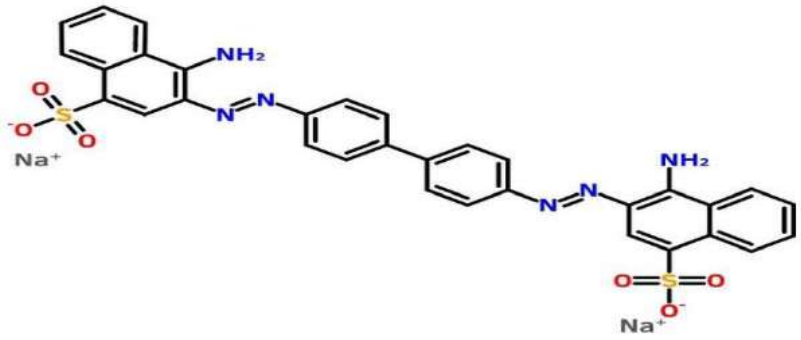

Figure I-1: Congo red structure.

Effluent containing CR can harm human health and aquatic ecosystems, as it can be metabolized to benzidine, which is human carcinogen[33].

It serves as a pH indicator, a histology stain for amyloid, a diagnostic tool for amyloidosis, and a test for free hydrochloric acid in gastric contents. It is used in the textile industries because of its great affinity for cellulose fibers. It is not only carcinogenic but also a mutagen and an effector on reproduction. It irritates the gastrointestinal tract, skin, and eyes.

It may cause breathing issues, sleeplessness, and an impact on blood components including clottin[34,35].

I.2.Organic-inorganic hybrid materials

Organic-inorganic hybrid materials, are nanocomposites formed by merging organic and inorganic components,on a scale ranging from a few angstroms to a few tens of nanometers. In which offer a groundbreaking approach to crafting novel materials boasting unique properties. Their unique two-phase structures, formed at low temperatures, lead to multifunctional materials with diverse applications. Chemistry holds the potential to manipulate the structure of these composites, enabling the disentanglement of individual contributions to the design of both phases and precise control over their interfaces[36].The interface properties or the nature of the bonds between the organic and inorganic phases have emerged as a key factor in the categorization of these materials into two separate classes:

In the class's one, weak interactions, including hydrogen bonds, van der Waals forces, or ionic bonds, govern the organic-inorganic components cohesion, resulting in a entire structure.Class two materials feature strong chemical bonds, including covalent and covalent-ionic bonds, responsible for the tight integration of the organic and inorganic phases[37].

I.2.1. Methods of synthesis materials using soft chemistry

Soft chemistry is a type of chemistry that uses mild conditions, such as low temperatures and ambient pressure, to synthesize materials. It is in contrast to traditional hard chemistry, which often uses high temperatures and pressures. it is inspired by the way that nature synthesizes materials. Soft chemistry has a number of advantages over traditional hard chemistry methods. It is more energy-efficient, less polluting, and easier to control. It is also possible to synthesize a wider range of materials using soft chemistry methods[38].There are different methods of synthesis materials using soft chemistry, among which we cite the following

I.2.1.1.Solid track

Crystallized molecules are produced via this synthesis route. It involves reacting the initial products, which are powdered carbonates and oxides, in an agate mortar in stoichiometric amounts. A uniaxial press can then be used to compact the powder into granules. Large amounts of product can be prepared simultaneously at the micrometric scale using this straightforward process [39, 40].

I.2.1.2.Mechanical activation

Mechanical activation is a process that disrupts the crystal structure of reactants, enabling synthesis with lower energy input and reduced processing temperatures. Utilizing a planetary mill facilitates the rapid and efficient grinding of both dry and suspended samples. Grinding balls are employed within the mill to achieve the desired size reduction, which primarily occurs through impact forces between the equipment and the powder [41,42].

I.2.1.3.Mechanosynthesis (high energy grinding)

High-energy mechanical grinding is a generally dry process of mixing powders of pure or alloyed elements in a high-energy mill. It is also a powerful method, capable of producing mixtures at the atomic scale.This process has been described as being a succession of repetitive fracture and rewelding phenomena responsible for the final product which is in the form of powders made up of micrometric particles with nanometric grains. The effect of reducing the grain size down to the nanometric scale and the significant proportion of defects induced within the ground powders give them original physicochemical properties[43,44].

I.2.1.4.The polymerizable complex method

The polymerizable complex approach makes use of the polyesters that are produced when metal complexes of citric acid react with ethylene glycol. In order to create metal chelates, metal cation salts are first dissolved in an aqueous solution of citric acid. After these chelates are esterified with ethylene glycol, a highly viscous polymer matrix containing uniformly dispersed metal cations is produced. The reaction mixture is pyrolyzed again to produce a precursor, which is then heat-treated at high temperatures to become the target chemical [45,46].

I.2.1.5.Hydro(solvo)thermal syntheses

The solvothermal process is used to describe a reaction in the presence of a solvent (aqueous = hydrothermal or non-aqueous = solvothermal) in stainless steel autoclave at a temperature higher than the boiling temperature (373 K-1273 K) and therefore a pressure higher than ambient pressure (1 MPa -100 MPa) [47,48].

I.2.1.1.6.Sol-gel synthesis

"Sol-gel" combines two terms: "sol," a suspension of colloidal particles in a liquid, and "gel," a semi-rigid solid in which the solvent is confined inside a solid network that may be polymeric or colloidal. This method makes use of organic precursors that generate oxide compounds during calcination. It is noteworthy because it allows for the creation of a solid by atomic-level mixing, guaranteeing the metallic elements' proper stoichiometry in the finished combination [49,50].

I.2.1.1.7.Co-precipitation

Co-precipitation involves the simultaneous precipitation of multiple metal hydroxides from a solution containing their respective metal salts and a precipitating agent like KOH or a ligand solution. The precipitated hydroxides are then filtered and dried. However, this technique faces challenges in achieving homogeneity and true mixed oxides due to varying reactivities of different metals. To control the process and ensure optimal precipitation, monitoring pH is crucial[51].

Furthermore, the co-precipitation method offers the advantage of low-temperature synthesis, leading to materials with very small grain sizes and superior crystallinity. The key principle lies in utilizing nitrates and/or chlorides as starting reagents within the synthesis protocol. Figure.I.2 shows a diagram of the co-precipitation method [52].

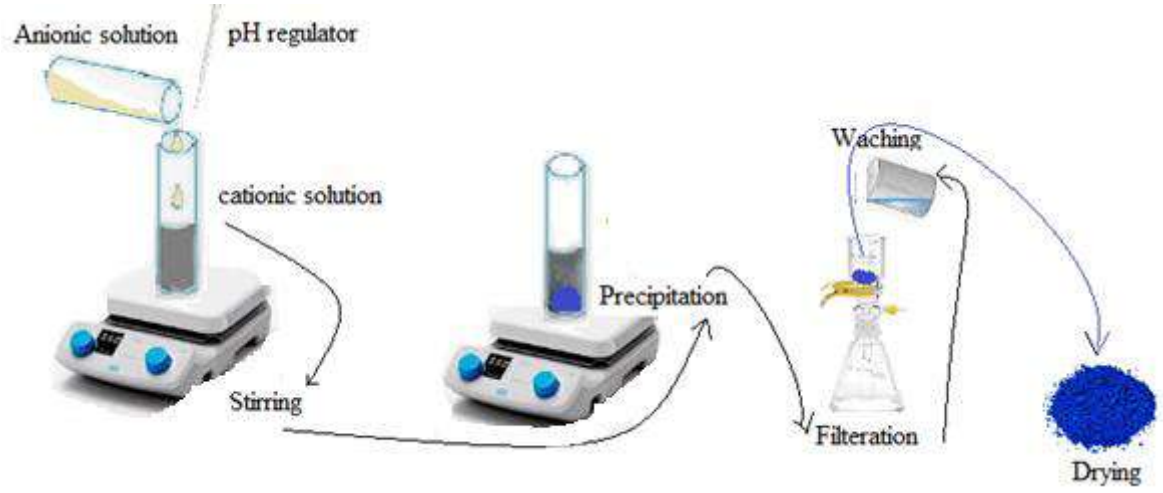

Figure.I.2: Schematic of the co-precipitation method[52].

For synthesize the compounds used in this thesis, we opted for a co-precipitation method conducted at ambient temperature. The co-precipitation approach, implemented at room temperature, allowed for the efficient production of CD which is reproduced here with

cadmium in instead of titanium reported in leturature, CMA proposal new isomorphous of [fluorenyllithium-2ethylenediamine] and FS.

I.3.Clay and Clay minerals

I.3.1.Clay

Clay is a naturally occurring, fine-grained material (<0.005mm diameter) composed mainly of clay particles based on clay and clay minerals and defined as primarily inorganic in composition. Exceptions include organic-rich materials like peat and certain soils. The weathering and erosion of rocks that contain soil, glacial clays, clay shales, and the mineral group feldspar also known as the mother of clay over very long epochs is what forms the clay particles[53].

I.3.2.Clay minerals

Clay minerals are commonly found in fine-grained sedimentary rocks such as shale, mudstone, and siltstone. Their unique property lies in their ability to act as (chemical sponges). This means they can hold onto water and dissolved plant nutrients eroded from other minerals. This exceptional ability stems from the unbalanced electrical charges present on their surface.As water plays a crucial role in the formation of clay minerals, most of them are classified as hydrous aluminosilicates or hydrous aluminum phyllosilicates. These terms highlight the key elements that make up these materials Each term carries a specific meaning. The term hydrated refers to the presence of water molecules within the clay mineral structure. Aluminum refers to the main component of the clay mineral structure, and is usually found in the octahedral layer. The term silicates refers to the presence of silicon and oxygen atoms arranged in tetrahedral units. Finally, the term phyllosilicate refers to the sheet-like structure of clay minerals, which consists of stacking tetrahedral and octahedral layers[54].

Physically the clay consists of very fine grains not exceeding 2 micrometers and is characterized by the fact that it forms a multi-layered structure consisting of frequently spaced tetrahedral and octahedral layers. In addition, it has other unique properties such as wide surface area, high mechanical strength, excellent thermal and chemical stability, high porosity and cation exchange ability, catalytic properties, and ability to control interlayer spacing [55].

I.3.3.The building blocks of clay

Clay minerals belong to the family of plate silicates and are probably the most common materials on Earth's surface.It is classified according to the thickness of its layers into simple basic units, Its structure is a stack of tetrahedral and octahedral layers that form the skeleton (lamina) of any clay mineral aggregate[56].Structurally, clay minerals can be classified into:

I.3.3.1. Tetrahedral structural unit

The silicon element predominates in it. The structural unit of this slide consists of one silicon atom(Si^{4+}) surrounded by four silica oxygen atoms, forming a four-faceted shape. Therefore, the slide is called the quaternary silica slide. The quaternary silica units are linked in horizontal chains by sharing oxygen ions, forming the quaternary silica segment.The thickness of one such layer is 0.7 nm [57].

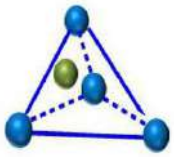

Figure.I.3: Tetrahedral unit of clay minerals.[58]

I.3.3.2. Octahedral structural unit

The strip contains aluminum or magnesium or aluminum and magnesium together, and it is called aluminum-magnesia eight strips. The building blocks are surrounded by six oxygen atoms to give an octagonal shape. The facet is called the octahedra.The thickness of one such layer is 0.9 nm[57].

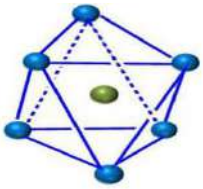

Figure.I.4: Octahedral unit of clay minerals.[58].

I.3.4. Types of clay

Clay minerals are divided based on the crystalline fraction to Amorphous: This portion represents a very small fraction of naturally occurring clay minerals. It lacks a defined crystal structure, making its composition and properties more variable. Crystalline: The majority of clay minerals fall into this category, characterized by a well-defined, repeating crystal

structure. This structure is formed by layers of tetrahedral and octahedral, giving rise to three main types:

I.3.4.1. Type 1:1 or T-O type: This type features one tetrahedral layer for every octahedral layer of equidistance, resembling a simple "sandwich" structure (distance between two layers close to 7Å). Examples include kaolinite and dickite [59].

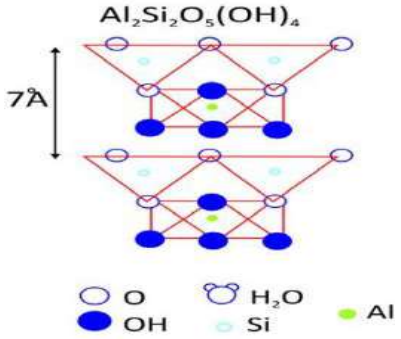

Figure.I.5: The structure of kaolinite [60].

I.3.4.2. Type 2:1 or T-O-T: As the name suggests, these clay minerals have two tetrahedral layers flanking a single octahedral layer. This configuration creates a "sandwich-with-filling" structure (with variable equidistance between 9.4 and 7Å), Examples include illite and smectite[61].

The properties of clay minerals are intimately linked to the intricate structures they possess, their ability to exchange cations and anions, and their powerful adsorption capabilities.

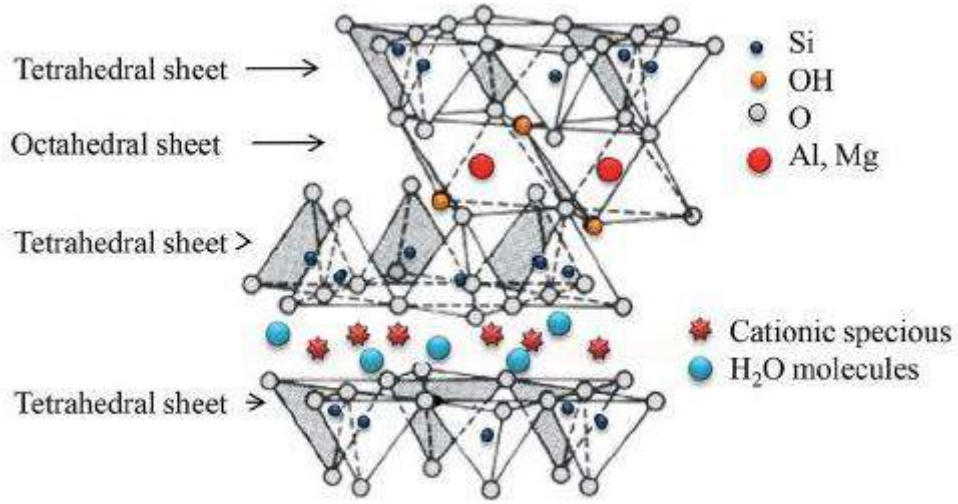

Figure.I.6: The structure of smectite[62].

I.3.4.3.Type 2:1:1 or T-O-T-O: This intricate structure consists of two tetrahedral layers sandwiching two octahedral layers, separated by a central octahedral layer. (The characteristic equidistance is then about 14Å).This "double-decker" arrangement is characteristic of chlorite[61].

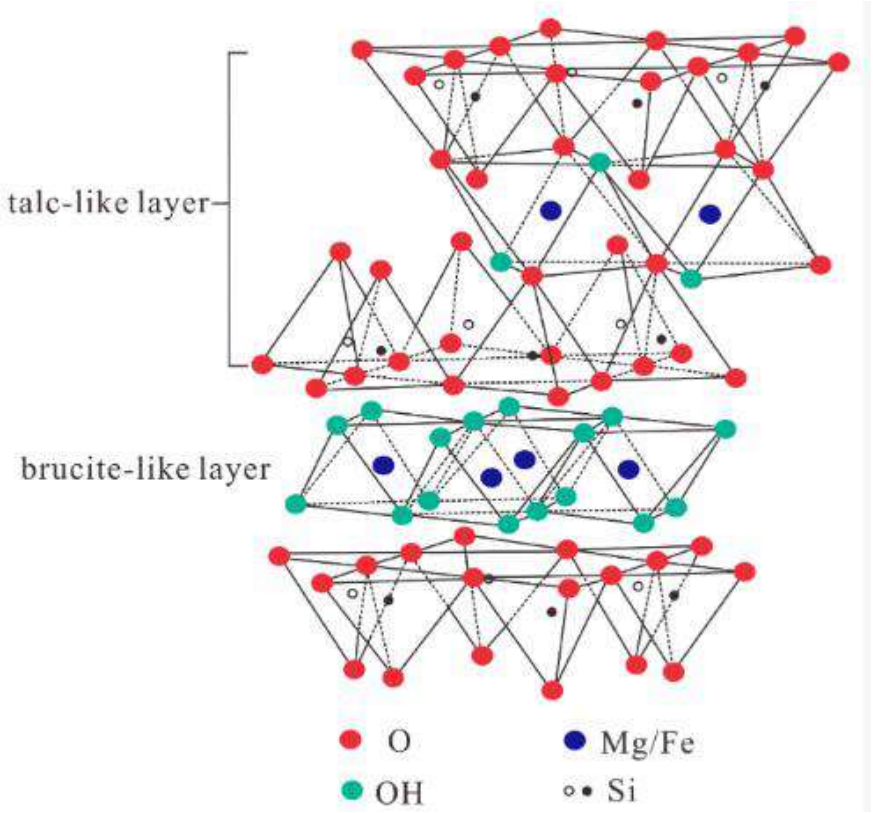

Figure. I.7: The structure of chlorite[63].

I.3.5.Physical and chemical properties of clay minerals

I.3.5.1. Cation–exchange capacity

Clay minerals possess a remarkable property known as cation exchange capacity (CEC). This refers to their ability to attract and retain certain positively charged ions (cations) on their surfaces. This ability arises from positive or negative charge deficiencies within their mineral structure [64].

These attracted cations are held onto the surface of the clay mineral, but they are not permanently fixed. Instead, they can be exchanged with other cations present in the surrounding soil water. This exchange process is what makes CEC distinct from simple sorption, where ions are simply adsorbed and not readily exchanged.The CEC value quantifies this exchange capacity, measuring the number of cations a clay mineral can hold onto per unit weight (usually expressed in milliequivalents per 100 grams of dry clay) [65,66].

I.3.5.2.Swelling capacity

The driving force behind the expansion lies of Clay minerals in the hydration energy forces associated with the clay particles. These forces arise from the interaction of water molecules with the charged surfaces of the clay mineral. As water enters the spaces between the layers, the electrostatic attraction between the water molecules and the charged surfaces draws the layers further apart, leading to the characteristic swelling. However, the extent of swelling in clay minerals is not constant. It depends on several factors: Layer charge density, Type of interlayer ions, Concentration of surrounding ions and Water content[67].

I.3.5.3.Surface charge properties

Through changes in surface charge density and electrical charge quantity, clay mineral surface charge influences a range of chemical characteristics. The creation of clay mineral organo compounds, ion movement, swelling, and shrinking are all influenced by the surface charge characteristics. Clay minerals can be categorized into two groups based on the nature of their surface charge:

Permanent Negative Charge:This type of charge arises from isomorphous substitution within the crystal structure of the clay mineral. This substitution involves the replacement of certain atoms within the mineral's building blocks (tetrahedral and octahedral layers) with atoms of similar size but different charge. This creates a permanent imbalance, resulting in a net negative charge on the surface of the clay mineral. This type of charge is also known as structural charge and is independent of the surrounding pH. It remains constant across a wide range of pH values, allowing clay minerals to attract and hold onto positively charged ions (cations) like potassium, calcium, and magnesium. Variable Charge:This type of charge arises from the protonation of Si-OH groups located at the edges of the clay mineral's surface. These Si-OH groups can gain or lose protons depending on the surrounding pH. [68,69].

I.3.5.4.Adsorptive properties

Clay minerals possess a remarkable ability to attract and hold onto various substances, these abilities are influenced by a number of variables. Clay minerals' wide surface area, limited permeability, high cation exchange capacities, and high retention abilities are the reasons for their high adsorption capacities for metal ions, organic materials, and other compounds. The structure and chemical makeup of clay minerals are among the numerous elements that influence their adsorption capacity. The clay minerals contain a variety of active sites where adsorption occurs.The hydroxyl group on the surface facilitates the Vander wall

interaction of hydrogen bonding, which causes physical adsorption between the active sites on the surface and the structural components. Second, chemisorption also occurs as a result of a chemical link that is created when molecules and surfaces contact more strongly[70,71].

I.3.5.5.Specific surface area (SSA)

Specific surface area (SSA) refers to the total surface area of soil particles per unit mass (usually expressed in m2/g) or volume (m2/m3). This seemingly simple concept holds immense significance in understanding the behavior of clay minerals, particularly their high reactivity. Compared to other soil constituents, clay minerals have a significantly larger surface area due to their small particle size and intricate layered structure. This vast surface area provides numerous "binding sites" for interacting with other molecules, leading to enhanced reactivity. However, the reactivity varies depending on the specific type of clay mineral and also Two primary factors govern the SSA of clay minerals: Particle size and shape and Internal surface area [72].

I.3.5.6.Plasticity

The sheet-like structure of clay minerals, with their ability to slide past each other when lubricated by water, gives them the remarkable property of plasticity. Adding water to clay minerals increases their plasticity until a maximum is reached, which depends on the specific type of clay. Plasticity is also known as extrudability, ductility, consistency, or workability. [73].

I.3.5.7.Dispersion/flocculation

Dispersion occurs when the forces repelling the clay particles are stronger than the forces attracting them. This leads to the separation of the particles and their suspension within the liquid medium. And Flocculation is the opposite of dispersion. When the attractive forces between the clay particles overcome the repulsive forces, the particles come together and form larger clusters known as "flocs" or "aggregates".Several factors influence the behavior of clay particles in suspension: Surface charge, Exchangeable cations, Ionic strength and pH[74].

I.3.6.Modifying (activating) clay

Clay modification refers to those chemical and physical treatments used to enhance the surface area, pore size, and number of active sites on the surface. Through this treatment or

modification, clay minerals become hydrophobic and organic, thus enhancing the absorption of small, non-ionic organic compounds [75]. As there are different methods for modifying clay minerals, we mention chemical activation with acids and salts [76], physical activation (Thermal activation) [77], treatment with organic cations [78]. Addition of polymer [79]. Biomodification [80], mechanical and chemical treatment [81], adsorption of organic polar molecules [82], ion exchange with inorganic and organic cations [83],modification with cationic surfactants and anionic surfactants[84,85], and many other methods.

I.3.6.1. Methods for modifying clay minerals:

a.Thermal activation

Thermal activation of mineral clay is a natural treatment that involves baking the clay at high temperatures in order to remove any impurities or moisture associated with the clay silt. Thermal activation changes the adsorption capacity by releasing active zones occupied by adsorption water. The change in the chemical composition of the clay upon heating is related to the type of clay and largely depends on the particle size and heating system [86,87].

b. Chemical activation:

Chemical activation of clay is the treatment of clay with inorganic acids at high temperatures. It is a two-step procedure in which molecules are divided into octahedral sheets. In the first step, exchangeable cations are replaced by protons (H^+). The second step involves leaching octahedral cations such as Mg^{+2} Al^{+3} and Fe^{+3} from the octahedral and tetrahedral sheets[88] . the clay is often activated by treating it with hydrochloric acid (HCI) or sulfuric acid (H_2SO_4) [89]. Activation of clay leads to a change in physical properties, such as improving the surface area and average pore size [90]. It is also possible to change chemical properties, such as the cation exchange characteristic and the acidity of the clay surface, thus providing the required properties for the effective meter [91]. Acid activation is a favorable method to increase the surface area as the decomposition of the crystal structure can be controlled [92].

I.4. Methods for removing Pollutants from water

I.4.1.Photocatalysis

Photocatalysis is a green chemical pathway and is a branch of chemistry which studies chemical reactions that occur when light and a photocatalyst are present. A semiconductor known as a photocatalyst increases the rate of reaction just by being there. Numerous uses for

photocatalysis exist, including water purification[93], self-cleaning[94], antimicrobial [95], deodorizing[96], air purifying[97], and antifogging[98].

I.4.2.Photocatalysts

Photocatalysts are materials that act as catalysts, accelerating chemical reactions when exposed to light. Their name reflects their dual nature, combining the Greek words 'photo' (light) and 'catalyst' (agent of change) [99].

a. Fenton process

The Fenton reaction, discovered in 1894 by H.J.H. Fenton, is a chemical process that involves the reaction of peroxides, typically hydrogen peroxide (H_2O_2), with iron ions to generate highly reactive oxygen species that break down organic or inorganic compounds. Iron, present in small amounts, serves as a catalyst, while H_2O_2 is gradually consumed to produce hydroxyl radicals, the primary oxidizing agents. The Fenton reaction has found widespread application in wastewater treatment, effectively removing a variety of hazardous organic compounds from wastewater streams [99].

The Fenton process can be conducted at room temperature and atmospheric pressure, making it a convenient and energy-efficient method. Additionally, the required reagents are readily available, easy to store and handle, and non-toxic, posing minimal environmental concerns. However, two key limitations have been identified with the Fenton process:

- The consumption of H_2O_2 can be inefficient due to the scavenging of radicals by the peroxide itself and its natural tendency to decompose over time.
- Iron ions are continuously consumed, leading to the formation of solid sludge [100].

b. Photo- Fenton process

It is a combination of hydrogen peroxide (H_2O_2) and UV radiation with Fe_2^+ or Fe_3^+ oxalate ion. Or in other words it is a combination of the Fenton reaction with conventional radiation zone of the visible and near ultraviolet. Reduces more hydroxyl radicals compared to conventional Fenton method or photolysis and in turn increases the rate of degradation of organic pollutants. The foundation of photo-Fenton lies in its ability to significantly augment hydroxyl radical (•OH) production, the primary catalysts responsible for organic pollutant breakdown. UV radiation plays a pivotal role in this process, triggering the photochemical reduction of Fe^{3+} ions back to Fe^{2+} ions, effectively renewing the catalyst pool and ensuring a

continuous supply of •OH generators. This self-sustaining cycle sustains the degradation process at an accelerated pace, surpassing the capabilities of traditional Fenton[99].

I.4.3.Adsorption

Adsorption is the process by which molecules (adsorbates) adhere to the surface of a solid or liquid (adsorbent). This phenomenon occurs due to the interaction between the adsorbate molecules and the surface forces of the adsorbent (interactive physical attractive forces). Adsorption is confined to the surface. Unlike absorption, which involves the uptake of molecules into the bulk of a material [101].Adsorption is one of the most popular methods and is currently considered an effective, efficient and economical method of water purification. Sorbents used include activated carbon [102,103], clay minerals[104,105], zeolites[106], metal oxides[107,108], agricultural waste[109], biomass[110] and polymeric materials[111].

In the following, we will review studies investigating the removal of Congo red and nitrates from water, employing synthetic materials and clay, and utilizing the previously discussed removal methods.

Porous hybrid organic-inorganic materials showed high effectiveness in degradation of Congo red dye from contaminated water. For example, the use of a two dimensionel dimeric hybrid compound synthetised by J-G Zhang, with general formula {[$Cd_2(H_2O)_2(tpeb)_2(1,2\text{-}CHDC)_2$]•$H_2O$}n, where (tpeb : 1,3,5-tri-4-pyridyl-1,2-ethenylbenzene) and $(1,2\text{-}CHDC)_2$: 1,2-cyclohexanedicarboxylic acid) represents a promising approach to the traitment of water contaminated with Congo red after being exposed to visible light irradiation and can be reused for either utilization [112].

Xue Dong et al in 2020 .were able to integrate acetamide, thioacetamide, or urea into UiO-67 (figure.I.8) during Zr-MOF synthesis, the number of adsorption sites and surface area were amplified, leading to a substantial enhancement in Congo red absorption. (2360 $mg.g^{-1}$ of NU-UiO67, 1986.3 $mg.g^{-1}$ of NT-UiO-67 and 1493 $mg.g^{-1}$ of NA-UiO-67)[113].

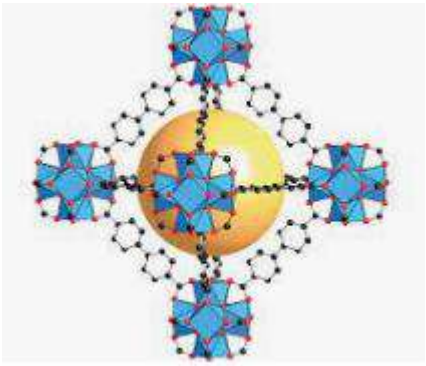

Figure.I.8:Analog Structure of UIO-67. [113]

In a groundbreaking study, Li and colleagues in 2019 successfully synthesized a novel metal-organic framework (MOF) designated as ZTB-1 and explored its potential applications in magnetic materials. Their efforts resulted in the development of a highly water-stable MOF-based magnetic material, Fe_3O_4@ZTB-1, which demonstrated exceptional adsorptive capabilities for the rapid removal of Congo red (CR) from aqueous solutions. With an adsorption capacity of 458 mg of CR per gram, Fe_3O_4@ZTB-1 exhibits remarkable promise as an adsorbent in wastewater treatment applications. The strong binding of CR to Fe_3O_4@ZTB-1 is attributed to electrostatic interactions and hydrogen bonding [114].

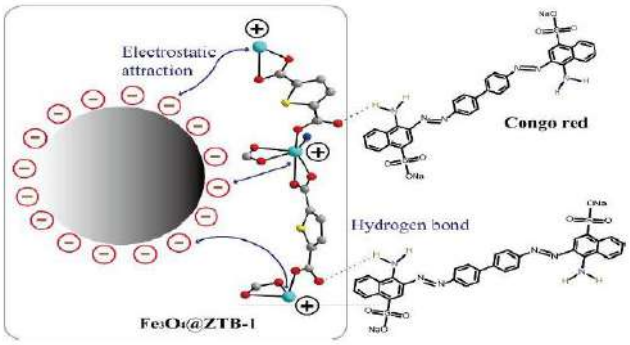

Figure.I.9: scheme of adsorbintion of congo red using Fe_3O_4@ZTB-1[114].

In the same context, C.Sobhan and all in 2020 used a new material Fe_3O_4@BTCA (BTCA= 1,2,3,4-Butanetetracarboxylic *acid)* to investigate Congo red adsorption. The result shows that this compound rapidly and selectively adsorbs Congo red dyes with very high adsorption capacity (630 $mg.g^{-1}$) the adsorption is assured by stronger H-bounding through three carboxylate anion into NH_2groupment of Congo red as showed (figure.I.11) [115].

Figure.I.10: Schematic of the preparation of surface-modified Fe_3O_4@BTCA. [115]

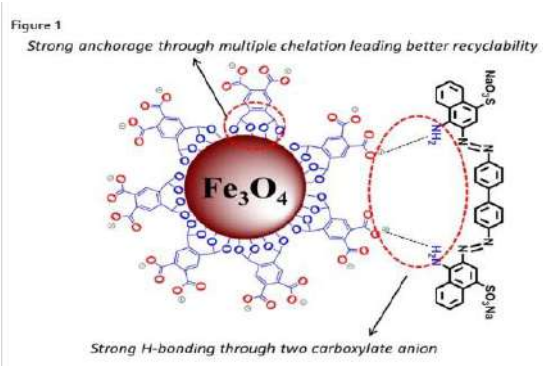

Figure.I.11: Schematic diagram of the adsorption of Congo red dye by Fe_3O_4BTCA through H-bonding carboxyl anions. [115]

Liu et al developed a manganese-based metal-organic framework (MOF) ($[Mn_3$(**L1**)2(**L2**)$_2(H_2O)_8]\cdot 4H_2O)n$ (H_3**L1** = 6-sulfonaphthalene-1,4-dicarboxylic acid, **L2** = 1,3,5-tris(1*H*-imidazol-1-yl)benzene)) . that effectively removes Congo Red (CR) from water through a host-guest interaction mechanism. The compound exhibited exceptional selectivity towards CR, in two minutes. Moreover, the MOF demonstrated an impressive maximum adsorption capacity of 1393 mg/g and could be conveniently recovered for reuse [116].

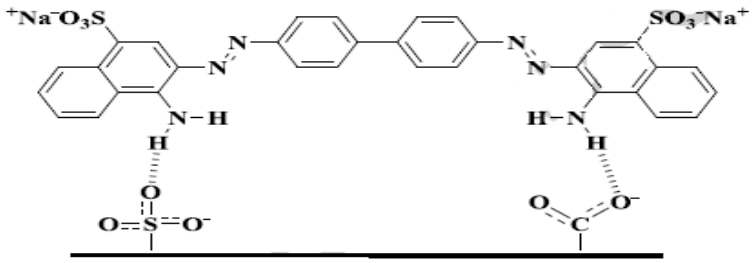

Figure.I.12: Possible mechanism of CR adsorption by ([Mn_3(**L1**)2(**L2**)2(H_2O)8]·4H_2O)n [116].

Fu-hua Wei and colleagues successfully synthesized a compound, H3BTC, $Co(OAc)_2.4H_2O$, derived from trimesic acid and cobalt(II) acetate tetrahydrate. This compound exhibited remarkable adsorption capabilities, effectively removing Congo red from water. After 300 minutes, the adsorption rate reached an impressive 85.54% [117] .

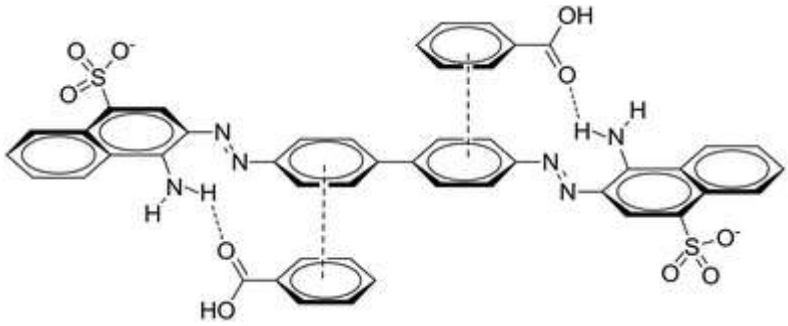

Figure.I.13:removal of Congo red by H3BTC. [117]

In 2018, Qingfeng Yang and collaborators successfully employed UiO-67,Which was previously prepared by (Zhu et al., 2015)[118] and was slightly modified, a bifunctional adsorbent, to remove illegal food dyes. Notably, the maximum adsorption capacity for Congo red was an impressive 1236.9 mg/g. The Zr-OH groups in UiO-67 played a crucial role in facilitating the binding of target molecules. Moreover, UiO-67 exhibited exceptional reusability, maintaining its adsorption capacity after seven cycles without significant loss [119].

In a separate study(2019), Ming Yang, B, and Qianhui Bai successfully synthesized Ni-Zn MOF pellets. The synergistic presence of nickel and zinc significantly altered the shape and microstructure of the pellets, leading to enhanced adsorption performance. The Ni-Zn MOF exhibited an exceptional adsorption capacity for Congo red (CR) dye, reaching an impressive 460.90 mg/g, far surpassing the capabilities of Ni MOF (276.70 mg/g) and Zn MOF (132.20 mg/g) [120].

A study by KholiswaYokwana et al in 2018 .demonstrated the effectiveness of NGOs derived from graphite powder in removing CR dye from aqueous solutions. These NGOs proved to be excellent adsorbents, achieving a remarkable removal rate of approximately 99.9%. The adsorption mechanism was primarily driven by electrostatic interactions, complemented by hydrogen bonding and/or van der Waals interactions depending on the specific NGO employed. This study highlights the promising potential of NGOs as eco-friendly and efficient adsorbents for wastewater treatment applications [121].

WondalemMisganawGolieand SreedeviUpadhyayula in 2017 investigated the effectiveness of three chitosan-based organic-inorganic hybrid biocomposites, namely chitosan/bentonite (ChBT), chitosan/titanium oxide (ChTi), and chitosan/alumina (ChAl), in removing nitrate from water. The results demonstrated that these biocomposites were efficient, low-cost, and reusable for nitrate removal, offering a promising approach to water purification [122].

Researchers led by Guoshuai Liu successfully synthesized a highly efficient photocatalyst, lithium niobate ($LiNbO_3$), using a hydrothermal method. This novel photocatalyst demonstrated remarkable effectiveness in removing nitrates from water under neutral pH conditions. $LiNbO_3$ achieved an impressive 98.4% overall nitrate removal and 95.8% N_2 selectivity [123].

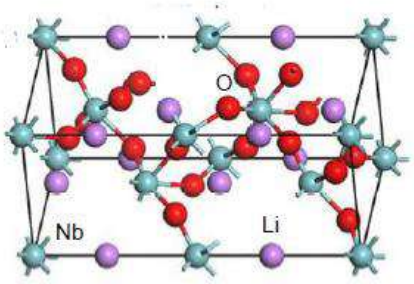

Figure.I.14: $LiNbO_3$trigonal structure [123].

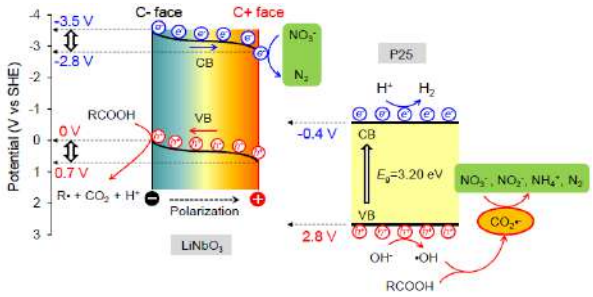

Figure.I.15:A scheme showing the method of removing nitrates from water using a photocatalyst$LiNbO_3$ [123].

ManikandanVelu and al (2021) employed a sol-gel method to synthesize aluminum oxide nanoparticles (Al_2O_3NPs)/Moringaoleifera gum activated carbon (MOGAC)-based nanocomposites. The synthesized nanocomposites exhibited promising photocatalytic activity towards nitrate removal under different LED light spectra. Under red LED light irradiation and a 10 mg/L nanocomposite dosage, nitrate ions were effectively removed by up to 94%

after 105 and 75 minutes. Notably, the Al_2O_3/MOGAC nanocomposites maintained remarkable stability after four cycles of nitrate reduction, demonstrating their potential for long-term use in wastewater treatment applications [124].

Figure.I.16:synthesis stages of aluminum oxide nanoparticles (Al_2O_3NPs)/Moringaoleifera gum activated carbon (MOGAC)-based nanocomposites

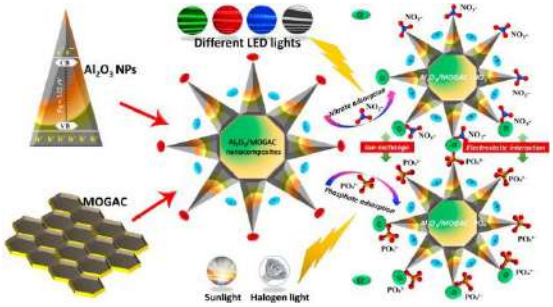

Figure.I.17:suggestion of mechanisms to removal of nitrate ion by Al_2O_3/MOGAC nanocomposites [124].

In a study by Ne¸seÖztürk and T. Enn˙ ilBekta¸s, the adsorption capacity of sepiolite and hydrochloric acid-activated sepiolite for nitrate removal was evaluated. Experimental results revealed that hydrochloric acid-activated sepiolite exhibited superior nitrate removal efficiency compared to unmodified sepiolite. The adsorption process demonstrated rapid kinetics, particularly during the initial stages of treatment. Considering the natural abundance of sepiolite, the hydrochloric acid activation method appears economically feasible for nitrate remediation applications [125].

Marcela N. Gatti and colleagues modified montmorillonite clay using silylation with γ-aminopropyltrimethoxysilane, resulting in an effective adsorbent for nitrate removal. The highest adsorption capacity was achieved for Mn-S clay at pH 3, reaching 0.80 mmol NO_3^-/g clay. For Mn-S-Ag clay, the maximum adsorption capacity was 0.77 mmol NO_3^-/g clay at pH 3. These findings demonstrate the potential of silylated montmorillonite, with or without prior silver treatment, as a promising sorbent for nitrate remediation under acidic conditions [126].

A modified form of calcium montmorillonite, treated with hydrochloric acid by C.J. Mena-Duran et al., exhibited promising nitrate removal capabilities, achieving up to 22.28% nitrate elimination from aqueous solutions [127].

In 2010, Yunfei Xi and colleagues significantly enhanced the nitrate removal potential of bentonite clay by treating it with HDTMA surfactant . This modification yielded an impressive 14.76 mg of nitrate ions removed per gram of organic clay, offering valuable insights into the mechanism of anion pollutant absorption from wastewater [128].

Cláudia G. Silva et al used monometallic (Pd) and bimetallic (Pd-Cu) catalysts loaded on hybrid materials of multi-walled carbon nanotubes and TiO_2 in the catalytic and photocatalytic reduction of nitrate in aqueous suspensions. They showed high catalytic activity in the dark and under near ultraviolet to visible light irradiation, in the presence of H_2 and CO_2. The efficiency of hybrid materials depends on the CNT load, and the best performing materials are those composed of 20 wt% CNTs. Very low nitrate conversion (4%) was achieved using the Pd-TiO_2 monometallic catalyst, where the presence of copper is essential for the reaction to occur. Moreover, as expected, it can be observed that the support has a decisive influence on the performance of the bimetallic catalysts [129].

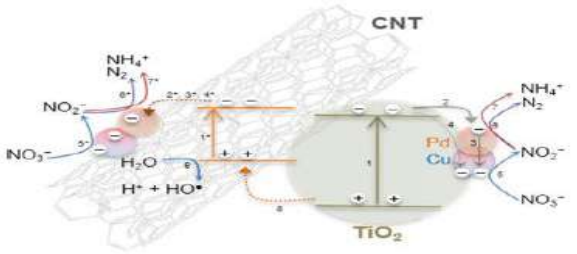

Figure.I.18: Schematic of the correlation of nitrate over Pd-Cu/CNT-TiO_2 catalysts in the presence of H_2 and CO_2[129].

SafaeBentahar and her colleagues delved into the adsorption behavior of Congo red, onto natural clay sourced from the Agadir region in southern Morocco. Their findings revealed that the adsorption of Congo red onto natural clay is significantly influenced by pH, initial dye concentration, and temperature. The maximum adsorption capacity of Congo red onto the clay was determined to be 74.62 $mg \cdot g^{-1}$. An assessment of thermodynamic parameters indicated that the adsorption of Congo red onto natural clay is a physical process, spontaneous in nature, and exhibits an endothermic character [130].

Vimonses et al. (2009) investigated the suitability of three Australian clay minerals – sodium bentonite, kaolin, and zeolite – for removing Congo red dye from aqueous solutions. Their findings revealed that sodium bentonite exhibited superior adsorption capacity, reaching 19.9 mg/g of Congo red removed. Kaolin and zeolite followed with 5.6 mg/g and 4.3 mg/g, respectively. Furthermore, sodium bentonite and kaolin displayed minimal sensitivity to pH changes and remarkable thermodynamic stability. These properties suggest that these Australian clay minerals hold significant potential as alternative adsorbents for the effective removal of recalcitrant dyes from industrial wastewater streams [131].

Original montmorillonite Mt generally shows weak adsorption capacity toward anionic dyes, because its surface is negatively charged, which causes electrostatic repulsion between Mt and anionic dyes [113]. So Lifang Zhu and others modified the montmorillonite (Mt) (from Inner-Mongolia, China) with both hexadecyltrimethylammonium (HDTMA) and chitosan (CTS), with the purpose of synthesizing multifunctional adsorbents that can efficiently adsorb hydrophobic organic contaminants, heavy metal cations, and dyes from water. This resulted in hybrid montmorillonite (C/T-Mt) with positively charged surfaces contributed to, together with the hydrophobic interactions between C/T-Mt and contaminants, contributed to the effective uptake of CR on C/T-Mt [132].

According to studies, organic contaminants from industrial effluent were adsorbed onto banntonite clay [133].

According to Lund and Nessen (1986), the best value for impurity removal is a pH of less than 8. They also found that adding banntonite clay to raw water eliminates most of the contaminants within the temperature range of (20–37) degrees Celsius [134].

Regarding (Gersberg and others) observed that the COD value of the treated water was less than 20 mg/L after treating urban wastewater with banntonite clay used as an adsorbent [135] .

According to (Francisco and al.) vegetable oils like soybean, cottonseed, and sunflower could be effectively removed from smectite clay from certain Brazilian states by acid activation with HCl or H_2SO_4[89].

Susan Sadeghi and colleagues developed novel, eco-friendly, and cost-effective adsorbents for removing acidic dyes from water. These adsorbents were prepared by grafting poly(methyl methacrylate) (P(MMA)) onto a natural gum (tragacanth gum, TG) and further combining it with bentonite (from the city of Birjand in South Khorasan, Iran) (TG-g-P(MMA)/B). The researchers evaluated the efficiency of these materials in removing various acidic dyes, including Congo red (CR). Notably, the experimental removal efficiency for CR exceeded 200 mg/g [137].

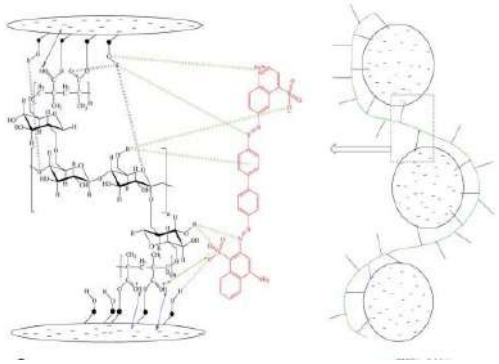

Figure.I.19: Link method between a compound TG-g-P(MMA)/B and Congo red [137].

To improve the adsorption capacity of bentonite clay for anionic dyes like Congo red, ManjotToor and Bo Jin implemented three modification methods: thermal activation (TA), acid activation (AA), and a combined approach of acid and thermal activation (ATA). Their investigation revealed that the ATA-modified bentonite exhibited the highest adsorption capacity, effectively removing over 95% of the Congo red [138].

VipasiriVimonses and colleagues conducted a comprehensive investigation to evaluate the kinetics and potential removal mechanisms of clay mixtures containing natural clay and lime for the anionic dye Congo red (CR). Their study involved testing the removal effectiveness of these mixtures, which demonstrated significantly improved dye removal capacity and efficiency. Furthermore, these mixtures displayed promising potential for application in wastewater treatment. The mixture composed of 70% $Ca(OH)_2$, 15% sodium bentonite, 10% kaolin, and 5% zeolite exhibited the fastest color removal, achieving an impressive 94% color removal efficiency [139].

Lili Lian et al. (2009) investigated the capacity of Ca-bentonite to remove Congo Red dye from aqueous solutions. Their findings revealed that a mere 0.2 grams of Ca-bentonite can effectively remove over 90.0% of the dye from a solution containing 100 mg/L of Congo Red. This remarkable removal efficiency was observed across a temperature range of 20-50°C, demonstrating the effectiveness of Ca-bentonite in a range of environmental conditions [91].

Reference bibliographique

[1] Mehndiratta, P.; Jain, A.; Srivastava, S.; Gupta, N. Environmental Pollution and Nanotechnology. *Environ. Pollut.***2013**, *2* (2), p49. https://doi.org/10.5539/ep.v2n2p49.

[2] Khasanova, S.; Alieva, E.; Shemilkhanova, A. Environmental Pollution: Types, Causes and Consequences. *BIO Web Conf.***2023**, *63*, 07014. https://doi.org/10.1051/bioconf/20236307014.

[3] Briggs, D. Environmental Pollution and the Global Burden of Disease. *Br. Med. Bull.***2003**, *68*, 1–24. https://doi.org/10.1093/bmb/ldg019.

[4] Alrumman, S.; El-kott, A.; Keshk, S. Water Pollution: Source and Treatment. *Am. J. Environ. Eng.***2016**, *6*, 88–89. https://doi.org/10.5923/j.ajee.20160603.02.

[5] *L'Eau pour les hommes, l'eau pour la vie: rapport mondial sur la mise en valeur des ressources en eau, résumé - UNESCO Bibliothèque Numérique*. https://unesdoc.unesco.org/ark:/48223/pf0000129556_fre (accessed 2023-12-18).

[6] Baig, J. A.; Kazi, T. G.; Arain, M. B.; Afridi, H. I.; Kandhro, G. A.; Sarfraz, R. A.; Jamal, M. K.; Shah, A. Q. Evaluation of Arsenic and Other Physico-Chemical Parameters of Surface and Ground Water of Jamshoro, Pakistan. *J. Hazard. Mater.***2009**, *166* (2), 662–669. https://doi.org/10.1016/j.jhazmat.2008.11.069.

[7] Wang, X. L.; Han, J.; Xu, L. G.; Zhang, Q. Spatial and Seasonal Variations of the Contamination within Water Body of the Grand Canal, China. *Environ. Pollut.***2010**, *158* (5), 1513–1520. https://doi.org/10.1016/j.envpol.2009.12.018.

[8] Mian, I. A.; Begum, S.; Riaz, M.; Ridealgh, M.; Mcclean, C.; Cresser, M. Spatial and Temporal Trends in Nitrate Concentrations in the River Derwent, North Yorkshire, and Its Need for NVZ Status. *Sci. Total Environ.***2009**, *408*, 702–712. https://doi.org/10.1016/j.scitotenv.2009.11.020.

[9] Khan, Dr. N.; Hussain, S.; Saboor, A.; Jamila, Dr. N.; Kim, K. Physicochemical Investigation of the Drinking Water Sources from Mardan, Khyber Pakhtunkhwa, Pakistan. *Int. J. Phys. Sci.***2013**, *8*, 1661–1671.

[10] Herrmann, W. A. New Materials – The Potential of Modern Synthetic Chemistry. *Chem. Eng. Technol.***1998**, *21* (7), 549–558. https://doi.org/10.1002/(SICI)1521-4125(199807)21:7<549::AID-CEAT549>3.0.CO;2-Q.

[11] Pawari, M. J.; Gawande, S. Ground Water Pollution & Its Consequences. **2015**, *3* (4).

[12] Organization, W. H.; Fund, U. N. C. Global Water Supply and Sanitation Assessment 2000 Report. *Glob. Water Supply Sanit. Assess. 2000 Rep.***2000**.

[13] Lin, L.; Yang, H.; Xu, X. Effects of Water Pollution on Human Health and Disease Heterogeneity: A Review. *Front. Environ. Sci.***2022**, *10*.

[14] Chowdhary, P.; Bharagava, R.; Mishra, S.; Khan, N. Role of Industries in Water Scarcity and Its Adverse Effects on Environment and Human Health; 2020; pp 235–256. https://doi.org/10.1007/978-981-13-5889-0_12.

[15] Parris, K. Impact of Agriculture on Water Pollution in OECD Countries: Recent Trends and Future Prospects. *Int. J. Water Resour. Dev.***2011**, *27* (1), 33–52. https://doi.org/10.1080/07900627.2010.531898.

[16] Lu, Y.; Song, S.; Wang, R.; Liu, Z.; Meng, J.; Sweetman, A. J.; Jenkins, A.; Ferrier, R. C.; Li, H.; Luo, W.; Wang, T. Impacts of Soil and Water Pollution on Food Safety and Health Risks in China. *Environ. Int.***2015**, *77*, 5–15. https://doi.org/10.1016/j.envint.2014.12.010.

[17] Xiao, J.; Wang, L.; Deng, L.; Jin, Z. Characteristics, Sources, Water Quality and Health Risk Assessment of Trace Elements in River Water and Well Water in the Chinese Loess Plateau. *Sci. Total Environ.***2019**, *650*, 2004–2012. https://doi.org/10.1016/j.scitotenv.2018.09.322.

[18] Baig, J. A.; Kazi, T. G.; Arain, M. B.; Afridi, H. I.; Kandhro, G. A.; Sarfraz, R. A.; Jamal, M. K.; Shah, A. Q. Evaluation of Arsenic and Other Physico-Chemical Parameters of Surface and Ground Water of Jamshoro, Pakistan. *J. Hazard. Mater.***2009**, *166* (2–3), 662–669. https://doi.org/10.1016/j.jhazmat.2008.11.069.

[19] *C Wu,; C Maurer,; Y Wang,; S Xue,;D L Davis. Water pollution and human health in China. | Environmental Health Perspectives. 1999, Vol. 107, No. 4*. https://ehp.niehs.nih.gov/doi/abs/10.1289/ehp.99107251 (accessed 2023-12-18).

[20] Zhang, X.; Zhang, Y.; Shi, P.; Bi, Z.; Shan, Z.; Ren, L. The Deep Challenge of Nitrate Pollution in River Water of China. *Sci. Total Environ.***2021**, *770*, 144674. https://doi.org/10.1016/j.scitotenv.2020.144674.

[21] Carey, R. O.; Migliaccio, K. W.; Brown, M. T. Nutrient Discharges to Biscayne Bay, Florida: Trends, Loads, and a Pollutant Index. *Sci. Total Environ.***2011**, *409* (3), 530–539. https://doi.org/10.1016/j.scitotenv.2010.10.029.

[22] Hoagland, B.; Schmidt, C.; Russo, T. A.; Adams, R.; Kaye, J. Controls on Nitrogen Transformation Rates on Restored Floodplains along the Cosumnes River, California. *Sci. Total Environ.***2019**, *649*, 979–994. https://doi.org/10.1016/j.scitotenv.2018.08.379.

[23] *Kharroubi M,; Bouselsal B,; Ouarekh M,; Benaabidate L,; Khadri R. Water quality assessment and hydrogeochemical characterization of the Ouargla complex terminal aquifer (Algerian Sahara).Arabian Journal of Geosciences, 2022, № 3* https://ouci.dntb.gov.ua/en/works/9jJvOAj9/ (accessed 2023-12-18).

[24] Kharroubi, M.; Bouselsal, B.; Ouarekh, M.; Benaabidate, L.; Khadri, R. Water Quality Assessment and Hydrogeochemical Characterization of the Ouargla Complex Terminal Aquifer (Algerian Sahara). *Arab. J. Geosci.***2022**, *15* (3), 251. https://doi.org/10.1007/s12517-022-09438-z.

[25] Eren, Z.; Acar, F. N. Adsorption of Reactive Black 5 from an Aqueous Solution: Equilibrium and Kinetic Studies. *Desalination***2006**, *194* (1), 1–10. https://doi.org/10.1016/j.desal.2005.10.022.

[26] Zaharia, C.; Suteu, D. Textile Organic Dyes Characteristics, Polluting Effects and Separation/Elimination Procedures from Industrial Effluents A Critical Overview. In *Organic Pollutants Ten Years after the Stockholm Convention - Environmental and Analytical Update*; 2012. https://doi.org/10.5772/32373.

[27] Zafar, M. S.; Ahmad, S. W.; Zia-Ul-Haq, M.; Mubeen, A.; Khan, W. A. Removal of Residual Carcinogenic Dyes from Industrial Wastewater Using Flocculation Technique. *Chem. Ind. Chem. Eng. Q.***2018**, *24* (1), 69–76. https://doi.org/10.2298/CICEQ160429024Z.

[28] Banat, I. M.; Nigam, P.; Singh, D.; Marchant, R. Microbial Decolorization of Textile-Dyecontaining Effluents: A Review. *Bioresour. Technol.***1996**, *58* (3), 217–227. https://doi.org/10.1016/S0960-8524(96)00113-7.

[29] *Material Safety Data Sheet Congo Red .according to Regulation (EC) No. 1907/2006 (REACH)*

[30] Zenasni, M. A.; Meroufel, B.; Merlin, A.; George, B. Adsorption of Congo Red from Aqueous Solution Using CTAB-Kaolin from Bechar Algeria. *J. Surf. Eng. Mater. Adv. Technol.***2014**, *4* (6), 332–341. https://doi.org/10.4236/jsemat.2014.46037.

[31] *Optimization of Parameters for Adsorption of Methylene Blue on a Low-Cost Activated Carbon | Journal of Chemical & Engineering Data*. https://pubs.acs.org/doi/10.1021/je900408s (accessed 2023-12-18).

[32] Wang, S.; Zhu, Z. H.; Coomes, A.; Haghseresht, F.; Lu, G. Q. The Physical and Surface Chemical Characteristics of Activated Carbons and the Adsorption of Methylene Blue from Wastewater. *J. Colloid Interface Sci.***2005**, *284* (2), 440–446. https://doi.org/10.1016/j.jcis.2004.10.050.

[33]Zenasni, M. A.; Benfarhi, S.; Merlin, A.; Molina, S.; George, B.; Meroufel, B. Adsorption of Cu(II) on Maghnite from Aqueous Solution: Effects of pH, Initial Concentration, Interaction Time and Temperature. *Nat. Sci.***2012**, *04* (11), 856–868. https://doi.org/10.4236/ns.2012.411114.

[34] *Bhatnagar A. Ebook - Application of Adsorbents for Water Pollution Control | Bentham Science*. volume/1128/related-journals (accessed 2023-12-18).

https:// *DOI: 10.2174/97816080526911120101*.

[35] Slater, A. G.; Cooper, A. I. Function-Led Design of New Porous Materials. *Science***2015**, *348* (6238), aaa8075. https://doi.org/10.1126/science.aaa8075.

[36] Judeinstein, P.; Sanchez, C. Hybrid Organic–Inorganic Materials: A Land of Multidisciplinarity. *J. Mater. Chem.***1996**, *6* (4), 511–525. https://doi.org/10.1039/JM9960600511.

[37] Ribot, F.; Sanchez, C. Organically Functionalized Metallic Oxo-Clusters: Structurally Well-Defined Nanobuilding Blocks for the Design of Hybrid Organic-Inorganic Materials. *Comments Inorg. Chem.***1999**, *20* (4–6), 327–371. https://doi.org/10.1080/02603599908021449.

[38] Figlarz, M. Soft Chemistry: Thermodynamic and Structural Aspects. *Mater. Sci. Forum***1994**, *152–153*, 55–68. https://doi.org/10.4028/www.scientific.net/MSF.152-153.55.

[39] Navar, R.; Tarantino, G.; T. Beynon, O.; Padovan, D.; Botti, L.; K. Gibson, E.; P. Wells, P.; Owens, A.; A. Kondrat, S.; J. Logsdail, A.; Hammond, C. Tracking the Solid-State Incorporation of Sn into the Framework of Dealuminated Zeolite Beta, and Consequences for Catalyst Design. *J. Mater. Chem. A***2022**, *10* (41), 22025–22041. https://doi.org/10.1039/D2TA03837D.

[40]Inaguma, Y.; Liquan, C.; Itoh, M.; Nakamura, T.; Uchida, T.; Ikuta, H.; Wakihara, M. High Ionic Conductivity in Lithium Lanthanum Titanate. *Solid State Commun.***1993**, *86* (10), 689–693. https://doi.org/10.1016/0038-1098(93)90841-A.

[41] Tamura, S.; Imanaka, N.; Adachi, G. Trivalent Ion Conduction in NASICON Type Solid Electrolyte Prepared by Ball Milling. *Solid State Ion.***2002**, *154–155*, 767–771. https://doi.org/10.1016/S0167-2738(02)00478-2.

[42] Gaffet, E.; Bernard, F.; Niepce, J.-C.; Charlot, F.; Gras, C.; Le Caër, G.; Guichard, J.-L.; Delcroix, P.; Mocellin, A.; Tillement, O. Some Recent Developments in Mechanical Activation and Mechanosynthesis. *J. Mater. Chem.***1999**, *9* (1), 305–314. https://doi.org/10.1039/a804645j.

[43] M. Titi, H.; Do, J.-L.; J. Howarth, A.; Nagapudi, K.; Friščić, T. Simple, Scalable Mechanosynthesis of Metal–Organic Frameworks Using Liquid-Assisted Resonant Acoustic Mixing (LA-RAM). *Chem. Sci.***2020**, *11* (29), 7578–7584. https://doi.org/10.1039/D0SC00333F.

[44] Afshariazar, F.; Morsali, A. The Unique Opportunities of Mechanosynthesis in Green and Scalable Fabrication of Metal–Organic Frameworks. *J. Mater. Chem. A***2022**, *10* (29), 15332–15369. https://doi.org/10.1039/D2TA02699F.

[45] Pechini, M. P. Method of Preparing Lead and Alkaline Earth Titanates and Niobates and Coating Method Using the Same to Form a Capacitor. 3330697, July 11, 1967. https://www.freepatentsonline.com/3330697.html (accessed 2023-12-19).

[46] Li, P.; Li, F.; Deng, G.; Guo, X.; Liu, H.; Jiang, W.; Wang, T. Polymerized-Complex Method for Preparation of Supported Bimetallic Alloy and Monometallic Nanoparticles. *Chem. Commun.***2016**, *52* (14), 2996–2999. https://doi.org/10.1039/C5CC08848H.

[47] Ye, N.; Yan, T.; Jiang, Z.; Wu, W.; Fang, T. A Review: Conventional and Supercritical Hydro/Solvothermal Synthesis of Ultrafine Particles as Cathode in Lithium Battery. *Ceram. Int.***2018**, *44* (5), 4521–4537. https://doi.org/10.1016/j.ceramint.2017.12.236.

[48] Cao, W. *The Development and Application of Microwave Heating*; BoD – Books on Demand, 2012.*DOI10.5772/2619*

[49] Mahato, S. S.; Mahata, D.; Panda, S.; Mahata, S.; Mahato, S. S.; Mahata, D.; Panda, S.; Mahata, S. Perspective Chapter: Sol-Gel Science and Technology in Context of Nanomaterials – Recent Advances. In *Sol-Gel Method - Recent Advances*; IntechOpen, 2023. https://doi.org/10.5772/intechopen.111378.

[50] Acharya, S. S.; Singh, J. P.; Acharya, S. S.; Singh, J. P. Introductory Chapter: Sol-Gel Synthesis. In *Sol-Gel Method - Recent Advances*; IntechOpen, 2023. https://doi.org/10.5772/intechopen.112248.

[51] Bader, N.; Benkhayal, A.; Zimmermann, B. Co-Precipitation as a Sample Preparation Technique for Trace Element Analysis: An Overview. *Int. J. Chem. Sci.***2014**, *12*, 519–525.

[52] *Mascolo M C,; Pei Y ,; Ring T A. Room Temperature Co-Precipitation Synthesis of Magnetite Nanoparticles in a Large pH Window with Different Bases*.*Materials 2013, 6(12), 5549-5567; https://doi.org/10.3390/ma6125549*

[53] Djamel, A.; Ammar, Z. An Investigation into the Mineralogical and Physicochemical Characterization of El-Oued (Algeria) Clay An Investigation into the Mineralogical and

Physicochemical Characterization of El-Oued (Algeria) Clay. **2023**, *20*, 1048–1058. https://doi.org/10.48047/NQ.2022.20.4.NQ22329.

[54] Guggenheim, S.; Martin, R. T. Definition of Clay and Clay Mineral: Joint Report of the Aipea Nomenclature and CMS Nomenclature Committees. *Clays Clay Miner.***1995**, *43* (2), 255–256. https://doi.org/10.1346/CCMN.1995.0430213.

[55] Dassanayake, S. M.; Perera, U. P.; Jayawardena, C. L.; Emmanuel, E. Clay Mineral Composites as Environmental Catalysts. In *Clay Composites: Environmental Applications*; Vithanage, M., Lazzara, G., Rajapaksha, A. U., Eds.; Advances in Material Research and Technology; Springer Nature: Singapore, 2023; pp 343–371. https://doi.org/10.1007/978-981-99-2544-5_16.

[56] *Clauer, N.; Chaudhuri, S. Clays in Crustal Environments: Isotope Dating and Tracing; Springer Science & Business Media, 2012.*

[57] *Budhu, M. Soil Mechanics and Foundations; John Wiley and Sons, 3rd edition. ISBN 978-0-470-55684-9 (hardback). 2010.*

[58] *Nascimento, G. M. D. Clay and Clay Minerals; BoD – Books on Demand, ISBN978-1-83969-564-3. 2021.https://doi 10.5772/intechopen.95640*

[59] Bailey, S. W. Odinite, a New Dioctahedral-Trioctahedral Fe3+-Rich 1:1 Clay Mineral. *Clay Miner.***1988**, *23* (3), 237–247. https://doi.org/10.1180/claymin.1988.023.3.01.

[60] Brindley, G. W.; Robinson, K. The Structure of Kaolinite. *Mineral. Mag. J. Mineral. Soc.***1946**, *27* (194), 242–253. https://doi.org/10.1180/minmag.1946.027.194.04.

[61] Bauluz Lázaro, B. Halloysite and Kaolinite: Two Clay Minerals with Geological and Technological Importance. *Rev. Acad. Cienc. Exactas Físicas Quím. Nat. Zaragoza***2015**, No. 70 ( ), 7–38.

[62] Ghadiri, M.; Chrzanowski, W.; Rohanizadeh, R. Biomedical Applications of Cationic Clay Minerals. *RSC Adv.***2015**, *5* (37), 29467–29481. https://doi.org/10.1039/C4RA16945J.

[63] Dahai H.; Yuzeng Y.; Jianfei F.; Joseph R.; Michalski.; Kun S. *The Laboratory-Based HySpex Features of Chlorite as the Exploration Tool for High-Grade Iron Ore in Anshan-Benxi Area, Liaoning Province, Northeast China.Appl. Sci. 2020, 10(21), 7444; https://doi.org/10.3390/app10217444*

[64] Schoonheydt, R. A.; Johnston, C. T. The Surface Properties of Clay Minerals. In *Layered Mineral Structures and their Application in Advanced Technologies*; Brigatti, M. F., Mottana, A., Eds.; Mineralogical Society of Great Britain and Ireland, 2011; Vol. 11, p 0. https://doi.org/10.1180/EMU-notes.11.10.

[65] Kahr, G.; Madsen, F. T. Determination of the Cation Exchange Capacity and the Surface Area of Bentonite, Illite and Kaolinite by Methylene Blue Adsorption. *Appl. Clay Sci.***1995**, *9* (5), 327–336. https://doi.org/10.1016/0169-1317(94)00028-O.

[66] Aran, D.; Maul, A.; Masfaraud, J.-F. A Spectrophotometric Measurement of Soil Cation Exchange Capacity Based on Cobaltihexamine Chloride Absorbance. *Comptes Rendus Geosci.***2008**, *340* (12), 865–871. https://doi.org/10.1016/j.crte.2008.07.015.

[67] Karpiński, B.; Szkodo, M. Clay Minerals – Mineralogy and Phenomenon of Clay Swelling in Oil & Gas Industry. *Adv. Mater. Sci.***2015**, *15* (1), 37–55. https://doi.org/10.1515/adms-2015-0006.

[68] Karak, T.; Das, D. K.; Singh, U. K.; Maiti, D. Influence of pH on Soil Charge Characteristics and Cadmium Sorption in Some Noncontaminated Soils of Indian Subtropics. *Sci. World J.***NaN/NaN/NaN**, *5*, 183–194. https://doi.org/10.1100/tsw.2005.26.

[69] Moghimi, A. H.; Hamdan, J.; Shamshuddin, J.; Samsuri, A. W.; Abtahi, A. Physicochemical Properties and Surface Charge Characteristics of Arid Soils in Southeastern Iran. *Appl. Environ. Soil Sci.***2013**, *2013*, e252861. https://doi.org/10.1155/2013/252861.

[70] *Dehmani Y, Dison S. P. Franco , Georgin J, Taibi L , Brahmi Y, Oukhrib R, Belfaquir M, Moussout H, Ouallal H Comparison of Phenol Adsorption Property and Mechanism onto Different Moroccan Clays. Water 2023, 15(10), 1881; https://doi.org/10.3390/w15101881Water 2023, 15(10), 1881; https://doi.org/10.3390/w15101881*

[71] Gulen, B.; Demircivi, P. Adsorption Properties of Flouroquinolone Type Antibiotic Ciprofloxacin into 2:1 Dioctahedral Clay Structure: Box-Behnken Experimental Design. *J. Mol. Struct.***2020**, *1206*, 127659. https://doi.org/10.1016/j.molstruc.2019.127659.

[72] Schweizer, S. A.; Mueller, C. W.; Höschen, C.; Ivanov, P.; Kögel-Knabner, I. The Role of Clay Content and Mineral Surface Area for Soil Organic Carbon Storage in an Arable Toposequence. *Biogeochemistry***2021**, *156* (3), 401–420. https://doi.org/10.1007/s10533-021-00850-3.

[73] Andrade, F. A.; Al-Qureshi, H. A.; Hotza, D. Measuring the Plasticity of Clays: A Review. *Appl. Clay Sci.***2011**, *51* (1), 1–7. https://doi.org/10.1016/j.clay.2010.10.028.

[74] Tankosić, L.; Sredić, S.; Tančić, P.; Nedić, Z. The Dispersion-Flocculation Behaviour of the Natural Raw Clay Samples from Omarska Mine. *Contemp. Mater.***2019**, *10* (1), 71–81. https://doi.org/10.7251/COMEN1901071T.

[75] Clay Soil Modification Techniques for the Adsorption of Heavy Metals in Aqueous Medium: A Review. *Int. J. Adv. Res. Chem. Sci.***2019**, *6* (6). https://doi.org/10.20431/2349-0403.0606003.

[76] Temuujin, J.; Senna, M.; Jadambaa, T.; Burmaa, D.; Erdenechimeg, S.; MacKenzie, K. J. Characterization and Bleaching Properties of Acid-Leached Montmorillonite. *J. Chem. Technol. Biotechnol.***2006**, *81* (4), 688–693. https://doi.org/10.1002/jctb.1469.

[77] Adams, I.; F.W., A.; Hassan, L. G.; S.A., M.; Itodo, H. Physicochemical Parameters of Adsorbents from Locally Sorted H3PO4 and ZnCl2 Modified Agricultural Wastes. *N. Y. Sci. J.***2010**, *3*, 17.

[78] *Prajyot D, Ravindra V. G. Green and Sustainable Chemistry Vol.14 No.1, 2024. DOI: 10.4236/gsc.2024.141001* .

[79] Liu, P. Polymer Modified Clay Minerals: A Review. *Appl. Clay Sci.***2007**, *38* (1), 64–76. https://doi.org/10.1016/j.clay.2007.01.004.

[80] Pawlowska, A.; Sadowski, Z. The Role of Biomodification in Mineral Processing. *Minerals***2023**, *13* (10), 1246. https://doi.org/10.3390/min13101246.

[81] Hongo, T.; Yoshino, S.; Yamazaki, A.; Yamasaki, A.; Satokawa, S. Mechanochemical Treatment of Vermiculite in Vibration Milling and Its Effect on Lead (II) Adsorption Ability. *Appl. Clay Sci.***2012**, *70*, 74–78. https://doi.org/10.1016/j.clay.2012.09.016.

[82] Shen, Y.-H. Preparations of Organobentonite Using Nonionic Surfactants. *Chemosphere***2001**, *44* (5), 989–995. https://doi.org/10.1016/S0045-6535(00)00564-6.

[83] López-García, S.; Sanchez, S.; Ramos, L. Effect of Type and Concentration of Ionomer Compatibilizer on the Hdpe/ Ionomer/ Clay Nanocomposites Morphology. *Mater. Sci. Forum***2010**, *644*, 17–20. https://doi.org/10.4028/www.scientific.net/MSF.644.17.

[84] Nathaniel, E.; Kurniawan, A.; Soeteredjo, F. E.; Ismadji, S. Organo-Bentonite for the Adsorption of Pb(II) from Aqueous Solution: Temperature Dependent Parameters of Several Adsorption Equations. *Desalination Water Treat.***2011**, *36* (1–3), 280–288. https://doi.org/10.5004/dwt.2011.2572.

[85] *Pankil S.; Rajeev M.; Siddh N. Clay Modification by the Use of Organic Cations. Green and Sustainable Chemistry, 2012, 2, 21-25. https://doi:10.4236/gsc.2012.21004*

[86]Komadel, P.; Schmidt, D.; Madejová, J.; Čičel, B. Alteration of Smectites by Treatments with Hydrochloric Acid and Sodium Carbonate Solutions. *Appl. Clay Sci.***1990**, *5* (2), 113–122. https://doi.org/10.1016/0169-1317(90)90017-J.

[87]Churchman, G. J.; Gates, W. P.; Theng, B. K. G.; Yuan, G. Chapter 11.1 Clays and Clay Minerals for Pollution Control. In *Developments in Clay Science*; Bergaya, F., Theng, B. K. G., Lagaly, G., Eds.; Handbook of Clay Science; Elsevier, 2006; Vol. 1, pp 625–675. https://doi.org/10.1016/S1572-4352(05)01020-2.

[88] Steudel, A.; Batenburg, L. F.; Fischer, H. R.; Weidler, P. G.; Emmerich, K. Alteration of Swelling Clay Minerals by Acid Activation. *Appl. Clay Sci.***2009**, *44* (1), 105–115. https://doi.org/10.1016/j.clay.2009.02.002.

[89] *Francisco R. Valenzuela D; Pérsio S. Studies on the acid activation of Brazilian smectitic clays: Ingenta Connect*. *Química Nova, Volume 24, Number 3, 2001, pp. 345-353(9). https://doi.org/10.1590/S0100-40422001000300011.*

[90] Doulia, D.; Leodopoulos, Ch.; Gimouhopoulos, K.; Rigas, F. Adsorption of Humic Acid on Acid-Activated Greek Bentonite. *J. Colloid Interface Sci.***2009**, *340* (2), 131–141. https://doi.org/10.1016/j.jcis.2009.07.028.

[91] Lian, L.; Guo, L.; Guo, C. Adsorption of Congo Red from Aqueous Solutions onto Ca-Bentonite. *J. Hazard. Mater.***2009**, *161* (1), 126–131. https://doi.org/10.1016/j.jhazmat.2008.03.063.

[92] Chaari, I.; Fakhfakh, E.; Chakroun, S.; Bouzid, J.; Boujelben, N.; Feki, M.; Rocha, F.; Jamoussi, F. Lead Removal from Aqueous Solutions by a Tunisian Smectitic Clay. *J. Hazard. Mater.***2008**, *156* (1), 545–551. https://doi.org/10.1016/j.jhazmat.2007.12.080.

[93] *Jorge B,; Virginia M,; Manuel P,; Almudena G,; Juan J.; Carolina B. A Review on the Synthesis and Characterization of Metal Organic Frameworks for Photocatalytic Water Purification*. Catalysts, 2019, 9(1), 52; https://doi.org/10.3390/catal9010052.

[94] McGuinness, N.; John, H.; M K, K.; Banerjee, S.; Dionysiou, D.; Pillai, S. Self-Cleaning Photocatalytic Activity: Materials and Applications; 2016; pp 204–235. https://doi.org/10.1039/9781782627104-00204.

[95] Lofrano, G.; Ubaldi, F.; Albarano, L.; Carotenuto, M.; Vaiano, V.; Valeriani, F.; Libralato, G.; Gianfranceschi, G.; Fratoddi, I.; Meric, S.; Guida, M.; Romano Spica, V. Antimicrobial Effectiveness of Innovative Photocatalysts: A Review. *Nanomaterials***2022**, *12* (16), 2831. https://doi.org/10.3390/nano12162831.

[96] Zhang, H.; Ge, C.; Zhu, C.; Li, Y.; Tian, W.; Cheng, D.; Pan, Z. Deodorizing Properties of Photocatalyst Textiles and Its Effect Analysis. *Phys. Procedia***2012**, *25*, 240–244. https://doi.org/10.1016/j.phpro.2012.03.078.

[97] *Hangjuan R, Pramod K, Wen-Fan C, Shaohua Q, Charles C. Photocatalytic materials and technologies for air purification. Hazardous Materials. 325, 340-366.2017. https://doi.org/10.1016/j.jhazmat.2016.08.072*

[98] Mavengere, S.; Kim, J.-S. Anti-Fogging, Photocatalytic and Self-Cleaning Properties of TiO2-Transparent Coating. *Korean J. Mater. Res.***2021**, *31* (1), 8–15. https://doi.org/10.3740/MRSK.2021.31.1.8.

[99] *Suresh C. A.*; *Advanced Oxidation Processes for Wastewater Treatment*.*Emerging Green Chemical Technology.* 2018, 1-12.https://doi.org/10.1016/B978-0-12-810499-6.00001-2.

[100] Babuponnusami, A.; Muthukumar, K. A Review on Fenton and Improvements to the Fenton Process for Wastewater Treatment. *J. Environ. Chem. Eng.***2014**, *2* (1), 557–572. https://doi.org/10.1016/j.jece.2013.10.011.

[101] Qu, J. Research Progress of Novel Adsorption Processes in Water Purification: A Review. *J. Environ. Sci.***2008**, *20* (1), 1–13. https://doi.org/10.1016/S1001-0742(08)60001-7.

[102] Nouri, S.; Haghseresht, F.; Lu, G. Q. M. Comparison of Adsorption Capacity of P-Cresol & p-Nitrophenol by Activated Carbon in Single and Double Solute. *Adsorption***2002**, *8* (3), 215–223. https://doi.org/10.1023/A:1021260501001.

[103] Pereira, M. F. R.; Soares, S. F.; Órfão, J. J. M.; Figueiredo, J. L. Adsorption of Dyes on Activated Carbons: Influence of Surface Chemical Groups. *Carbon***2003**, *41* (4), 811–821. https://doi.org/10.1016/S0008-6223(02)00406-2.

[104] Abollino, O.; Aceto, M.; Malandrino, M.; Sarzanini, C.; Mentasti, E. Adsorption of Heavy Metals on Na-Montmorillonite. Effect of pH and Organic Substances. *Water Res.***2003**, *37* (7), 1619–1627. https://doi.org/10.1016/S0043-1354(02)00524-9.

[105] *Heavy metal adsorption by functionalized clays.Rafael C,; Carmen H,; Juan C. Environ. Sci. Technol. 2000, 34, 21, 4593–4599. https://doi.org/10.1021/es000013c.*

[106] Oliveira, L. C. A.; Petkowicz, D. I.; Smaniotto, A.; Pergher, S. B. C. Magnetic Zeolites: A New Adsorbent for Removal of Metallic Contaminants from Water. *Water Res.***2004**, *38* (17), 3699–3704. https://doi.org/10.1016/j.watres.2004.06.008.

[107] Wu, R.; Qu, J.; Chen, Y. Magnetic Powder MnO–Fe2O3 Composite—a Novel Material for the Removal of Azo-Dye from Water. *Water Res.***2005**, *39* (4), 630–638. https://doi.org/10.1016/j.watres.2004.11.005.

[108] Zhang, G.; Qu, J.; Liu, H.; Cooper, A. T.; Wu, R. CuFe2O4/Activated Carbon Composite: A Novel Magnetic Adsorbent for the Removal of Acid Orange II and Catalytic Regeneration. *Chemosphere***2007**, *68* (6), 1058–1066. https://doi.org/10.1016/j.chemosphere.2007.01.081.

[109] Robinson, T.; Chandran, B.; Nigam, P. Removal of Dyes from a Synthetic Textile Dye Effluent by Biosorption on Apple Pomace and Wheat Straw. *Water Res.***2002**, *36* (11), 2824–2830. https://doi.org/10.1016/s0043-1354(01)00521-8.

[110] Loukidou, M. X.; Matis, K. A.; Zouboulis, A. I.; Liakopoulou-Kyriakidou, M. Removal of As(V) from Wastewaters by Chemically Modified Fungal Biomass. *Water Res.***2003**, *37* (18), 4544–4552. https://doi.org/10.1016/S0043-1354(03)00415-9.

[111] Atia, A. A.; Donia, A. M.; Abou-El-Enein, S. A.; Yousif, A. M. Studies on Uptake Behaviour of Copper(II) and Lead(II) by Amine Chelating Resins with Different Textural Properties. *Sep. Purif. Technol.***2003**, *33* (3), 295–301. https://doi.org/10.1016/S1383-5866(03)00089-3.

[112] Zhang, J.-G.; Gong, W.-J.; Guan, Y.-S.; Li, H.-X.; Young, D. J.; Lang, J.-P. Carboxylate-Assisted Assembly of Zinc and Cadmium Coordination Complexes of 1,3,5-Tri-4-Pyridyl-1,2-Ethenylbenzene: Structures and Visible-Light-Induced Photocatalytic Degradation of Congo Red in Water. *Cryst. Growth Des.***2018**, *18* (10), 6172–6184. https://doi.org/10.1021/acs.cgd.8b01040.

[113] Dong, X.; Lin, Y.; Ma, Y.; Zhao, L. N-Contaning UiO-67 Derived Multifunctional Hybrid Materials as Highly Effective Adsorbents for Removal of Congo Red. *Inorganica Chim. Acta***2020**, *510*, 119748. https://doi.org/10.1016/j.ica.2020.119748.

[114] Han, L.-J.; Ge, F.-Y.; Sun, G.-H.; Gao, X.-J.; Zheng, H.-G. Effective Adsorption of Congo Red by a MOF-Based Magnetic Material. *Dalton Trans.***2019**, *48* (14), 4650–4656. https://doi.org/10.1039/C9DT00813F.

[115] Chatterjee, S.; Guha, N.; Krishnan, S.; Singh, A. K.; Mathur, P.; Rai, D. K. Selective and Recyclable Congo Red Dye Adsorption by Spherical Fe3O4 Nanoparticles Functionalized with 1,2,4,5-Benzenetetracarboxylic Acid. *Sci. Rep.***2020**, *10* (1), 111. https://doi.org/10.1038/s41598-019-57017-2.

[116] Liu, J.; Zhang, X.-Y.; Hou, J.-X.; Liu, J.-M.; Jing, X.; Li, L.-J.; Du, J.-L. Functionalized Mn(II)-MOF Based on Host-Guest Interaction for Selective and Rapid Capture of Congo Red from Water. *J. Solid State Chem.***2019**, *270*, 697–704. https://doi.org/10.1016/j.jssc.2018.12.039.

[117] Wei, F.; Chen, D.; Liang, Z.; Zhao, S.; Luo, Y. Synthesis and Characterization of Metal–Organic Frameworks Fabricated by Microwave-Assisted Ball Milling for Adsorptive Removal of Congo Red from Aqueous Solutions. *RSC Adv.***2017**, *7* (73), 46520–46528. https://doi.org/10.1039/C7RA09243A.

[118] Yang, Q.; Wang, Y.; Wang, J.; Liu, F.; Hu, N.; Pei, H.; Yang, W.; Li, Z.; Suo, Y.; Wang, J. High Effective Adsorption/Removal of Illegal Food Dyes from Contaminated Aqueous Solution by Zr-MOFs (UiO-67). *Food Chem.***2018**, *254*, 241–248. https://doi.org/10.1016/j.foodchem.2018.02.011.

[119] Yang, M.; Bai, Q. Flower-like Hierarchical Ni-Zn MOF Microspheres: Efficient Adsorbents for Dye Removal. *Colloids Surf. Physicochem. Eng. Asp.***2019**, *582*, 123795. https://doi.org/10.1016/j.colsurfa.2019.123795.

[120] Yokwana, K.; Kuvarega, A. T.; Mhlanga, S. D.; Nxumalo, E. N. Mechanistic Aspects for the Removal of Congo Red Dye from Aqueous Media through Adsorption over N-Doped Graphene Oxide Nanoadsorbents Prepared from Graphite Flakes and Powders. *Phys. Chem. Earth Parts ABC***2018**, *107*, 58–70. https://doi.org/10.1016/j.pce.2018.08.001.

[121] Golie, W. M.; Upadhyayula, S. An Investigation on Biosorption of Nitrate from Water by Chitosan Based Organic-Inorganic Hybrid Biocomposites. *Int. J. Biol. Macromol.***2017**, *97*, 489–502. https://doi.org/10.1016/j.ijbiomac.2017.01.066.

[122] Liu, G.; You, S.; Ma, M.; Huang, H.; Ren, N. Removal of Nitrate by Photocatalytic Denitrification Using Nonlinear Optical Material. *Environ. Sci. Technol.***2016**, *50* (20), 11218–11225. https://doi.org/10.1021/acs.est.6b03455.

[123] Velu, M.; Balasubramanian, B.; Velmurugan, P.; Kamyab, H.; Ravi, A. V.; Chelliapan, S.; Lee, C. T.; Palaniyappan, J. Fabrication of Nanocomposites Mediated from Aluminium Nanoparticles/Moringa Oleifera Gum Activated Carbon for Effective Photocatalytic Removal of Nitrate and Phosphate in Aqueous Solution. *J. Clean. Prod.***2021**, *281*, 124553. https://doi.org/10.1016/j.jclepro.2020.124553.

[124] Öztürk, N.; Bektaş, T. E. Nitrate Removal from Aqueous Solution by Adsorption onto Various Materials. *J. Hazard. Mater.***2004**, *112* (1–2), 155–162. https://doi.org/10.1016/j.jhazmat.2004.05.001.

[125] Gatti, M.; Fernández, L.; Sánchez, M.; Parolo, M. Aminopropyltrimethoxysilane- and Aminopropyltrimethoxysilane-Silver-Modified Montmorillonite for the Removal of Nitrate Ions. *Environ. Technol.***2016**, *37*, 1–44. https://doi.org/10.1080/09593330.2016.1158868.

[126] Mena-Duran, C. J.; Sun Kou, M. R.; Lopez, T.; Azamar-Barrios, J. A.; Aguilar, D. H.; Domínguez, M. I.; Odriozola, J. A.; Quintana, P. Nitrate Removal Using Natural Clays Modified by Acid Thermoactivation. *Appl. Surf. Sci.***2007**, *253* (13), 5762–5766. https://doi.org/10.1016/j.apsusc.2006.12.103.

[127] Xi, Y.; Mallavarapu, M.; Naidu, R. Preparation, Characterization of Surfactants Modified Clay Minerals and Nitrate Adsorption. *Appl. Clay Sci.***2010**, *48* (1), 92–96. https://doi.org/10.1016/j.clay.2009.11.047.

[128] Silva, C. G.; Pereira, M. F. R.; Órfão, J. J. M.; Faria, J. L.; Soares, O. S. G. P. Catalytic and Photocatalytic Nitrate Reduction Over Pd-Cu Loaded Over Hybrid Materials of Multi-Walled Carbon Nanotubes and TiO2. *Front. Chem.***2018**, *6*.

[129] Chen, H.; Zhao, J. Adsorption Study for Removal of Congo Red Anionic Dye Using Organo-Attapulgite. *Adsorption***2009**, *15* (4), 381–389. https://doi.org/10.1007/s10450-009-9155-z.

[130] *Vipasiri V ,; Shaomin L,; Jin B ,; Chris W.K. Chow d,; Chris Saint b d. Kinetic study and equilibrium isotherm analysis of Congo Red adsorption by clay materials.Chemical Engineering Journal.148, (2–3), 2009,354-364*. https://doi.org/10.1016/j.cej.2008.09.009.

[131] Wang, L.; Wang, A. Removal of Congo Red from Aqueous Solution Using a Chitosan/Organo-Montmorillonite Nanocomposite. *J. Chem. Technol. Biotechnol.***2007**, *82* (8), 711–720. https://doi.org/10.1002/jctb.1713.

[132] Zhu, L.; Wang, L.; Xu, Y. Chitosan and Surfactant Co-Modified Montmorillonite: A Multifunctional Adsorbent for Contaminant Removal. *Appl. Clay Sci.***2017**, *146*, 35–42. https://doi.org/10.1016/j.clay.2017.05.027.

[133] Smith, J. A.; Galan, A. *Sorption of Nonionic Organic Contaminants to Single and Dual Organic Cation Bentonites from Water*. ACS Publications. https://doi.org/10.1021/es00003a016.

[134] Lund, E.; Nissen, B. Low Technology Water Purification by Bentonite Clay Flocculation as Performed in Sudanese Villages. Virological Examinations. *Water Res.***1986**, *20* (1), 37–43. https://doi.org/10.1016/0043-1354(86)90211-3.

[135] Gersberg, R. M.; Lyon, S. R.; Brenner, R.; Elkins, B. V. Performance of a Clay-Alum Flocculation (CCBA) Process for Virus Removal from Municipal Wastewater. *Water Res.***1988**, *22* (11), 1449–1454. https://doi.org/10.1016/0043-1354(88)90103-0.

[136]Francisco, R.,; Valenzuela, D.; S.S. Pérsio.. Studies on the acid activation of Brazilian smectitic clays. *Quim. Nova*, 24(3): 345-353. (2001)

[137] Susan Sadeghi, a Ali ZeraatkarMoghaddama and Mohammad Massinaei. Novel tunable composites based on bentonite and modified tragacanth gum for removal of acid dyes from aqueous solutions. 2015 DOI: 10.1039/c5ra07979a

[138] Toor, M.; Jin, B. Adsorption Characteristics, Isotherm, Kinetics, and Diffusion of Modified Natural Bentonite for Removing Diazo Dye. *Chem. Eng. J.***2012**, *187*, 79–88. https://doi.org/10.1016/j.cej.2012.01.089.

[139] *Vipasiri V,; Bo J,; Christopher W K. Insight into removal kinetic and mechanisms of anionic dye by calcined clay materials and lime. 2010 . 15;177(1-3):420-7.* https://*doi:10.1016/j.jhazmat.2009.12.049.*

Chapter TWO

MATERIALS AND METHODS

Introduction

The objective of this chapter is to list the precursors of chemical reactions used for the elaboration of hybrid particles, a description of the tools and equipment used in the preparation of the materials and a description of the natural materials used for the purification of the poled waters. The chapter is organized in two parts. First, we will describe the methodology used to synthesize catalysers. We will begin by describing the synthesis protocols of the studied systems. Then we will describe the choice of techniques used to identify the behavior of pollutants in solution.The second part will focus on the systems of natural materials (clays)

II.1.Chemical product(precursors)

The table II.1 includes the reactants used during syntheses of materials

Table.1: The natural and chemical materials used.

	Chemical formula	Name	Molar mass(MW)	Supplier
Metallic cation source				
1	$Cu(NO_3)_2.H_2O$	Copper(II) nitrate	241.60	Merck
2	$FeCl_3.6H_2O$	iron(III) chloride	270.30	Aldrisch
3	$CdCl_2.H_2O$	Cadmium chloride hidrated	201.32	E.Merck
Acidic ligand				
4	$C_4H_4O_4$	maleic acid	116.07 g/mol	(Biochem)
5	$H_2C_4O_4$	squaric acid	114.06 g/mol	Acros Organic
Amide template				
6	C_8H_9NO	Acetanilide	135.16	Biochem
7	$C_2H_8N_2O_4.H_2O$	Ammonium oxalat	142.12	Merck
Activating acid and **pH regulators**				
	H_2SO_4	Sulfuric acid	98.08 g/mol	Biochem
10	HCl (37%)	Hydrochloric acid.	36.5	Merck
11	NaOH	Sodium hydroxyd	28	Merck
12	H_2O_2	Hydrogen peroxide	pharmaceutic	Merck
Pollutant				
	$C_{32}H_{22}N_6Na_2O_6S_2$)	Red congo	696.68 g/mol	Merck
	KNO_3	Potassium nitrate	101.1032 g/mol	ProlaboChemicals

Solvent				
	C_2H_5OH	Ethanol	46.07	Merck
	CH_4O	Methanol	32.04	Comercial
cuvette test				
	LCK 339	Nitrate LCK cuvette test		Hach Lange
	LCK 314	COD LCK cuvette test		Hach Lange
	LCK114	COD LCK cuvette test		Hach Lange
indicators				
	$AgNO_3$	Silver nitrate		
	$BaCl_2$	Barium chlorid		

II.2.Natural product

In this study, two kinds of natural clay mineralswere used, the first one (clay1) was obtained in march 2020from El M'Guer state(Algeria) (46.73° N, 33.42° E),.(figI-1) display the geographical location where it was collected.

Figure II.1. The location of the clay(CM) sample by Google Earth.

and the second one (clay2)was acquired in january2022from Wad Al-Nisaa (32°34'22.20"N) (5°21'41.64"E) on altitude 129.49 km affiliated to Al-Hujaira inOuargla state (Algeria).(figII-2) display the clay sample and the geographical location where it was collected.

Figure.II.2: Thelocation of theclay (CH) sample by Google Earth.

II.3.Wastewater

II.3.1.Synthetic wastewater

In this study, we used two types of contaminated water: Industrial contaminated water that were synthetic wastewater contening both of nitrate and Congo red and urban contaminated water.

Nitrates (NO^{3-}) are a common pollutant, especially in wastewater and can cause a number of problems in aquatic ecosystems .Contaminated water was prepared by mixing KNO_3 with the water slowly, stirring constantly until completely melted. The concentration of nitrates in water was measured using the nitrate tester.

Congo red is a toxic dye and should be handled with care. To prepare wastewater with Congo red, we dissolve Congo red in distilled water to prepare a stock solution. The concentration of the stock solution will depend on the desired concentration of Congo red in the wastewater.

II.3.2.urban wastewater

urban wastewater was taken from ONA (Office National de l'assinisement). ONA is the Algerian national water and sanitation company, responsible for the collection, treatment, and disposal of wastewater in Algeria. It collects wastewater from households, businesses, and industries. This wastewater is then transported to wastewater treatment plants, where it is treated to remove pollutants before being discharged into the environment.The use of treated urban wastewater for these purposes can help to conserve water resources and reduce environmental pollution.

II.4.Physico-chemical measurements

II.4.1.Fourier Transform Infrared Spectroscopy(FTIR)

Fourier Transform Infrared Spectroscopy (FTIR) was utilized in this study to analyze powder samples of the mentioned materials, as well as clay, using the FTIR-7600 Fourier-Transform Infrared spectrometer of Tlemcen Universit(figure 1 Annexe1) This technique enabled us to identify chemical bonds and functional groups in the synthesized compounds and clay.

The resulting spectrum from FTIR appears as peaks, each representing specific reactions for the sample. This allows for a deeper understanding of the chemical and physical properties of the materials.

The FTIR-7600 Fourier-Transform Infrared devises operates by measuring the interaction between infrared radiations and the analyzed materials. This is achieved by generating infrared radiations using a radiation source such as a halogen lamp or laser. These radiations are then directed towards the sample, passing through it. At this point, some of these radiations are absorbed based on the chemical and structural properties of the sample.

II.4.1.1.Sample preparation

Samples preparing for analysis were carried according to the following: The first step was to ensure that the sample was clean, dry, and free of any contaminants that could interfere with the analysis. Then ground the material into a fine powder to ensure homogeneity and improve interaction with infrared light. After mix the powder well to ensure a representative sample for analysis is obtained and placed it on holder. Performed the baseline measurement with a blank sample holder to account for any background signals. Finally, we set appropriate measurement parameters such as wavelength range, resolution and perform FTIR analysis by exposing the sample to infrared radiation and recording the resulting absorption spectrum.

II.4.2.Visible (UV-Vis)

Using the Ultraviolet-Visible (UV-Vis) spectroscopy devices, at the University of Tlemcen and also (Optizen 2120 UV) at the VPRS laboratory of the University Kasdi Merbah Ouargla (figure 2 Annexe1Cary Series UV-Vis Spectrophotometer of crapc(figure 3 Annexe1),we analyzed the interaction of molecules with ultraviolet and visible light for the samples. We also analyzed the concentration of absorbed Congo Red dye in the solution, studied kinetics, determined equilibrium constants.

In UV-Vis spectroscopy analysis, the sample is exposed to light in the UV-Vis region (typically 190-900 nanometers). The sample absorbs light at specific wavelengths depending on its composition and electronic structure. Absorption of light corresponds to transitions between electronic energy levels.The instrument measures the amount of light absorbed by the sample, generating a spectrum that shows absorption peaks at certain wavelengths. These peaks are related to electronic transitions, providing information about the compound's structure, concentration, and sometimes its environment.

II.4.3.Scanning Electron Microscope

The primarily surface analysis technique SEM/EDS on powder samples of the materials reported in this work as well as the clay using aZEISS EVA 15 SEM/EDS apparitus of (CRAPC-Ouargal). (Figure4 Annexe 1)provided valuable information on morphology such as the size and shape of individual particles providing information on its physical characteristics. The SEM images have shown the surface topographic characteristics, which are: pores, agglomerates and crystalline structures allowing the understanding of the properties and stability of the material.EDS allowed the qualitative identification of the elements present in the samples. By analyzing the characteristic X-ray spectra emitted by the sample during the excitation of the electron beam and had also provided quantitative information on the elemental composition of the synthetized complex and clay, to determine the relative proportions of the different elements in the different samples we studied.

The ZEISS EVO 15 is characterized by the simultaneous acquisition of up to 4 single photo detectors up to 24000 x 32000 pixels, it is equipped with an advanced SmartSEM control panel with a SE C2DX detector (VP, EP), a SE Everhart Thornley Detectors: SE1 (HV): Reduces spurious SE3 signals and reduces buildup, a door mounted color navigation camera used for navigation monitoring to guide the SEM to the correct sample and area of interest and an infrared camera.

II.4.3.1.Sample preparation

The sample was homogenized to avoid bias and carefully spread on a carbon adhesive tape ensuring a uniform distribution (figure 5 Annexe 1) without clumping or excessive aggregation thereafter covered with a thin layer of conductive material (platine)to dissipate the load during the runusing Metallizer Quorum Technologies (figure 6 Annexe 1).

II.4.4.The BET method

The specific surface area for both FS and CMA was measured using the (Micromeritics 3Flex 5.00) device at the University of Tlemcen, (figure 7, annexe 1). The (Micromeritics 3Flex 5.00) instrument functions by adsorbing nitrogen gas molecules onto the surface of the solid sample. The amount of adsorbed gas is measured at pressureand temperature 200 C°. These data are then used to calculate the specific surface area of the material.BET analysis is performed to determine the specific surface of the material. The statistical evaluation of the BET adsorption curves provided information on the FS's specific surface and pore distribution from the measurements of the nitrogen gas adsorption isotherm.

II.4.5.Structural identification of powders by x-ray techniques

Identification of $(Fe_2(OH)_2(C_4O_4).2H_2O).2H_2O$, CMA, CD and clay formula wereconfirmed by recording of X-ray diffractometers on the powders corresponding to each sample. The apparatus used was aRigaku-binary diffractometer(figure 8, annexe 1) is equipped with a copper anticathode (λ = 1.542 Å) Kα1 = 1,54060 Å, Kα2 = 1,54443 Å, Kβ =1,39225 Å, K α2/ K α1 Ratio = 0,50000 and a θ-2θ goniometer (MiniFlex 300/600), it works in reflection mode where the sample is in rotary motion, and the detector and the source are in mouvement. The collimation of the incident beam is in fixed mode, the appratus is piloted by PDXL softward. Lattice strain and crystallite size can be calculated by using HalderWagner method and Williamson-Hall plot (implemented in PDXL). and geologys univ ouargla . Routine preliminary diffractograms were recorded in the 2θ angular domain with a start-end Position [2θ] = 2.5-60°, Step Size = 0.0200°θ, Scan Step Time = 1.0000 s using Pre-set time Scan Type, Offset = 0.0000°θ. The divergence Slit Type was Fixed and the divergence Slit Size was about 1.0000°. The specimen Length measured 10.00 mm with a receiving Slit Size of 0.1000 mm at 25.00°C. More information on the devise are given in (table 1, annexe 2).

Particle size analysis

Particle size analysis is a fundamental tool for characterizing the particle size distribution of various materials, including sand, soil and powders. This information is essential for evaluating the suitability of materials for specific applications, understanding their behavior in different environments and optimizing their performance.

II.4.7. Multi-parameter device

The pH, temperature(T), and electrical conductivity(EC) of the wastewater were measured using a WTW (multi 9310 IDS) device (Figure .., Appendix 1). The device is equipped with various IDS sensors for pH, T, and ECthat transmit sensor data to the device.

II.4.8. Turbidity Meter

The turbidity of the wastewater was measured using a device WTW(Turb.550), with tungsten lamp , universal power supply 90...250 VAC, single unit with calibration set (standards 0,02 - 10,0 - 1000 NTU), 3 empty cuvettes, optional continuous flow measurement with the flow vessel D-Turb.

II.5. Informatic support

II.5.1.FullProf Suite

FullProf Suite, a program for analyzing and improving X-ray diffraction data. However, the program has "structure determination" features using the simulation method to improve overall performance[56]. FullProf is made up of crystallographic programs mainly developed for Rietveld analysis (refinement of the structure profile), and has powerful tools for the indexing of the recorded diffractograms, by which we have indexed our data and assessed the quality of our synthesized products.

II.5.2.HighScore Plus and QualX

The recorded data are processed using the HighScore Plus and QualXprograms, by which the databases are consulted, and were used for the identification of peaks and the selection of iso-structural compounds. The databases are provided with the QualX program (PDF–14, ICSD, CDD, COD…)

II.5.3.Mercury 3.8

Mercury 3.8 program was used for reading and viewing rotating and translating crystal structures in three dimensions display. The theoretical diffractograms are also calculated using this program and are used for the superposition of experimental and theoretical data to facilitate comparisons.

In order to visualize the crystal structure of the compounds we synthesized and understand their properties, we used Mercury program, which is a free and open source software package for visualizing, analyzing, and processing crystallographic data. It was

developed by the Cambridge Crystallographic Data Center (CCDC) and is used by researchers in a variety of fields, including chemistry, materials science and biology.

Mercury translates the crystallographic information (CIF) of compounds into a variety of graphical formats for crystal structures, including 3D models, 2D plots, and tables. It also calculates bond lengths, angles, and surface areas. Manipulates crystal structures, such as creating new structures, and merging structures. , calculate properties and generate reports on crystallographic data.

II.5.4.ImageJ software

ImageJ is a Java-based program for image processing and analysis. It's a useful tool for graphic designers due to its support of multiple formats and various functions. This program was used in the calculation of particle sizes using images from scanning electron microscopy analysis

II.5.5.Origin

A proprietary computer tool called Origin is used for data processing and interactive scientific visuals. It is made by OriginLab Corporation and requires Windows to function. Statistics, signal processing, curve fitting, and peak analysis are examples of data analytics in Origin. We used this program in parallel with ImageJ in the particle size calculation.

II.6. Database

The COD PDF andICSD were used in this work to identify and characterize materials.

II.6.1.COD powder diffraction file database

The COD powder diffraction file database (COD PDF) is a collection of powder diffraction patterns of inorganic, organic, and metal-organic compounds. It is the world's largest and most comprehensive powder diffraction database, containing over 500,000 patterns.

II.6.2. ICSD (Inorganic crystal structure database)

The Inorganic crystal structure database (ICSD) is a database of inorganic crystal structures and information on all inorganic crystal structures published since 1913, including elements, minerals, metals and intermetallic compounds.

II.7.Crystallographic Data File (Cif)

Cif is a standard format for storing and exchanging crystallographic data. They are typically used to store the crystal structure of a material, and can be used to store other information, such as the experimental data used to determine the crystal structure.There are a number of software packages that can be used to read and write CIF files, such as Mercury and VESTA.

PART THREE

CHAPTER THREE : $NH_4[Cd(C_2O_4)2H_2O]$

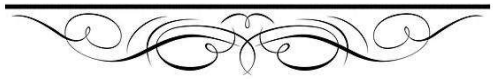

Investigation of $NH_4[Cd(C_2O_4)2H_2O]$ in Nitrite removal fromsynthtique wastewater

Introduction

This chapter introduces a novel compound, $NH_4[Cd(C_2O_4)_2].2H_2O$, belonging to the $NH_4[Ti(C_2O_4)_2].2H_2O$ family, where cadmium replaces titanium. Employing RDX, IR, and SEM techniques, the compound's identity was confirmed, and its efficacy in removing NO_3 and Congo red from water was evaluated. The crystalline structure of $NH_4[Ti(C_2O_4)_2].2H_2O$ was elucidated by (Englishe al. 1993)[1] and later by Shue.h.s et al. in 1996 [2] in order to examine both the charge density distribution and the wavelength influence in these studies.Weares English e al. 1993 were interested about its structure, magnetic and spectral properties of the title compound have been reported recently

III.1.Synthesis of $NH_4[Cd(C_2O_4)_2].2H_2O$ (CD)

A powder of Cadmium chloride monohydrate ($CdCl_2 \cdot H_2O$) (0.20132 g, 0.001099 mol) was dissolved in distilled water (5 mL) and was added to a solution of Ammonium oxalate monohydrate ($C_2H_8N_2O_4 \cdot H_2O$) (0.14212 g, 0.001 mol) in distilled water (5 mL) under stirring at room temperature, subsequently a solution of acetanilide 0.1351 g was added drop by drop to the preceding homogeneous solution. The final ph of the solution is 1.7. A white precipitate was obtained. The precipitate was then washed with distilled water, and then dried.

III.2.Identification of $NH_4[Cd(C_2O_4)_2].2H_2O$

III.2.1.InfraRed Spectroscopie analysis

Figure III.1 depicts the infrared spectrum of the sample acquired using an infrared spectrometer in the 400-3800 cm^{-1} range. The spectrum exhibits a variety of peaks which collectively represent the functional groups present in the complex. Spectral profile of theproduct shows the absence of peaks in the range (1700-1800) $cm^{-1}$and (2500-3300) cm^{-1}indicating respectively the elongation of the C=O bond and the elongation of the O-H bond of aliphatic acid. These data are consistent with the results of powder X-ray diffraction because the oxygene carbon bonds in this compound are characteristic of cordination polyhedra. A broad absorption band at around 3588.326 cm^{-1}due to the O-H stretching vibrations of the water molecules and can also be assigned to the free elongation N-H in amonium. Moreover a narrow absorption band at around 1646.401 cm^{-1}due to the C=C stretching vibrations of the oxalate ions [3].Whereas, While the wide and low absorption band at about 2108,199 cm^{-1}attributed to stretching vibrations C=O as well as to 1646,4 cm^{-1} of the

acetanilide ketone group. a wide absorption band with several narrow peaks at about 3298,656 cm^{-1} due to the N-H stretch vibrations of the acetanilide.

The sharp and narrow absorption band shown at 788,847 cm^{-1}represents the symmetric tension vibration of the C-C bond in the oxalate ion, while The metal-oxygen bond, which is often in the range of 490-750 cm^{-1}, which in turn confirms the existence of an organic-inorganique compound [4,5]This indicates that the product marks the presence of a second minority phase; it is a low recrystallization of acetanilide [6].

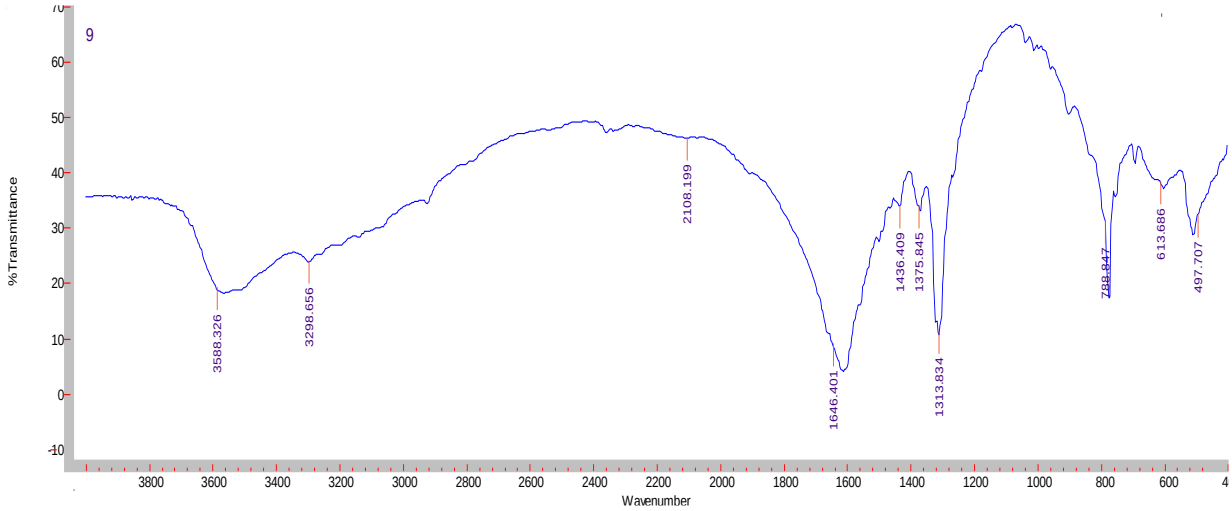

Figure.III.1: Infrared spectrum of the prepared compound

There have been numerous unsuccessful attempts to create a chemical that combines acetanilides, oxalate anions, and metal cations at the same time. The chemical was wached many imes by ethanolIn order to ensure the dissolution of the whole wolf in the compound to produce a pure product.

III.2.2.Elemental analysis

The product grain morphology of the pure product was assessed using SEM microstructure of the CD particles as shown in Figure III.2 and reveals the presence of crystallite agglomerations. These agglomerates include fine opaque white crystallite and Homogeneous with a Cuboid regular shape vertically nested into each other.The powders are all different shapes and sizes. The grain sizes were calculated using Image software. The average value is 30 micrometer which indicates that the material is micrometer

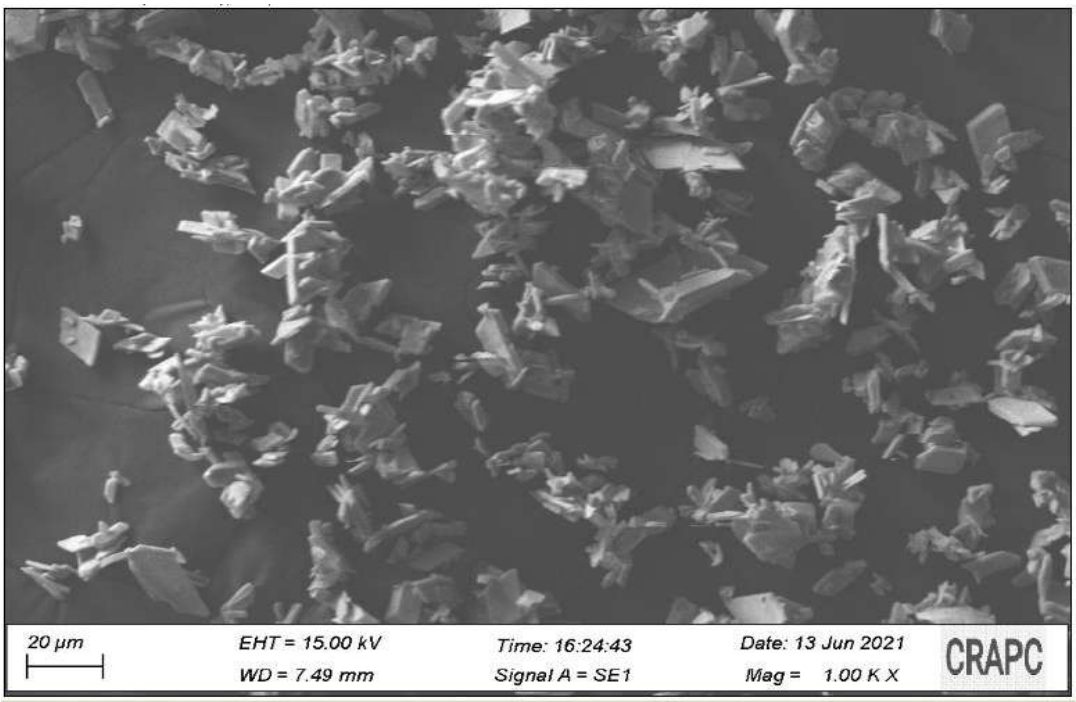

Figure.III.2: SEM image of the compound CD

Table III.1 illustrate the quantitative and qualitative percentage of mass and atomic intensity total of elements that made composition of the CD sampleand the spectrum offigure III.3 reveals the intensity of each element present in the sample.

Table.III.1: The quantitative and qualitative composition of the CD sample recorded by the EDS device

Element	% ofmass	%atomic	Intensitytotal
C K	31.81	54.53	375.33
O K	30.11	38.75	164.59
N M	3.19	0.33	13.50
Cd L	34.88	6.39	112.89

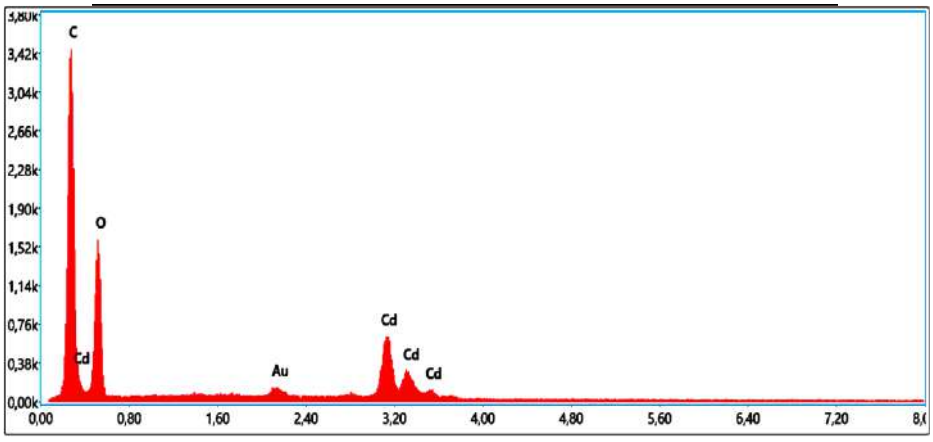

Figure.III.3:EDS spectrum for CD sample

From the table III.2, we can deduce that the sample comprises the following elements: carbon C(31.81%), oxygen O(30.11%), Nitrogen N(3.19%), and cadmium Cd(34.88%).This elemental composition aligns with the conclusion that will be presented from the DRX analyses.

III.2.3.Results of crystal structure analyzeby X-ray diffraction

Figure III.4 depicts the X-ray diffraction (XRD) spectrum of the sample, recorded within the examined angular range of (2θ) from 10 to 80 degrees. Diffracted X-rays are transformed into signals that are amplified and plotted as a histogram (I = f(2θ)). The X-ray source and a scanning angle of incidence θ allow for a comprehensive representation of the sample's crystal structure, providing insights into its lattice dimensions.

III.2.3.1. Qualitative Analysis Results

The experimental X-ray diffractogram of the prepared compound (red) was compared to the containt of ICDD (PDF-2 Release 2014 RDB) database, and was found that it agree with the DB card number 01-075-7257 as shown in table III.2 which summarizes the specific details of phase identification (formula, figure of merit, database, and card number).However, non-attributability of some pics was observed, indicating impurities in the sample.

Table.III.2: Specific details of phase identification

Phase name	Formula	Figure of merit	Phase reg. detail	DB card number
Ammonium dioxalatotitanate(III) dihydrate	$(NH_4)(Ti(C_2O_4)_2)(H_2O)_2$	1.381	ICDD (PDF-2 Release 2014 RDB)	01-075-7257

Using the information obtained from the FT-IR analysis on the presence of impurities in the sample that are attributed to acetanilide due to having determined the functional groups C=O and N-H in the results, we searched in IUCR articles on the crystal structure of acetanilide [7-8], After downloading the cif crystal data file N° 614360 [10] an x-ray diffractogram was calculated using Mercury 3.8 and superimposed with the experimental as shown in the figureIII.4.

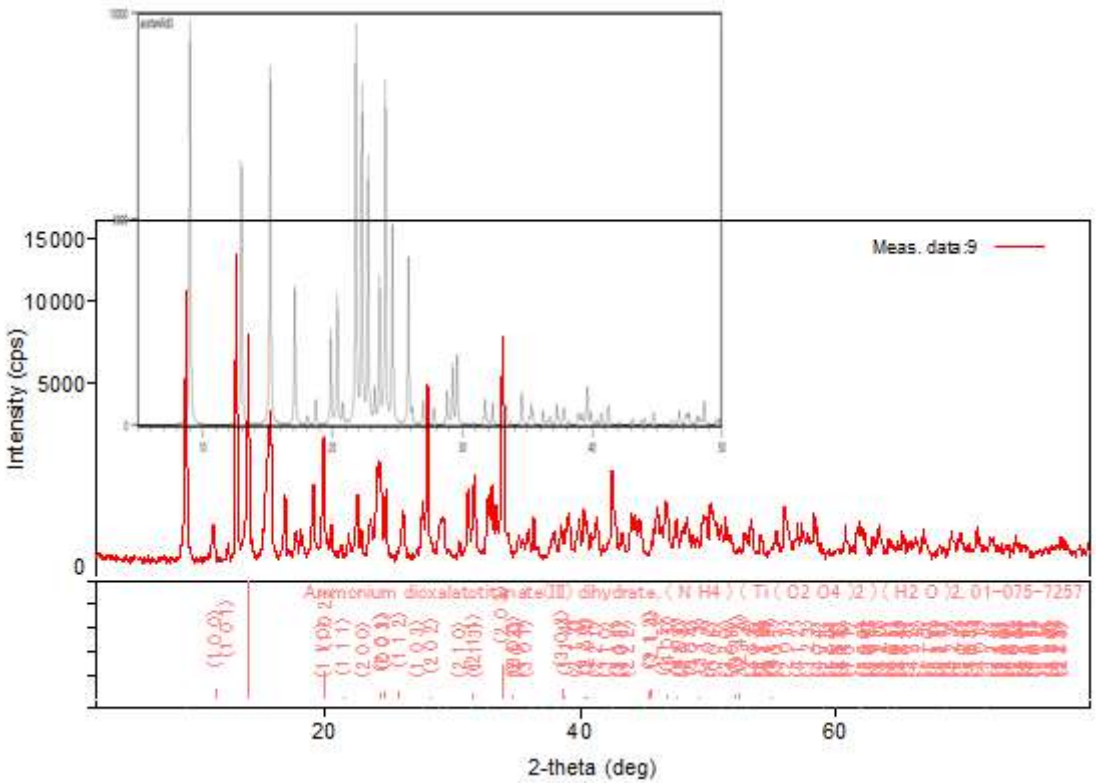

Figure.III.4: X-ray spectrum of the prepared sample (red) and trace of acetanilide (black)

III.2.3.2.Quantitative Analysis Results

Table III.3 and Figure III.5 summarize the automated quantitative characterization of the prepared compound. The data indicates that the sample comprises two distinct phases. The phase with the highest percentage of presence was identified, and its formula corresponds to that of the compound $NH_4[Ti(C_2O_4)_2].2H_2O$, with the Ti atom replaced by Cd. These results show that the predominant compound is $NH_4[Cd(C_2O_4)_2].2H_2O$by 82.7% of the total product, while the remaining 17.3% of the impurities is acetanilide, Which was then dissolved by waching the product withethanol.

Table.III.3: The two phases involved in the chemical composition of the sample under analysis

Phase	The proportion in the sample (%)
Ammonium dioxalato chrome(III) dehydrate	82.7(10)
Acetanilide	17.3(09)

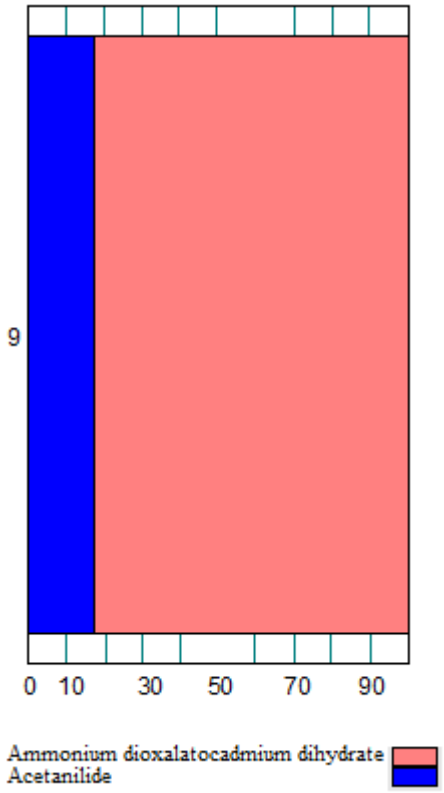

Figure.III.5:hystogramme of the qualitative composition of the sample

III.2.3.3.Indexing of the X-ray spectrum

We find in Table III-6 the results of indexing the X-ray spectrum for the phase with the overall formula $NH_4[Cd(C_2O_4)_2].2H_2O$and comparing it with its counterpart from the scientific publication of Shaw and companions for the compound $NH_4[Ti(C_2O_4)_2].2H_2O$We make sure that our characterization is correct.

Table.III.4: X-ray indexing results for the sample and compound of the scientific publication

Phase name	a(A)	b(A)	c(A)	V(A^3)	Space grope	Cell sitting	ref
$(NH_4)(Cd(C_2O_4)_2)(H_2O)_2$	8.94348	8.94348	10.8424	751.052	P6222	Hexagonal	This work
$(NH_4)(Ti(C_2O_4)_2)(H_2O)_2$	8.947	8.947	10.898	755.4	P6422	Hexagonal	1996 [2]

III.2.3.4. Cristallite size and lattice strain (Williamson-Hall method)

The Williamsons Hall (WH) method is a straightforward approach that may be used to calculate intrinsic stress in relation to particle size. It takes into account the impact of deformation-induced XRD peak enlargement [11]. It states that the size and microstrain of the

crystals cause the physical line widening of the X-ray diffraction peak, and the overall widening can be expressed as,

$$FW(s)\times\cos\theta = K\lambda size + 4\times strain\times\sin\theta$$

The strain component is obtained from the slope and the particle size component is obtained from the y intercept when we plot FW(s)×cosθ on the y axis against sinθ on the x axis.

The sample's strain and particle size are computed using the Williamson Hall plot, taking into account high intensity peaks (figure III.6) provide WH plots. Table III.5 provide the title compound grains' particle size (D) and strain (e) for the indicated peaks.

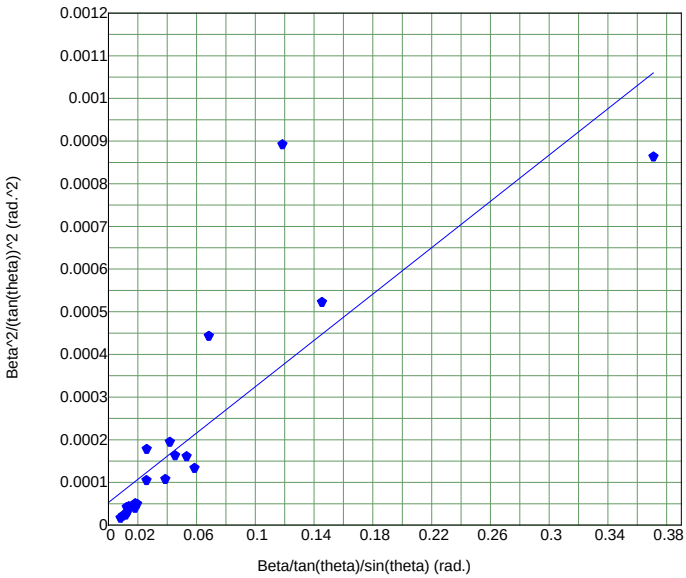

Figure.III.6: WH plots.

Table.III.5: Grains' particle size (D) and strain (e).

Phase name	Crystallite size(A)	Strain(%)
Ammonium dioxalatotitanate(III) dihydrate	347(14)	0.000000
Acetanilide	596(90)	0.18(7)

III.4. Description of the Crystal Structure

The crystal structure of the compound was investigated using the Mercury 3.8 program, based on the X-ray diffraction data obtained from the powder sample and the crystal data file (cif.) for the compound $NH_4[Ti(C_2O_4)_2].2H_2O$reported by Shu et al.

III.4.1.Asymmetric Molecular Unit:

The analysis of the asymmetric molecular unit of the compound (Figure III.7) revealed that it comprises one titanium atom, three oxygen atoms, two carbon atoms, two hydrogen atoms, and one nitrogen atom. This corresponds to one titanium atom, half of an oxalate ion $(C_2O4)_2$, one-quarter of an ammonium ion $(NH_4)^+$, and half of a water molecule (H_2O).

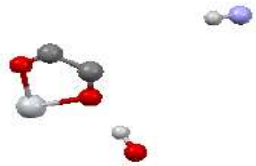

Figure.III.7: Asymmetric Molecular Structure

III.4.2.Molecule (Molecular Unit)

Figure III.7-a depicts the interconnection system between the asymmetric units in the compound to form the molecular units, as it appears that the central metal ion is surrounded by eight oxygen atoms, with each two atoms coming from the oxalate ion to give us a multifaceted geometric structure (Anti-prism with square base). To construct the molecular unit, each metal atom in the asymmetric unit is joined to the neighboring unit by two oxygen atoms of the oxalate ion.

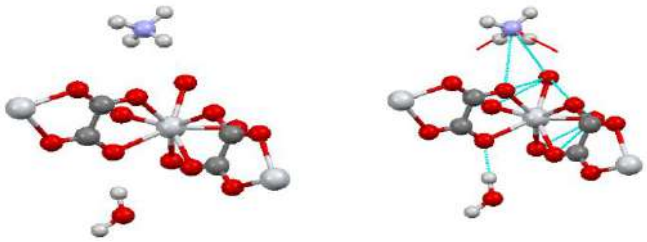

a b

Figure.III.8: Molecular unit of the prepared compound

III.4.3.primary cell's

The basic cell comprises six molecular units, resulting in a three-dimensional structure rich in hydrogen bonds, which occurs from the arrangement of ammonium ions and water molecules, and thus improves the structure's strength, as seen in Figure III.9.

While figure III.10 illustrates the primary cell's projection along the axes a, b, and c by clarifying the nature of the pores existing within the chemical edifice of the compound, which

could subsequently give information on the material's properties related to pollutant degradation or adsorption. It should be noted that the pore sizes were measured using the mercury 3.8 software.

The aforementioned substance has two types of tunnel-shaped pores (figure III.9): the first is completely empty and has the dimensions (8939 Å -8527 Å) at its base, while the second contains templates (water molecule and ammonium cation)(11,77 Å - 8,758 Å). These templates can be discarded using cation exchange without affecting crystallinity [2]. In this context, the phenomenon observed in this work for this compound is the vacancy of the contain of tunels without being replaced by the templates target (nitrate).

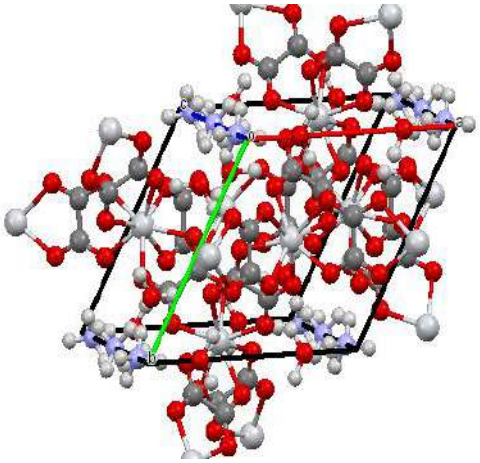

Figure.III.9: Primary network structure

Figure.III.9shows the projections of the primary cell at the level of the three axes a, b and c

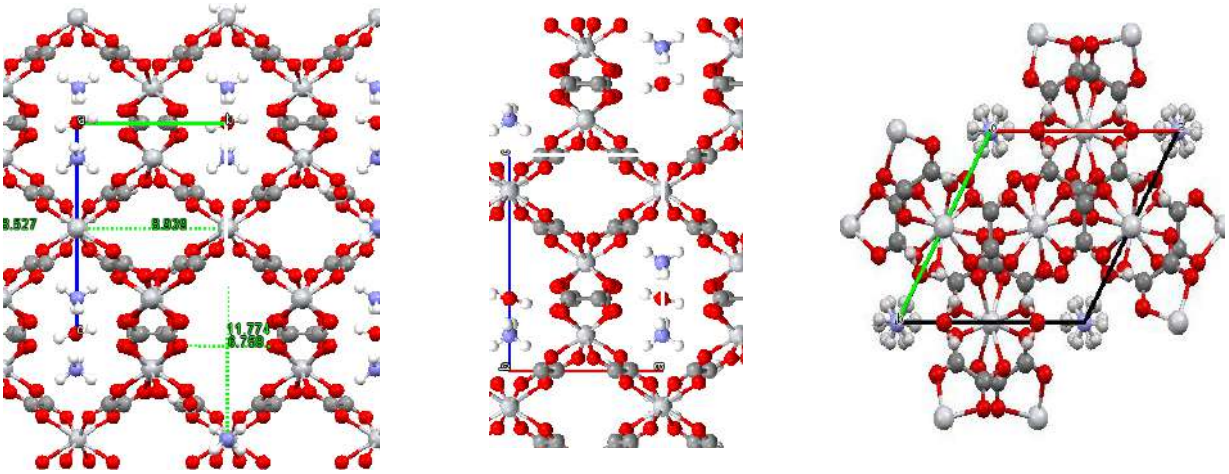

The axis a The axis b The axis c

Figure.III.10: Projection of the primary cell along the axes a, b, c

III.4.4.The role of hydrogen bonds in the cohesion of the compound

Hydrogen bonding is crucial to the cohesiveness of this compound's crystal structure. They are intermolecular in nature, having formed between the oxygen atoms in water molecules and the hydrogen atoms in ammonium ions on the one hand. The length of the bonds formed by water molecules lying within the plane of space was 1.870 Å. The length of those produced by water molecules organized along the axes was 1.869 angstroms.

In addition, hydrogen bonds arise between the oxygen atoms located on the level of the oxalate ion and the hydrogen atoms located in the water molecule on the other hand. The length of these bonds was 1.818 Å. As shown in Figure III.11.

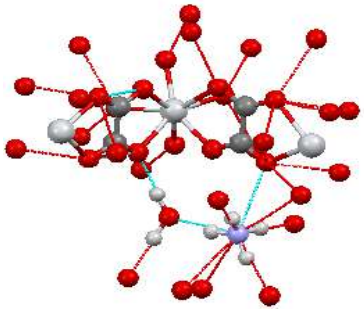

Figure.III.11: Representation of the hydrogen bonds formed at the level of the crystal structure of the compound

III.5.BET interpretation

A FIGUREIII-12 andIII-13 depicts the method surface erea and pore structure of the synthesized compoud as determined by the N_2 adsorption/desorption isotherm measurement at 77,099 K, and Table III-6display the results of a BET (Brunauer-Emmett-Teller) analysisand summarizes the characteristic results of the measurement method.First the sample was degassad for about 2 h at 2230K.

Table.III.6: Characteristic resultsof Brunauer-Emmett-Teller analysis

	Surface Area (m^2/g)	Pore Volume (cm^3/g)	Pore Size (nm)	Pore Size (Å)
Adsorption	6,7945	0,195304	14,9768	149.768
Desorption	9,6711	0,195439	14,9768	149.768

According to the data obtained the adsorption curve of (CD1) corresponds to a Type II isotherm, as per IUPAC classification.The measurement of the amount of active area per unit mass determined by the amount of nitrogen gas.adsorbed on a surface at a pressure by the BET analysis studied here shows that the specific area is 6.7945 m^2/g in adsorption and

9.6711 m^2/g in desorption. The measurement of the total pore volume per unit mass determined by the amount of gas adsorbed on a surface at nitrogen pressure gives pore volumes of 0.195304 cm^3/g in adsorption and 0.195439 cm^3/g in desorption.

This means that the specific surface area and pore volume values obtained indicate that the analyzed substance is porous, with a slightly higher pore volume in desorption than in adsorption.

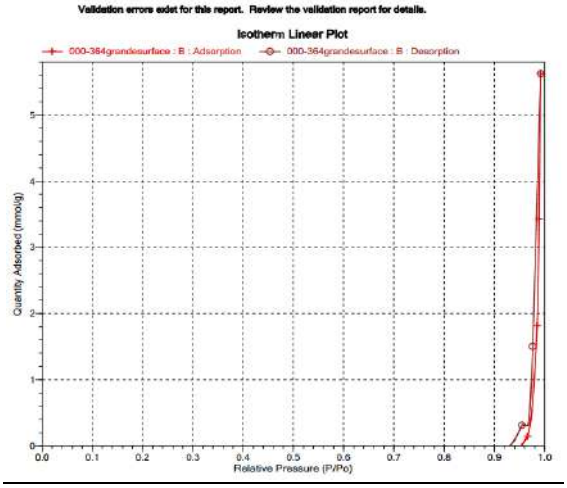

Figure.III.12: isotherme adsoption BET Plot

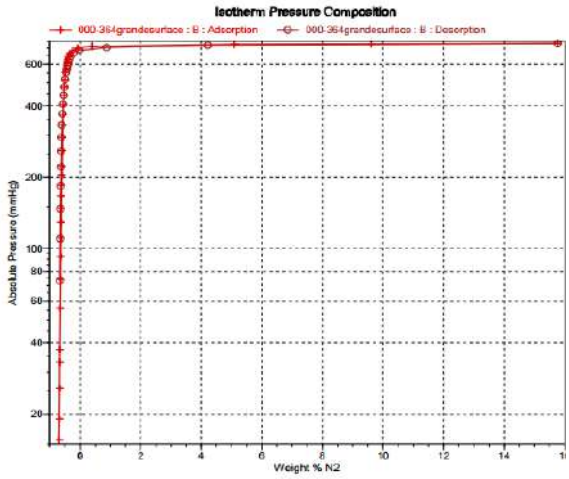

Figure.VI.13: isotherme pressure composition

In both adsorption and desorption, the measured mean pore diameter in the examined material is 14.9768 nm. This signifies that the substance has a uniform pore size, implying that the substance is made up of pores of identical size.

These results suggest that the product has the potential to be a medium catalyst. However, additional studies are needed to confirm this hypothesis.

III.6.Removing nitrates from synthetic wastewater

III.6.1.Preparation of the contaminated medium

To prepare the contaminated medium, a precise amount of potassium nitrate (0.0625g) was carefully weighed and transferred to a 250 ml volumetric flask. Distilled water was then added to the flask until it reached the volumetric mark. The flask was securely capped and thoroughly agitated using a shaking device until the potassium nitrate completely dissolved.

Prior to conducting the experiments, we employed the program DesignExper to identify the optimal values for the factors influencing the product's removal performance, (contact time, adsorbent mass, and shaking speed). This was achieved by designing suitable experiments based on the previously mentioned data and determining the number of experiments required to obtain precise results.

The tables III.7present the values of the variables, the number of experiments conducted, and the corresponding results.

Table.III.7: Values given to the program for design appropriate experiments

independent variable	levels		
	-1	0	+1
mass of product (CD) (g)	0.2	0.4	0.6
residence time (min)	20	40	60
stirring speed (t/min)	400	600	800

Table.III.8: The experiments conducted.

Test	Factor1	Factor2	Factor3	volume	Results1
	Mass	Time	Agitation	(10ml)	(mg/l)
0	/	/	/	/	14
1	-1	0	-1	/	13.6
2	0	-1	1	/	17.8
3	-1	-1	0	/	15.2
4	1	0	1	/	16.5
5	0	0	0	/	17.1
6	-1	1	0	/	15.3
7	0	-1	-1	/	18.5
8	1	1	0	/	16.5
9	0	1	-1	/	19.1
10	1	-1	0	/	13.5
11	-1	0	1	/	19.6
12	1	0	-1	/	11.3
13	0	0	0	/	17.1
14	0	1	1	/	18.2
15	0	0	0	/	17.1

Throughout the experiments presented in table III-8, a constant volume of 10 ml of potassium nitrate solution was utilized for each trial, while the remaining variables were adjusted as indicated.

III.6.2.Result

From the results shown in the table, we note that the values obtained for nitrate concentrations from all experiments are close, other than some high values. Nitrate absorption was recorded in only 3 experiments and at a very slight rate. The best result of the trial was 12 with a catalytic mass of 0.6 grams and a contact time of 40 minutes. Vibration speed: 400rpm. However, this cannot be said to be a good outcome. While an increase in the concentration of nitrates in the middle has been recorded, we can explain the emergence of an increase of nitrates into the NO_3 forming from $NH_4[Cd(C_2O_4)_2].2H_2O$as a catalyst in a KNO_3 aqueous solution through an interaction mechanism that includes the following steps:

The formation of NO_3 from $NH_4[Cd(C_2O_4)_2].2H_2O$can be interpreted as a catalyst in KNO_3 's aqueous solution through a reaction mechanism where the interaction of nitrate ions with the $NH_4[Cd(C_2O_4)_2].2H_2O$catalyst, leads to the formation of nitrous oxide (NO) and hydrogen ions (H^+). According to the following formula

$$NH_4[Cd(C_2O_4)_2].2H_2O + NO_3^- \rightarrow NO + NH_4^+ + Cd(C_2O_4).3H_2O(1)$$

The templates NH_4 can also be removed either by cation exchange or by thermal methods without losing the crystallinity [2].It is followed by nitrous oxide interaction with water, leading to the formation of nitric acid (HNO3). According to the following formula.

$$NO + H_2O \rightarrow HNO_3(2)$$

The nitric acid formed in the previous step disintegrates into the aqueous solution, leading to the formation of nitrate ions (NO_3^-) and hydrogen ions (H^+). As follows

$$HNO_3 \rightarrow H^+ + NO_3^-(3)$$

This explains why the compound was unable to continue to remove the nitrate contaminant from the medium.

On the other hand, the result of the chemical reaction (1) which was$Cd(C_2O_4).3H_2O$[12]corresponds to what was obtained experimentally when recording the X-ray diffractogram for the catalyst as appeared in figure III-14.Diffractometers reveal that the compound gradually abandons water and ammonium molecules over time without compromising the critallin network's cohesion and order.

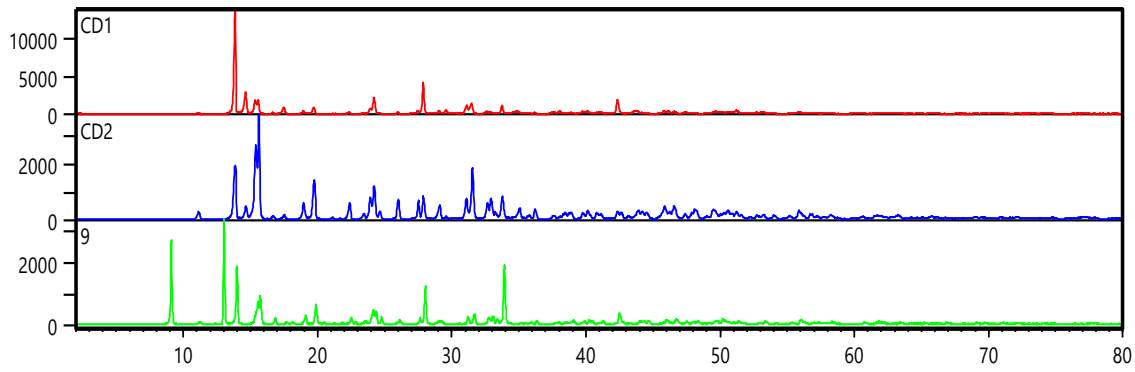

Figure.III.14: X-rays diffractometers of initial product (green) , after being washing with ethanol to disolve acetanilid, (bleu), calist residu (red).

Figure.III.14. shows the arrengemen of the pore channels befor and after losing water and amonium cation

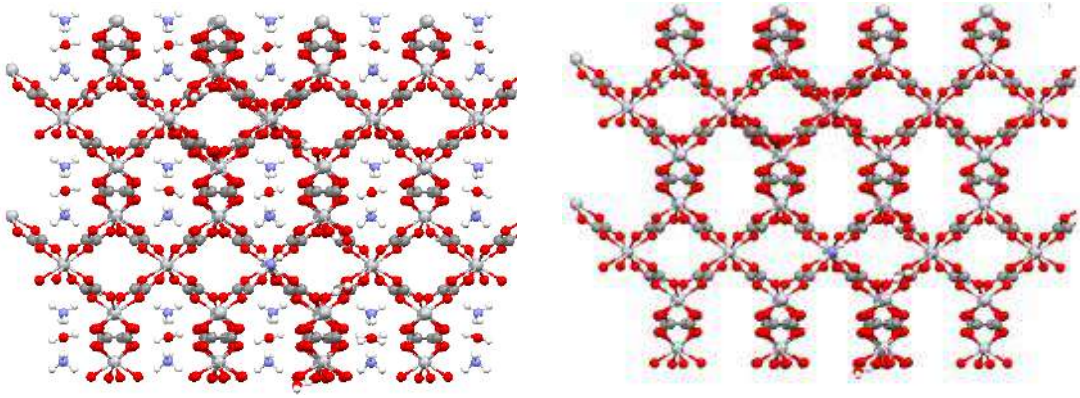

Figure.III.15: Representation showing the pore channels befor and after losing water and amonium cation

III.7.Removing Congo red from synthetic wastewater

The photocatalytic activity of the $NH_4[Cd(C_2O_4)_2].2H_2O$catalyst on the breakdown of Congo Red dye in aqueous solution was investigated in this study under three conditions:Fenton, photocatalysis, and photo-Fenton degradation, according to the parameters conditions reported in table III.9.

Table.III.9: Operating conditions of different parameters.

	pH	W (CD1) (g)	(CR) (mg/L)[13]	$V_{(H2O2)}$ (µL)	T (min)	V_{CR} (mL) [12]
Adsorption	7	0.05	24.5	100	120	100
Fenton	7	0.05	24.5	100	90	100
Photocatalysis	7	0.05	24.5	100	30	100
Photo-Fenton	7	0.05	24.5	100	30	100

III.7.1. Adsorption

The adsorption of CR on the catalyst $NH_4[Cd(C_2O_4)_2].2H_2O$ was carried out at room temperature by immersion of 0.05g of the catalyst (CD1) in 100 mL of the CR solution previously prepared in a beaker under continuous stirring for 120 min. The operation consists in taking 4 mL of the mixture at 15-minute intervals from the reaction beaker (figure III-15), the samples were centrifuged at 6000 rpm for 5 minutes, and the supernatant was analyzed by UV-Visible spectrophotometry in the wavelength range 280 to 700 nm. The maximum absorbance of the studied dye was recorded at 496 nm [14], which is attributed to the interaction of the chromophore bond (N = N).

III.7.2.Fenton's process

For the Fenton process, the catalyst was pre-equilibrated in adsorption for 30 minutes before initiating the reaction with the addition of 100 µL of H_2O_2 (30%) and taking samples at 10 minute intervals for a total of 90 minutes to be analyzed by UV-Visible spectrophotometry.

III.7.3.Photocatalysis

Photocatalysis was carried out in complete darkness for 30 minutes. Following complete adsorption of the synthesized catalyst in a CR solution, samples were collected at 10-minute intervals for UV-Visible examination (λ = 254 nm).

III.7.4.photo-Fenton

The photo-Fenton process was analogous to photocatalysis, but it began with the addition of H_2O_2(100 µL) in the presence of UV light. Following steps include sampling at 10 minute intervals for UV-Visible spectrophotometry analysis in accordance with the photocatalytic reaction method.

III.7.5.Result

Congo Red is a diazo dye that is often used as an indicator in various chemical experiments. It has a large conjugated system that allows it to exhibit different colors based on its interaction with substances [15].

To our knowledge, the properties of the compound (CD1) concerning the adsorption of Congo Red are not documented. However, in general, Congo Red is known to interact with various substances through ionic and/or hydrogen bonding interactions. To assess the adsorption properties of (CD1) with Congo Red, we involved an experimental studying marqued by the slow changes in the color of Congo Red solution before and after contact with the compound.

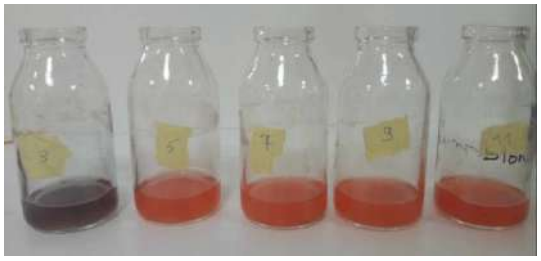

Figure.III.16: Photocatalytic degradation of Congo red under visible light irradiation using $NH_3[Cd(C_2O_4)_2].2H_2O$

The kinetics of coloran CR adsorption by catalyst (CD1) is depicted in Figure III.16. The adsorption-desorption equilibrium is attained after 30 minutes of response with an adsorption rate of 11.25% in this figure. This shows that (CD1) exhibits minimal adsorbent behavior.Before each catalytic reaction, the system was given 30 minutes to attain adsorption equilibrium.

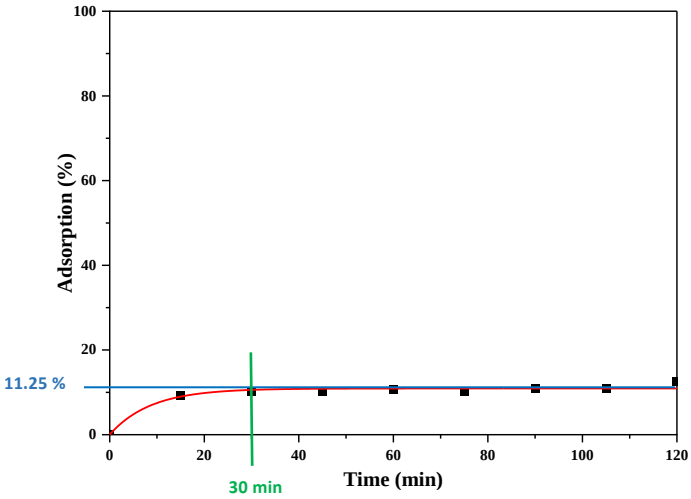

Figure.VI.17: The kineticsof coloran CR adsorption

The Fenton reaction in the presence of (H_2O_2) was not particularly successful, as seen in FigureIII.17. A considerable amount of dye worth 98% has not yet been degraded after 113 minutes of reaction. The second photocatalysis approach showed a small improvementunder dark condition, we see the removal of 23%, as 77% of the dye was not destroyed.

Higher degradation efficiency was observed for the photo-Fenton reaction, where degradation reached 77% at 92 min, indicating that the photocatalysis combination with the Fenton system produces more HO. These findings suggest that the photo-fenton reaction is the most effective for CR breakdown.

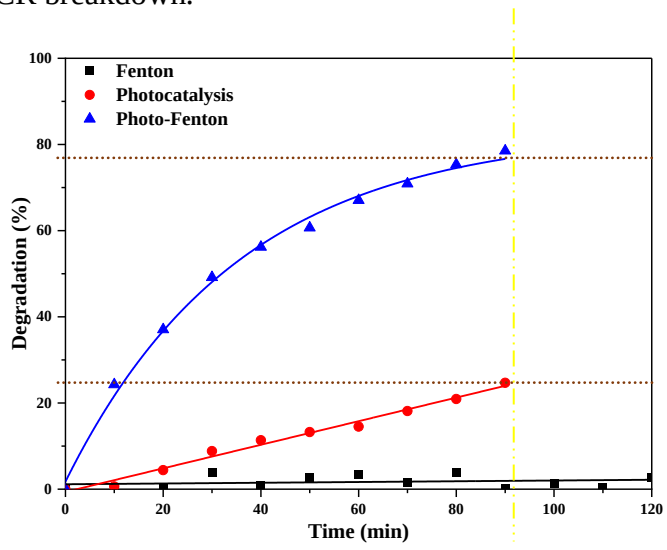

Figure.III.18:CR degradation efficiency in the presence of (CD1) catalyst in the various Advanced Oxidation Processes

In general, the photo-Fenton process involves the formation of highly reactive hydroxyl radicals (•OH) by the reaction of hydrogen peroxide (H_2O_2) with catalysts when exposed to

UV or visible light. These hydroxyl radicals are potent oxidizing agents that can destroy organic pollutants such as Congo Red dye by oxidation [16].

Cadmium-based compounds have been studied in photocatalytic reactions due to their ability to interact with light and generate reactive species [17-19]. In this chapter, $NH_4[Cd(C_2O_4)_2].2H_2O$ has shown to act as a catalyst (Figure III-17), which explains that it has potentially provided sites for the generation or activation of hydroxyl radicals in the photo-Fenton process.The Congo red degradation mechanism employing photo-fenton reation could comprise the following steps (figure III-18):

- When exposed to UV-visible light, the $NH_4[Cd(C_2O_4)_2].2H_2O$ catalyst reacts with hydrogen peroxide (H_2O_2), leading to produce hydroxyl radicals (•OH):

$$H_2O_2 + NH_4[Cd(C_2O_4)_2].2H_2O \rightarrow \bullet OH \text{ radicals}$$

- The hydroxyl radicals (•OH) produced assault the Congo Red dye molecules. Through oxidation reactions, these radicals degrade the dye's chemical structure, resulting in breakdown into smaller, less toxic compounds or even mineralization to carbon dioxide and water.

$$\bullet OH + \text{Congo Red} \rightarrow \text{Dye degradation}$$

- The degradation procedure was repeated until up to 77% of the dye molecules were broken down into chemicals.

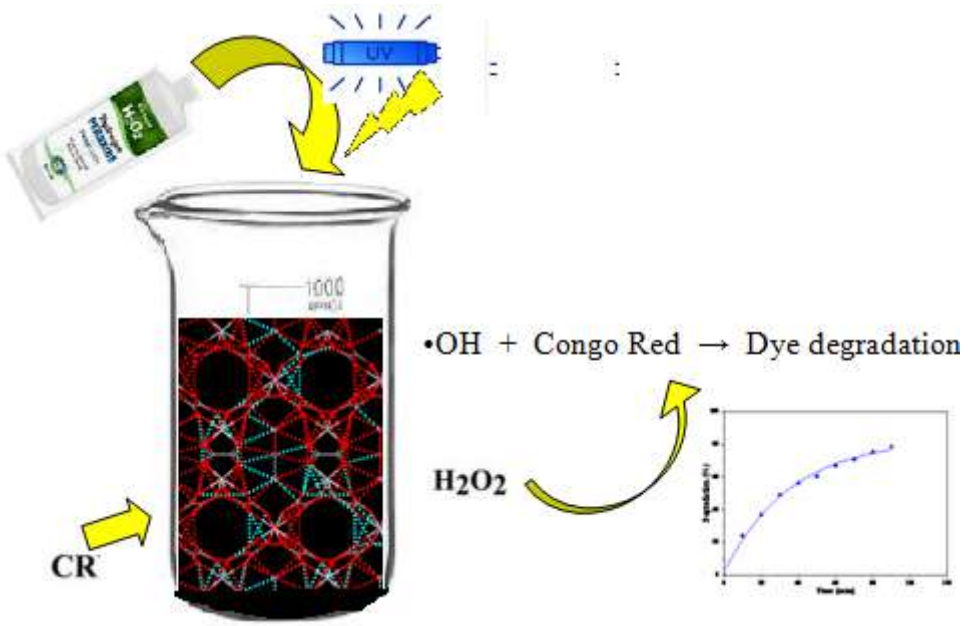

Figure.III.19: A schematic representation of CR deterioration over a $NH_4[Cd(C_2O_4)_2].2H_2O$ photocatalyst when exposed to UV light.

Conclusion:

During this part of our research, we succeeded in characterizing the substance with the formula $NH_4[Cd(C_2O_4)_2].2H_2O$. This was done using spectroscopic analysis techniques with the aim of determining its chemical composition quantitatively and qualitatively, identifying the vibrations of functional groups in the infrared field, and characterizing its crystal structure based on X-rays.

This compound's catalytic activity was initially tested to remove scattered nitrate in an aqueous medium; the results showed a low return of elimination, indicating that it was unsuitable for this mission. Next, the compound's catalytic activity was tested to degrade CR; this test produced positive results but required the use of the photo-Fenton process.

[1] English, R. B.; Eve, D. J. Ammonium Di-μ-Oxalatotitanate(III) Dihydrate: An Eight-Coordinate, Polymeric Titanium(III) Complex. *Inorganica Chimica Acta***1993**, *203* (2), 219–222. https://doi.org/10.1016/S0020-1693(00)81660-6.

[2] Sheu, H. S.; Wu, J. C.; Wang, Y.; English, R. B. Charge Density Studies in NH4[Ti(C2O4)2].2H2O Crystals at Two Wavelengths. *Acta Cryst B***1996**, *52* (3), 458–464. https://doi.org/10.1107/S0108768195012900.

[3] Wyncke, B.; Brehat, F.; Hadni, A. Spectres d'absorption de l'acide oxalique dihydraté dans l'infrarouge lointain. *J. Phys. France***1975**, *36* (9), 877–882. https://doi.org/10.1051/jphys:01975003609087700.

[4] Olczak-Kobza, M. IR Spectra, X-Ray Diffraction Studies and Thermal Analysis of Cadmium(II) Complexes with o-Aminobenzoic Acid and Imidazoles. *Journal of Analytical and Applied Pyrolysis***2007**, *78* (2), 400–405. https://doi.org/10.1016/j.jaap.2006.10.003.

[5] Sivakumar, S.; Venkatesan, A.; Soundhirarajan, P.; Khatiwada, C. P. Synthesis, Characterizations and Anti-Bacterial Activities of Pure and Ag Doped CdO Nanoparticles by Chemical Precipitation Method. *Spectrochimica Acta Part A: Molecular and Biomolecular Spectroscopy***2015**, *136*, 1751–1759. https://doi.org/10.1016/j.saa.2014.10.078.

[6] Singh, B.; Thakur, A.; Kumar, M.; Verma, S. K.; Jasrotia, D. Structural and Optical Properties of Inorganic–Organic Hybrid Material of Acetanilide Tetrachloromercurate(II). *J Mater Sci: Mater Electron***2017**, *28* (14), 10007–10011. https://doi.org/10.1007/s10854-017-6758-0.

[7] Brown, C. J.; Corbridge, D. E. C. The Crystal Structure of Acetanilide. *Acta Cryst***1954**, *7* (11), 711–715. https://doi.org/10.1107/S0365110X54002174.

[8] *Crystal Structure of Acetanilide at 15 and 295 K by Neutron Diffraction. Lack of Evidence for Proton Transfer along the N-H.cntdot..cntdot..cntdot.O Hydrogen Bond | The Journal of Physical Chemistry*. https://pubs.acs.org/doi/10.1021/j100044a009 (accessed 2023-12-20).

[9] Brown, C. J. Further Refinement of the Crystal Structure of Acetanilide. *Acta Cryst***1966**, *21* (3), 442–445. https://doi.org/10.1107/S0365110X66003128.

[10] Tsiaousis, D.; Munn, R. W.; Smith, P. J.; Popelier, P. L. A. Polarizability of Acetanilide and RDX in the Crystal: Effect of Molecular Geometry. *Chemical Physics***2004**, *305* (1), 317–323. https://doi.org/10.1016/j.chemphys.2004.07.013.

[11] *Warren B. E. ; Averbach B. L. The Separation of Cold-Work Distortion and Particle Size Broadening in X-Ray Patterns .J. Appl. Phys. 23, 497 (1952) https://doi.org/10.1063/1.1702234.*

[12] Sheng-Hua, H.; Ru-Ji, W.; Mak, T. C. W. Crystal Structures of Isomorphous Cadmium(II) and Lead(II) Oxalate Trihydrates. *Journal of Crystallographic and Spectroscopic Research***1990**, *20* (2), 99–104. https://doi.org/10.1007/BF01160959.

[13] M, M.; K, K.; A, N.; S, B.; N, A.; D, L.-Z.; K, B.; A, C.-B. Organometallic Modified Montmorillonite Application in the Wastewater Purification: Pollutant Photodegradation and Antibacterial Efficiencies. *Applied Surface Science***2021**, *569*, 151097. https://doi.org/10.1016/j.apsusc.2021.151097.

[14] Taghavi Fardood, S.; Moradnia, F.; Ramazani, A. Green Synthesis and Characterisation of ZnMn2O4 Nanoparticles for Photocatalytic Degradation of Congo Red Dye and Kinetic Study. *Micro & Nano Letters***2019**, *14* (9), 986–991. https://doi.org/10.1049/mnl.2019.0071.

[15] Oladoye, P. O.; Bamigboye, M. O.; Ogunbiyi, O. D.; Akano, M. T. Toxicity and Decontamination Strategies of Congo Red Dye. *Groundwater for Sustainable Development***2022**, *19*, 100844. https://doi.org/10.1016/j.gsd.2022.100844.

[16] Matavos-Aramyan, S.; Moussavi, M. Advances in Fenton and Fenton Based Oxidation Processes for Industrial Effluent Contaminants Control-A Review. *International journal of Environmental Science and Natural Resources***2017**, *2*, 1–18. https://doi.org/10.19080/IJESNR.2017.02.555594.

[17] Buta, I.; Nistor, M. A.; Lönnecke, P.; Hey-Hawkins, E.; Muntean, S. G.; Costisor, O. One-Dimensional Cadmium(II) Coordination Polymers: Structural Diversity, Luminescence and Photocatalytic Properties. *Journal of Photochemistry and Photobiology A: Chemistry***2021**, *404*, 112961. https://doi.org/10.1016/j.jphotochem.2020.112961.

[18] Paul, A. K.; Madras, G.; Natarajan, S. Adsorption–Desorption and Photocatalytic Properties of Inorganic–Organic Hybrid Cadmium Thiosulfate Compounds. *Phys. Chem. Chem. Phys.* **2009**, *11* (47), 11285–11296. https://doi.org/10.1039/B913407G.

[19] Jiao, Y.-Q.; Qin, C.; Sun, C.-Y.; Shao, K.-Z.; Liu, P.-J.; Huang, P.; Zhou, K.; Su, Z.-M. Hydrothermal Synthesis and Structural Characterization of a New Inorganic–Organic Hybrid Compound with Photocatalytic Activity Based on Keggin-Type Polyanion and Cadmium-1, 2, 4-Triazolate Units. *Inorganic Chemistry Communications* **2012**, *20*, 273–276. https://doi.org/10.1016/j.inoche.2012.03.025.

CHAPTER FOUR :

$Cu((C_4H_6O_5)_2(C_8H_9NO)_2$

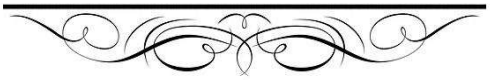

Synthesis, caracterization and design of a new isomorphous of [fluorenyllithium .2 ethylenediamine]

Itroduction

This fourth chapter, reports the synthesis, caracterization and design of a new isotype of [fluorenyllithium 2 ethylenediamine] with copper, malic acid and acetanilide co ligand. The prepared compound was identified by infrared spectroscopie, elemental analysis and powder X-rays diffraction. The identification using PDXL2 program shows that the structure consists of an isotype of fluorénylllithium 2 éthylènediamine.

The two compounds, different in the chemical entities contiguous to the molecule, where the [fluorenyllithium 2 ethylenediamine] molecule contains a lithium cation, florenyl and ethylenediamine cation, while the compound of the study is formed from the copper cation, maleic acid and acetanilide.

The solid-state crystal structure of [fluorenyllithium . 2 ethylenediamine]$_\infty$ was resolued in 1989 by S Buchholz et al [1]. In [fluorenyllithium . 2 ethylenediamine]$_\infty$, the ligands forms network structure by these bonds around the central cation, while fluorenyl occupies the pore formed by the crystalline network. S Buchholz et al mainly invested the length of bond between the atoms of this complex and determined the value of the length of the hydrogene bond and their role in the cohesion of the crystal network of this compound.

IV.1.Synthesis of $Cu((C_4H_6O_5)_2(C_8H_9NO)_2$

In view to synthesize copper (II) coordination polymer, two organi clinker species were used as precurssors maleic acid ($C_4H_6O_5$) and acetanilide solution (C_8H_9NO).A solution of trihydrous copper (II) nitrat(($NO_3)_2.3H_2O$) (0.24160 g) was dissolved in methanol (5 mL) and wasadded to a solution of maleic acid ($C_4H_6O_5$) (0.1161 g) inmethanol (5 mL) inder stiring. To this mixture was added dropwise acetanilide solution(C_8H_9NO) (0.06758g) in methanol (5 mL). After stirring for 6 min at room temperature, a blueprecipitate was obtained. The powder was then washed with methanol, and finally dried.

IV.2.$Cu(C_4H_6O_5)_2(C_8H_9NO)_2$ identification

IV.2.1.Elemental analysis

The blue crystallites seen under the optical microscope in figure 1-a, were captured with the scanning electron microscope. The high resolution scanning electron microscopy image Figure 1-b shows a regular agglomerates crystallites layered form with a thickness of about

avrage 2 µm micrometers a spacing of ~ 0.9 µm. The typical 2D morphology takes a look like the MXene. The chemical elemental qualitative and qualitative analysis reveals the présence of C(56.58 %) O(32.91) N(0.52 %) and Cu(1.99 %) in the sample**(**Table IV.1).

Table.IV.1: Quantitative and qualitative composition of the sample by the EDS device

Element	% ofmass	%atomic	Intensitytotal
C K	52.29	56.58	404.63
O K	33.90	31.91	175.99
Cu L	8.40	1.99	31.48
NL	5.41	0.52	12.63

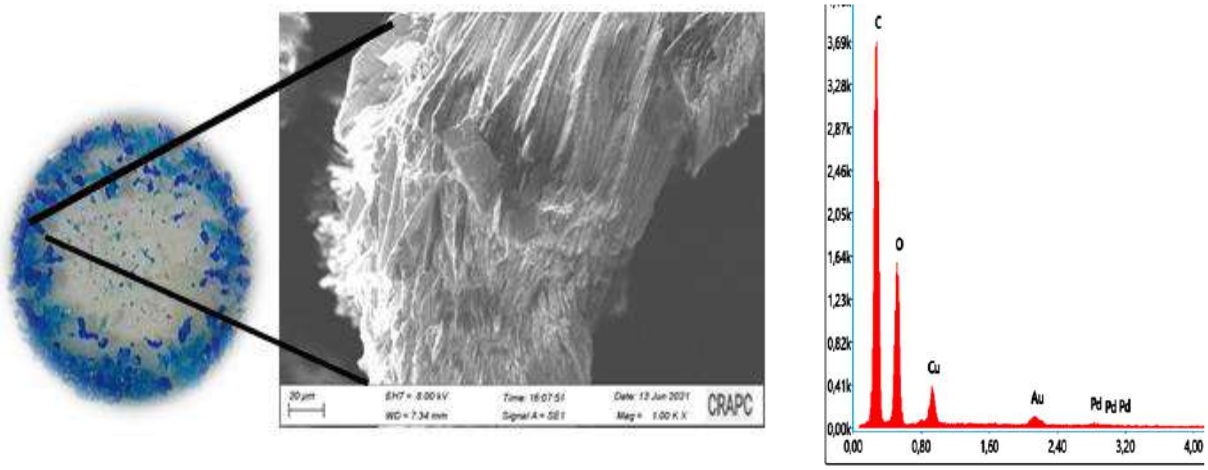

Figure.IV.1: SEM image of the compound

IV.2.2.Cristal structure analysis result

Figure IV.2 shows the measurement diffractogramprofilesrecorded by Rigaku-binary diffractometer in the range 2θ(°) [2.5 - 60] with scan speed/Duration time = 10deg/min, Step width = 0.0200 deg, Scan axis = θ/2θ, Incident slit = 1.250 deg, diffractogramrecorded.

Comparing the enregitred diffractogram with that generated by COD data base, the result concord with the card COD N° 1100300[2]cristallise in group 14: P_{121}/c_1(Table IV-4), the phase identification accomplished using PDXL2 program rice to an isomorphous of [fluorenyllithium .2 ethylenediamine], this by changing in the new synthetised compound entities: lithium by copper, ethylenediamine by malic acid and fluorenyl by acetanilide as explaind in table IV.2.

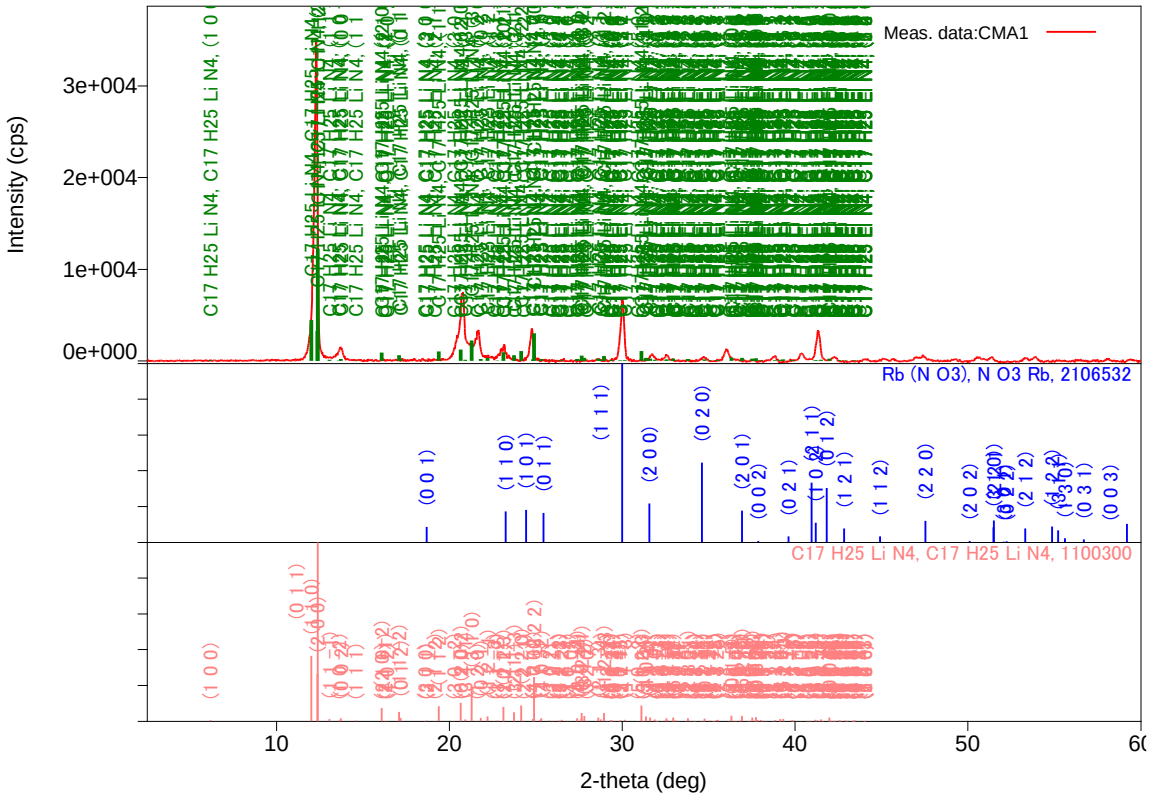

Figure.IV.2: Powder X-ray diffraction pattern, the red of the title compoud and the green of [fluorenyllithium .2 ethylenediamine] database

Table.IV.2: Comparison between the two compounds precursor

precurssor	A	B
Metallic cation	Li^+	Cu^{2+}
Linker 1	Ethylenediamine 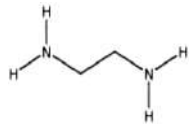	Maleic acid 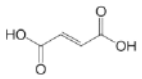
Template	Fluorinyl 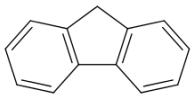	Acetanilid 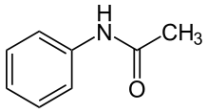
Similarity	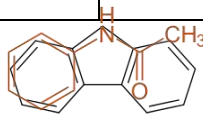	

The quantitative analysis shows that there are residues of recrystallized copper nitrate present, mostly represented by peak 2θ= 30, with a minimum presence percentage (Figure IV.2),table IV.3 reports the lattice parameters where the qualitative analysis of PDXL2 used the database of known materials $Rb(NO_3)$ (Table IV.4) to try to identify the material traces of

$Cu(NO_3)$ recrystallized during the chemical reaction from its diffraction diagram and provide the mesh parameters with relatively high accuracy.

IV.2.6.Lattice indexation

Indexing with PDXL2 program leads in a monoclinic unit cell with parameters noted in table IV-3 with figure of merite of 1.048 revealing crystallization quality. These results also show that the new structure is modeled in the same space group as that found in the work of Buchholz (1989) [1],with an exces of about 14 angestrom of the unit cell volume, due to the different arrangement of the chemical entities in the unit cell, as shown in Table IV.3.

Indexing with DIVCOL 06 program leads in a monoclinic unit cell with parameters noted in table IV-3 and figures of merit M (14) = 10.9, F (14) = 10.4(0.0128, 105) revealing crystallization quality. The value M (14) = 10.9 is likely represents a good quality of indexation.Values above 10 are generally considered acceptable, with higher values indicating better agreement between the proposed crystal structure and the observed diffraction data.The value F(14) = 10.4(0.0128, 105)represents a statistical measure of confidence in the indexation.This low value confirms the presence of impurity in the studied sample, which is copper nitrate that was in the medium in excess, and there was recrystallization.

Table.IV.3: Lattice parmeters found for the synthetised product

Phase name	a(A)	b(A)	c(A)	α(deg)	β(deg)	ϫ(deg)	V(Å^3)	
$Rb(NO_3)$	5.665128	5.178386	4.747997	90.00	90.00	90.00	139.280	
C17 H25 Li N4	14.724(3)	8.561(2)	13.267(3)	90.000	104.11(2)	90.000	1621.88	P121/c1
Title compound	14.765000	8.584839	13.303943	90.00	104.11	90.00	1635.46	P121/c1
Indexed	14.5499	8.1467	13.0358	90.00	102.91	90.00		

What is interesting about the composition of these two molecules is the similarity between the detailed structure of both ethylenediamine and malic acid(table IV.2). While we can accept that the two templates are similar considering the difference in their respective size, this is what is normal for some decalage des pics de diffraction.

The crystallographic data file (cif) number used is 1100300Powder X-ray diffraction confirms the crystalline state of the title compound.Phase identification was egain accomplished by comparing the experimental XRD pattern with the either simulated pattern from a database with mercury softward with different meusurement condition (figure 1 annex 2).

Table.IV.4:fluorenyllithium .2 ethylenediamine] caracteristics

Phase name	Formula	Figure of merit	DB card number (COD)	Space group
[fluorenyllithium .2 ethylenediamine]	C17 H25 Li N4	1.048	1100300	14 : P121/c1,unique-b,cell-1
Rb (N O3)	N O3 Rb	0.706	2106532	59 : Pmmn,choice-1

IV.2.4.Structure description

The crystalline structure of [fluorenyllithium-2ethylenediamine] is described by Stefan Buchholz et al [1]. It is composed of a crystalline lattice of metallic lithium cations in an antiperiplanar conformation figure tetracoordinated by four Li-N type ethylenediamine ligands. In row 2.80 A, fluoryl anions are bound together by hydrogen bonds N-H... C and are located in inter-network voids. Four antiperiplanar maleic acid ions encircle copper ions with tetrahedral geometry, just like in the original combination. Strong structural similarities arise from the acetanilide cation's attachment to the system via hydrogen bonds with acid type C-H... O, N-H... O from the -NH and -CH_3 groups of acetanide, respectively, to the carbonyl group of acid and C-O... H.

Based to this description, which was previously described, the prohibited compound has the same crystal structure as the complex fluorenyllithium-2ethylenediamine, with the chemical units substituted as shown in the table IV.2.Maleic acid and ethylenediamine share a similar size and shape table IV.5, which enables the two compounds to fit in the same packing configuration.

Table.IV.5: Similarity betweenMaleic acid and ethylenediamine [3]

Molécule	Longueur (Å)	Largeur (Å)	Hauteur (Å)
Éthylènediamine	1.39	1.22	1.47
Acide maléique	1.24	1.51	1.39

The similarity between fluorenyl and acetanilide extends beyond just size and shape, making them good candidates for forming isomorphous compounds with ethylenediamine and maleic acid substitutes. Both have a roughly planar aromatic ring system as their core, contributing to a similar overall shape.Fluorenyl has two benzene rings fused together, slightly larger than the single benzene ring of acetanilide. However, the additional ring in fluorenyl doesn't significantly alter the overall shape compared to acetanilide.Both exhibit relatively weak intermolecular forces due to their neutral charges and delocalized electrons.The similar size and shape of the aromatic core in both molecules allows them to

potentially fit into similar packing arrangements within a crystal lattice.The weak intermolecular forces of both molecules provide flexibility in how they can arrange themselves within the lattice, further enhancing the possibility of isomorphism.This means that they can also fit into the crystal structure in the same way [4-7].

Table.IV.6: Similarity between flurenyl and acetanilid [7,8]

Molécule	Longueur (Å)	Largeur (Å)	Hauteur (Å)
Fluorenyl	9.70	7.20	1.70
Acetanilide	7.70	7.70	1.20

Depending on this information the compound is designed as follows

	fluorenyllithium-2ethylenediamine	Studied compound
Asymetric unit model	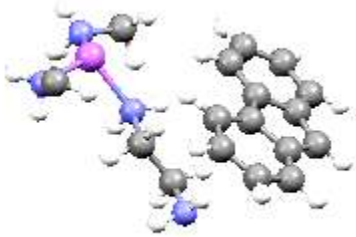	
Molecular unit model	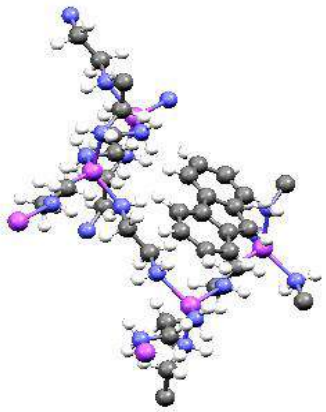	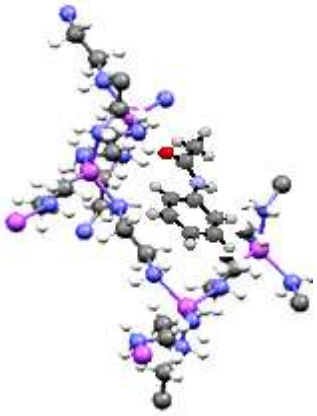
Lattice without fluorenyl	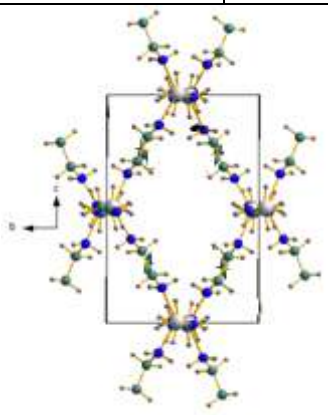	

lattice with fluorenyl	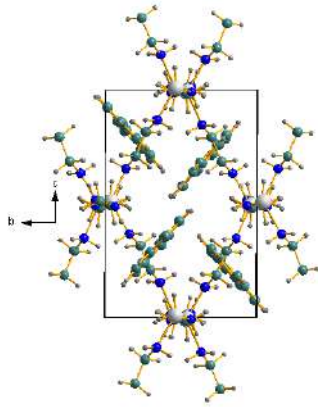

IV.2.5.Molecule conception

By comparing the experimental XRD pattern with the either simulated pattern from a database for card COD N° 1100300 with mercury softward we get. The powder X-ray diffraction confirms the crystalline state of the title compound.

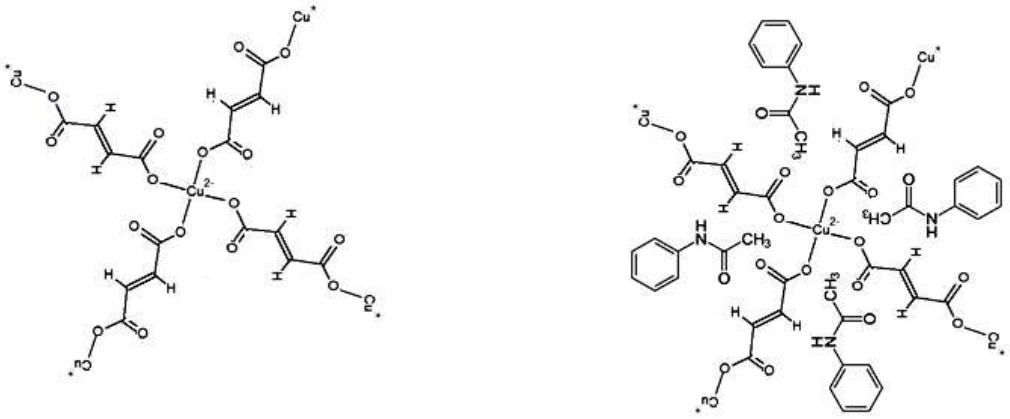

IV.3: primitive cell conception

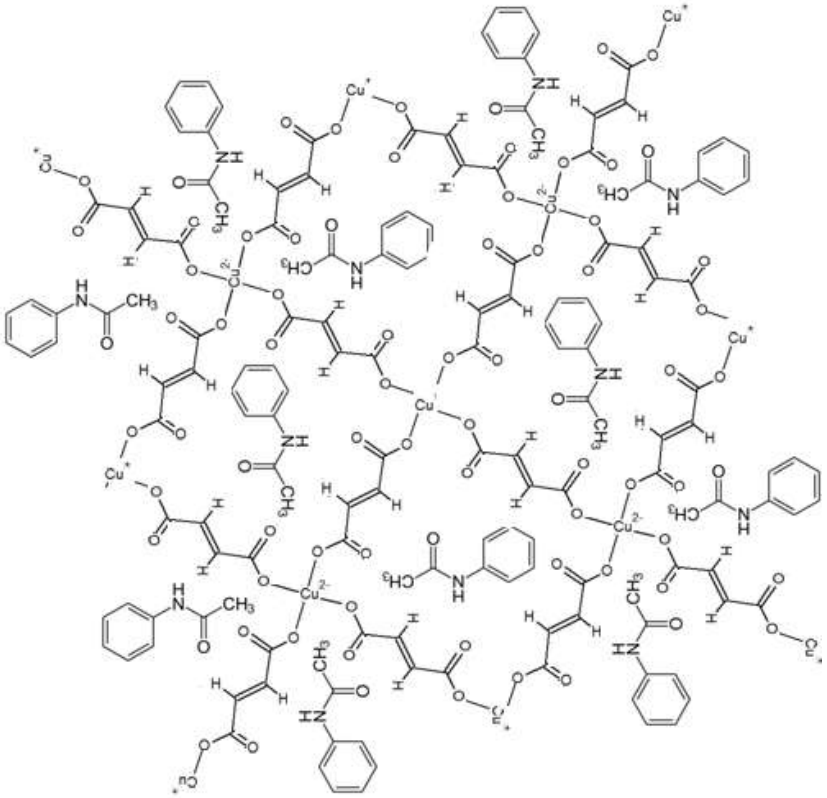

IV.4: cristalline lattice conception

Conclusion

In this chapter, a chemical compound was manufactured and designed based on the results of the qualitative quantitative analysis using X-ray and scanning electron microscope, which showed that this compound is a synchronizer of another known compound. Future possibilitiies for the synthetised compound could to be used in specific application such as cathalytic as done with other compounds in this thesis.

[1] Stefan Buchholz, Klaus Harms, Michael Marsch, Werner Massa, and Gernof Boche. “Model of a Solvent-Shared Ion Pair with N-H . . . C Hydrogen Bonds between Amine and Carbanion-Crystal Structure of [Fluorenyllithium· 2Ethylendiamin]∞”. Angewandte Chemie 101 (1), 57-58

[2] http://www.crystallography.net/cod/result.php

[3] Chemical and Engineering Data, 7e édition, par R. C. Weast et M. J. Astle (1982) "Crystallography of Organic Molecules" par H. A. Levy (1969)

[4] "Crystal Structure Analysis: A Primer" par D. W. Jones (2003)

[5] "The Principles of Crystallography" par M. J. Buerger (1970)

[6] "The Crystal Structure of Acetanilide" par D. W. Jones et J. E. F. Stocks (1956)

[7]"The Crystal Structure of Fluorenyl" par J. A. Friend et C. W. Bunn (1952)

[8] The Crystal Structure of Acetanilide" par D. W. Jones et J. E. F. Stocks (1956)

CHAPTER FIVE :

$[Fe_2(OH)_{2(}C4O4)_2H2O]_2.2H_2O$

Introduction

Organic-inorganic hybrid materials gained significant interest in a variety of sectors, including separating gases, energy storage, catalysis, adsorption and pharmacy due to their porous structure and high specific surface area. They can exist in their mono, bi or three-dimensional form as well as the reconstitution of zero-dimensional molecules, is possible. Zero-dimensional molecules are formed by discreteentitieswithoutextended structures, connected by strong hydrogen bonds and offerseveraladvantages for dye removal because of their high porosity, good stability in water. Various hybrid complexes have been developed, described, and used to eliminate organic waste.

Compounds of the squarate anion with many metal cations have been studied due to their diverse structures and properties [1]. in most cases, the reaction of squaric acid with the cation Fe (II) or Fe(III) result dihydroxy squarate of iron at the first contact between these two components.Dihydroxy squarate of iron was widely reported in the literature since its first synthesis by West and Niu[2-7].

Using a three-dimensional similar metal-organic framework with the chemical formula $[Fe_3(OH)_3(C_4O_4(C_4O_4)_{0.5}]_n$[8] at room temperature, Soumyabrata Goswami, et al. performed the degradation of tetrazines into oxadiazole. This compound is considered a heterogeneous catalyst, due to the presencec hydroxyl groups in it's structure and two different types of voids hydrophilic squarate ligands with hydroxyl groups at the surface and hydrophobic voids enclosed by aromatic ligands are present in the three dimensional framework, which is an infinite extension of nanoscopic cuboctahedral cages. In addition, it is simple, easy to handle, environmentally benign, and can be recovered and used again[9].

Herein, we report the syntheses, identification, crystal structures description, of the coordination dymer compound with chemical formula $Fe_2(OH)_2(C_4O_4).2H_2O)2H_2O$ based on the squarate ligand and iron ion and the various spectroscopic measurements carried out and by which it follows: Elemental analysis using the SEM electron microscope and X-ray diffraction. The catalytic analysis of the title compound was also caried. The surface area, crystal structure, and morphology of FS was all described. To comprehend the functionality and use of hybrid materials in the removal of organic dyes, the degradation behaviors of red Congo pigment on FS were examined. It was discovered that FS disperses in water with good stability and is completely insoluble in it before assessing its catalytic activity. Even at, this product is renowned for keeping its crystalline structure.

V.1. Synthesisof$[Fe_2(OH)_2(C_4O_4)_2.2H_2O]_2.2H_2O$

A mixture of squaric acid (0.11 g, 10 ml, 100 C°) and iron(III) chloride $FeCl_3.6H_2O$ (0.2705 g, 10 ml) was stirred (500 turns/minute) until being clear. We notice the change in the mixture solution color immediately after adding the first drop of acid $H_2C_4O_4$ from yellow to purple. After a few minutes, the solution take dark purple powder of the compound forms and increases over time with about 65% yield (based on Fe). The powder was filtered, washed with water then dried.

V.2.Physico-chemical characterization of $[Fe_2(OH)_2(C_4O_4)_2.2H_2O]_2.2H_2O$

V.2.1.Elementary analysis

Elemental composition of the title compound was studied by scanning electron microscopy. Figure V.1.Presents a SEM image obtained on a part of the powder shows a different sizes and shapes of grains, and they are loosely packed together. Their surface is rough and textured, with many small bumps and ridges.The sample looks homogeneous and this has also been confirmed from the diffractogram indexation using FULLPROF softward from the merite factors(annexe 5, table 1).Powder size reaches some micrometers.

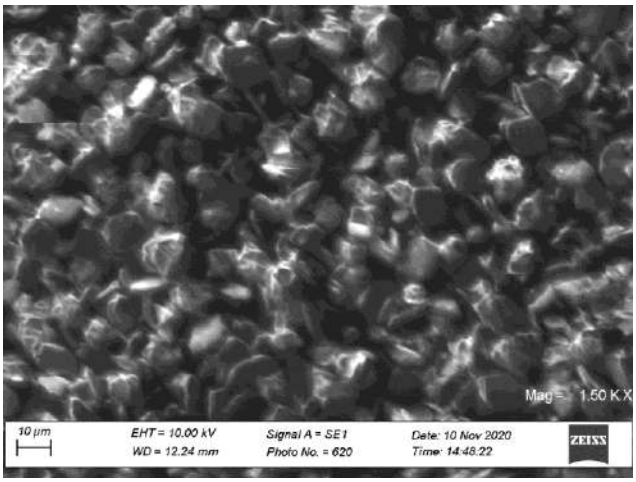

Figure.V.1: Surface morphology of FS compound by SEM analyses

The table V.2 shows the elemental composition of the compound and Figure V.2 the EDX. Based on the data in the table, the compound is composed primarily of carbon (C) and oxygen (O), with a smaller amount of iron (Fe). The weight percent of C is 48.46%, the atomic percent of C is 60.36%. The weight percent of O is 39.94%, the atomic percent of O is 37.35%. The weight percent of Fe is 7.37%, the atomic percent of Fe is 1.97%.

Table.V.1: Results of quantitative and qualitative analysis of the FS sample

Elément	% weight	% atomic	Total intensity
C K	48.46	60.36	513.64
O K	39.94	37.35	306.68
FeK	7.37	1.97	10.49

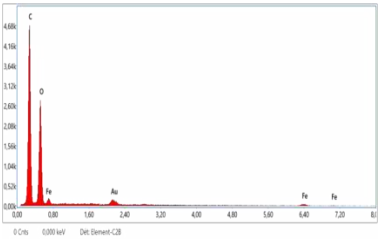

Figure.V.2: EDX spectrum of FS compound

V.2.2.Spectroscopy InfraRed analysis

FS infrared spectrum (figure V.3) exhibits the squaric acid ligand's distinctive bands. The OH bond of water molecules bonded to Fe produces a very strong, extraordinarily broad band between 2800 and 3400 cm^{-1} in the spectrum[3]. A faint band at 1800 is due to the squaric entity's free noncoordinated carbonyl. , at 1105, 1080, 860 [3], 760 and 430 cm^{-1} these bonds are attributed to C-C, Fe-OH and Fe-O respectively. A very weak band at 985 cm^{-1} and 490cm^{-1} attributedto Fe-OH. The region between 1700-1300 cm^{-1} essentially corresponds to the vibrations of the organic ligand. It appears two strong bands at 1620 is attributed to C-O [2], at 1500 is attributed to C-O /C-C [4].

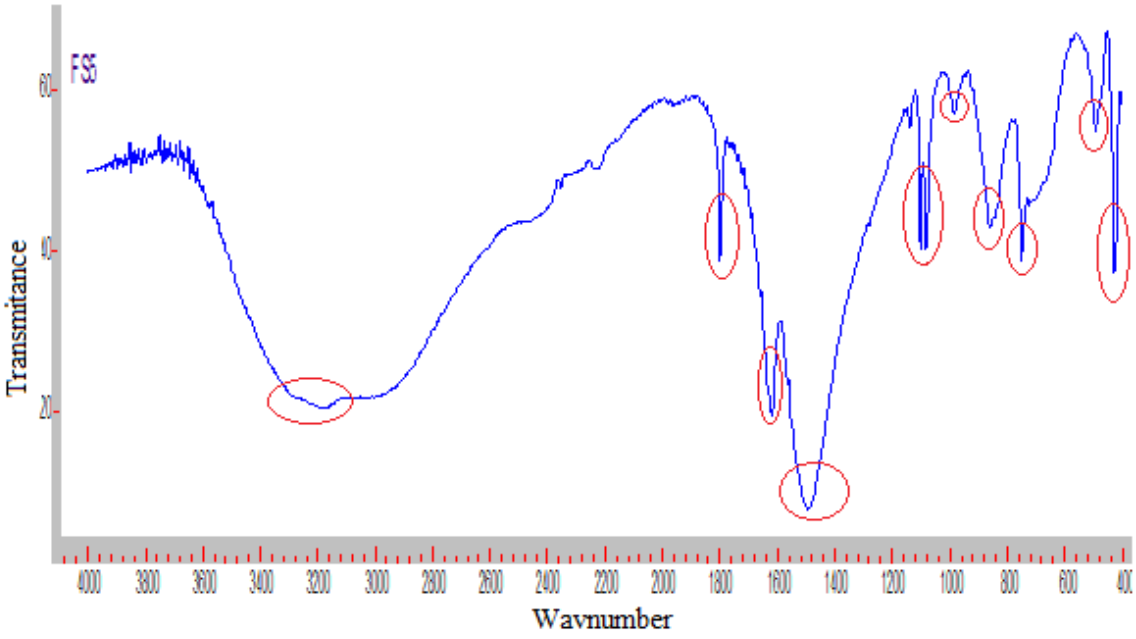

Figure.V.3: The infrared product spectra

The interpretation of the IR spectra reveals the establishment of many bonds between Fe and the ligand, confirming the complex formation.

V.2.3.X-ray powder diffraction study

Figure V.4matches the data gathered FS X-ray diffraction profile to a COD database equivalent, noticing that the recorded diffractogram contains isomers of coordination with the complex $V_2(OH)_2(C_4O_4)_2.4H_2O).2H_2O$ containing iron instead of vanadium and agree with card number 1532749 [5] (Table IV -4), with a merit figure of 0.445.

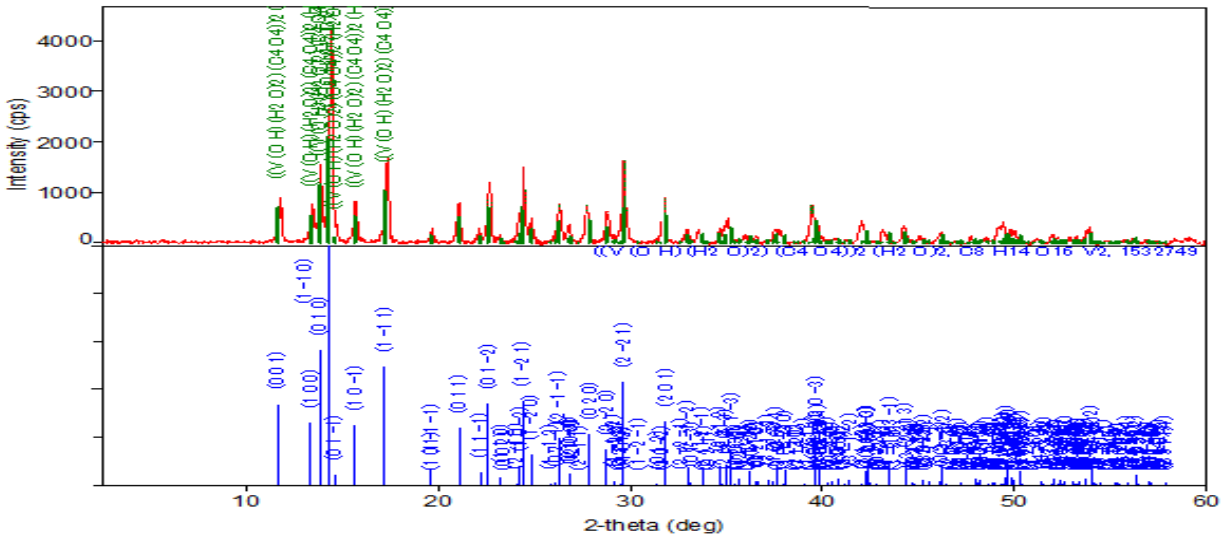

Figure.V.4: Phasis identification using X-ray's diffraction.

V.3. Qualitative analysis

In the table V.3 are given the qualitative analysis whitch are improved by the automatically search/match by using COD database and the combination of peak search and profile fitting.

as well as the values obtained from the indexing of the diffractogram using the implemeted WinPloter program in the FullProf software [10-12] confirms the validation of the phase and indicates the homogeneity of the product by the merite figure value(Table 1.Annexe 6)

Table.IV.2: lattice parameters

	a(Å)	b(Å)	c(Å)	α(°)	β (°)	γ (°)	ref
Exp	7.538942	7.5882	8.2488	106.9039	94.5100	113.9840	[5]
Theo	7.5112(10)	7.5603(8)	8.2185(8)	106.904(8)	94.510(10)	113.984(9)	index

Table.IV.3: COD Determinaton

Phase name	Figure of merit	DB card number	Space group
$((V(OH)\ (H_2O)_2)(C_4O_4))_2\ (H_2O)_2$	0.445	1532749	2 : P-1

V.4.Structure description

The coordination complex $[Fe_2(OH)_2(C_4O_4)_2.2H_2O]_2.2H_2O$ is dimeric (figure V.6), it is composed of two iron(II) ions, two hydroxyde ions, two squarate ions and four water molecules. The iron(II) ions are octahedral, four ligands surround them. Two of the water molecules and two squarate bidendate ions form a link with the iron (II) ions via two oxygen atoms.Figure V.5 shows the asymetric unit

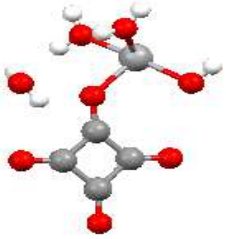

Figure.V.5: asymetric unit

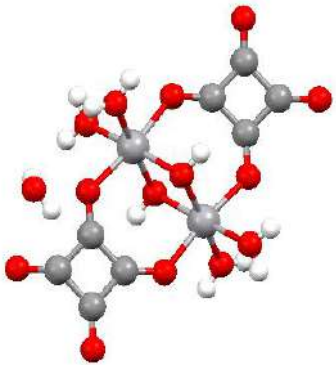

Figure.V.6: molecular unit

The elemental lattice projection for the crystalline structure along axes a, b, and c is shown in Figure V.7. The arrangement of the hydroxyl anion and water molecules in relation to the structure is avoided in figure V.7.c.

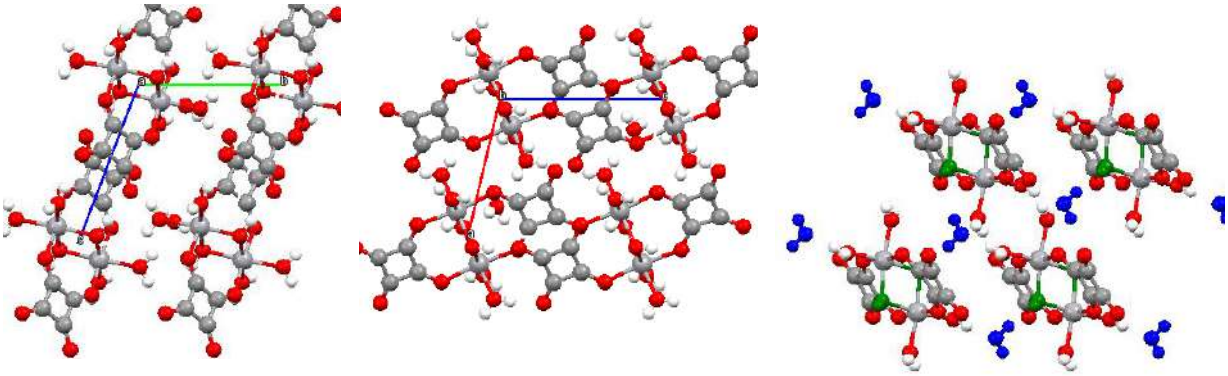

a **b** **c**

Figure.V.7: lattice presentation

V.4.1.H bounds

Hydrogen bonds are strong intermolecular interactions that play an important role in the cohesion of zero-dimensional crystalline networks. In these networks, the molecules are arranged in a regular structure, often in the form of a grid or network. Hydrogen bonds are formed between the hydrogen atoms of one molecule and the oxygen, nitrogen or other electronegative atoms of another molecule. Hydrogen bonds are weaker than covalent or ionic bonds, but they are still strong enough to hold molecules together in a solid structure.

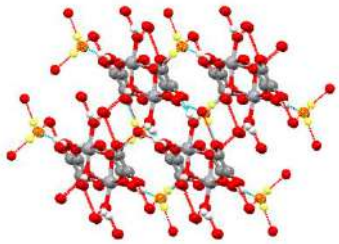

Figure.V.8:H bounds presentation

V.4.2.Water and OH

The presence of OH and water molecules linked to iron in $[Fe_2(OH)_2(C_4O_4)_2.2H_2O]_2.2H_2O$ can indirectly influence its reactivity in removing red congo dye. While FS itself doesn't directly interact with red congo, the presence of these ligands can affect the overall reactivity of the system in a few ways (figure V.7.c).

V.5.BET analysis of FS structure

The BET surface erea and pore structure of the synthesized FS is determined by the measurement of N_2 adsorption/desorption isotherm at 77,099 K. BET ploted in figure V.9 shows a starting section convex with respect to the pressure axis and which rises only slowly when the pressure increases. This behavior indicates a situation in which the amplitude of the adsorbate-adsorbent interaction is equal to or greater than that of the adsorbate-adsorbent interactions. Table V.5 brings together the characteristic of FS results of the meusure bet. First the sample was degassad for about h at K. the adsorption branch in the isotherm of FS belong to typeB

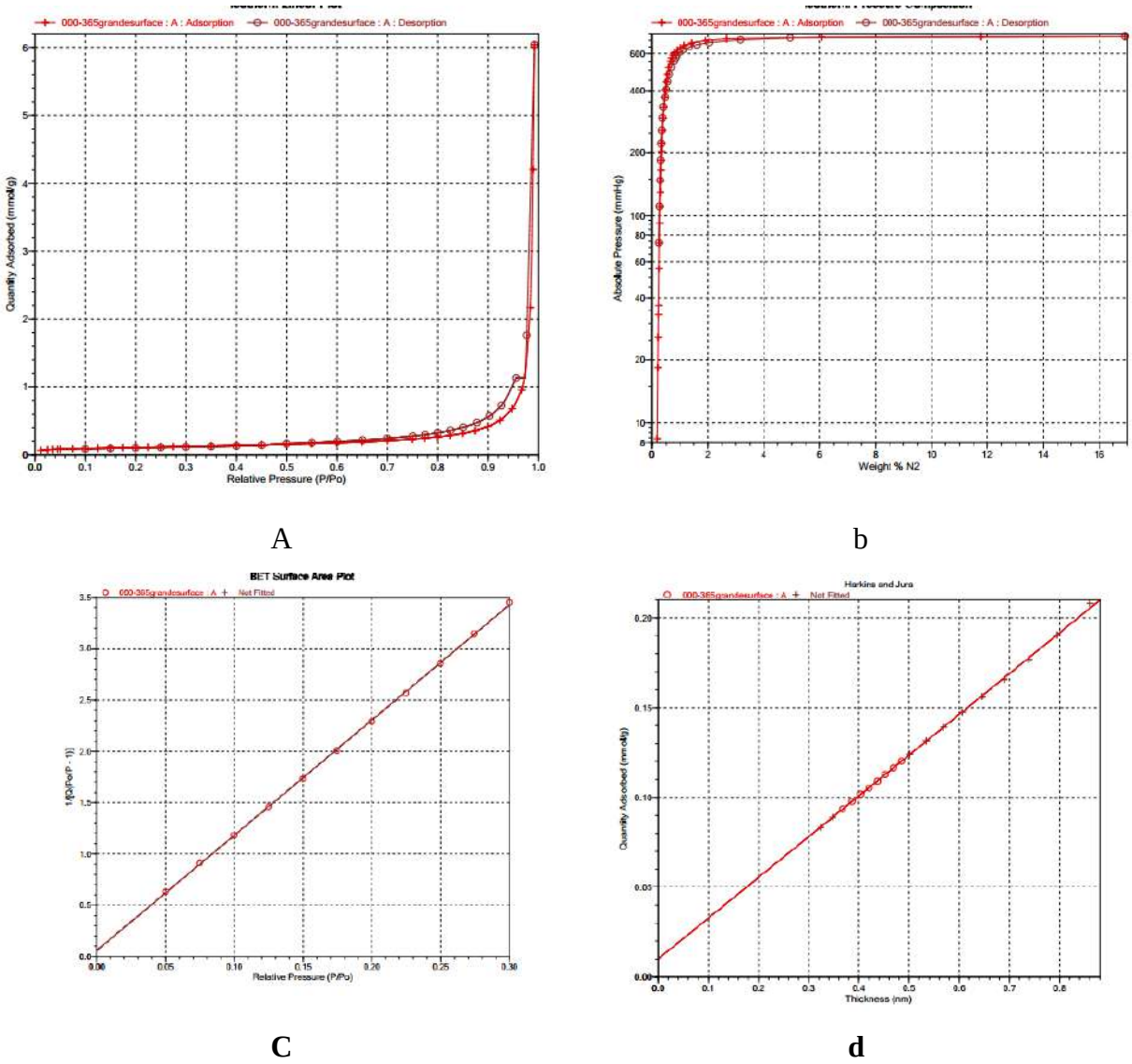

Figure.V.9:plot BET of FS

Table.V.4: The BET meusure characteristic of FS

Properties	**FS**
Single point surface area at P/Po = 0,299995844:	8,4774 m²/g
BET Surface Area:	8,6455 m²/g
t-Plot Micropore Area:	0,7666 m²/g
t-Plot external surface area:	7,8789 m²/g
BJH Adsorption cumulative surface area of pores width:	1,7000 nm - 300,0000 nm 9,5548 m²/g
BJH Desorption cumulative surface area of pores width:	1,7000 nm - 300,0000 nm 13,8349 m²/g
t-Plot micropore volume:	0,000349 cm³/g

BJH Adsorption cumulative volume of pores width:	1,7000 nm - 300,0000 nm 0,209672 cm^3/g
BJH Desorption cumulative volume of pores width:	1,7000 nm - 300,0000 nm 0,209678 cm^3/g
BJH Adsorption average pore width (4V/A):	87,7766 nm
BJH Desorption average pore width (4V/A):	60,6229 nm

The BET surface erea of FS is to be found at 8,6455 m^2/g, slop is 1 g/cm^3. The result of a BJH (Barrett-Joyner-Halenda) analysis used in conjunction with the BET analysis for a better characterization of the pore size distribution of FS gives "BJH Cumulative pore surface adsorption between 1.7000 nm and 300.0000 nm width: 9.5548 m^2/g". This indicates that the area calculated using the BJH method refers to the cumulative total of all pores in the specified pore width range, which is 1.7 (nm) to 300 (nm). 9.5548 m^2/g is the specific surface of FS). This means that for every gram of material, there are about 9.5548 m^2 of surface available for adsorption. This information provides a detailed breakdown of the available surface in a specific range of pore sizes in FS. It indicates that there is a large surface area available for adsorption within the specified pore width range. In the case of desorption, for the width range, the pores have a width range between 1.7 nm and 300 nm. The cumulative surface area of these pores in the specified width range is 13849 m^2/g.

The micropore volume of FS is given t-Plot is 0.000349 cm^3/g. Micropores are very small pores in FS, often smaller than 2 nanometers in diameter. This measurement is important for characterizing the porosity and surface of materials, especially in applications such catalysis studies.

BJH Adsorption cumulative pore volume between 1.7000 nm and 300.0000 nm width: 0.209672 cm^3/g and BJH Desorption cumulative volume of pores between 1,7000 nm and 300,0000 nm width: 0,209678 cm^3/g. These values characterize the porosity of FS to understand the distribution of pore sizes. It provides valuable information on the structure of FS and its potential applicationsin Congo red degradation.The BJH (Barrett-Joyner-Halenda) Desorption average pore width calculated as 4V/A is 60.6229 nm. This value represents the average pore width of a material, which is important for characterizing its porosity and understanding its potential applications in various fields, such as materials science, catalysis, and adsorption studies.

V.6.Degradation of Congo red

A porous MOF with OH hydroxyl and water molecule in the lattice is a promising catalyst for the degradation of Red Congo in solution. The porous structure of the MOF provides a high surface area for the adsorption of Red Congo molecules. The OH hydroxyl and water molecules in the lattice can act as active sites for the degradation of Red Congo.

Removal of Congo red was conducted at temperature (29.6 °C) in a 250 mL beaker. 51 mg of a Fs sample was added to 100 mL of congo red solution (~14.2 mg 500 mL^{-1}), under natural light and magnetic stirring. The pH was adjusted to 7 using NaOH and HCl solution of concentration 1M and 0.1M. For adsorption reactions, every 10 to 60 min, a 10 mL aliquot of the sample was analyzed by ultraviolet spectrometry (The SPECORD 200 PLUS-223E1769C spectrophotometer). The removal rate was calculated by $C = (C_0 - C_t)/C_0 \times 100\%$, where C_0 is the initial concentration and C_t is the concentration.

V.6.1. Adsorption

At room temperature, 0.05 g of the catalyst (CD1) was immersed in 100 mL of the CR solution that had been previously made in a beaker while being continuously stirred for 120 minutes. This allowed the CR to be adsorbed on the catalyst FS. The procedure is to remove 4 mL of the mixture from the reaction beaker every 15 minutes. The samples are then centrifuged for 5 minutes at 6000 rpm, and the supernatant is examined using UV-Visible spectrophotometry, which measures wavelengths between 280 and 700 nm. The interaction of the chromophore bond (N = N) is responsible for the highest absorbance of the dye under study.

V.6.2.Fenton's process

For the Fenton process, the catalyst was pre-equilibrated in adsorption for 30 minutes before initiating the reaction with the addition of 100 µL of H_2O_2 (30%) and taking samples at 10 minute intervals for a total of 90 minutes to be analyzed by UV-Visible spectrophotometry.

V.6.3.Photocatalysis

Photocatalysis was carried out in complete darkness for 30 minutes. Following complete adsorption of the synthesized catalyst in a CR solution, samples were collected at 10-minute intervals for UV-Visible examination (λ = 254 nm).

V.6.4.photo-Fenton

The photo-Fenton process was analogous to photocatalysis, but it began with the addition of H_2O_2(100 µL) in the presence of UV light. Following steps include sampling at 10 minute intervals for UV-Visible spectrophotometry analysis in accordance with the photocatalytic reaction method.

V.7.Result

Congo red degradation

Fenton's process

TableIV.5 lists the experimental conditions for the Red Congo degradation process for two samples of the separately prepared FS productused in the experiment, abreged FS5 and FS12. Degradation results are presented in the figure V.10.

Table.V.5: Experimental conditions for the Red Congo degradation process

Echantillon	pH_i	pH_f	T_i (C°)	T_f (C°)	m_{cat} (g/100ml)	m_{CR} (mg/ ml)	V_{H2O2} (µl)
FS5	6.60	4.95	19.2	29.6	0.0510	14.2/500	60
FS12	6.31	5.32	23.5	32.3	0.0501	14.2/500	60

Initial Adsorption: Both curves start at a degradation yield of around 20%, indicating that some initial adsorption of Congo red occurred, likely onto the catalyst.

Rapid Degradation: The curves show a steep increase in degradation yield within the first 20 minutes, suggesting a rapid degradation process.

Plateau: After about 30 minutes, the curves begin to plateau, reaching a maximum degradation yield of around 80% for the two curve. This suggests that the degradation rate slows down over time.

Interpretation:

Effective Degradation: The curves demonstrate that significant degradation of Congo red can be achieved under the experimental conditions, with up to 80% degradation observed within 60 minutes.

Factors Affecting Degradation: The difference in degradation yields between the two curves suggests that certain factors, such as the extent of initial adsorption or the specific conditions of each sample, can influence the degradation process.

The initial adsorption of Congo red is a possible role of adsorption witch might play a role in facilitating its subsequent degradation, as it brings the dye molecules into close proximity with the catalyst or other reactive species.

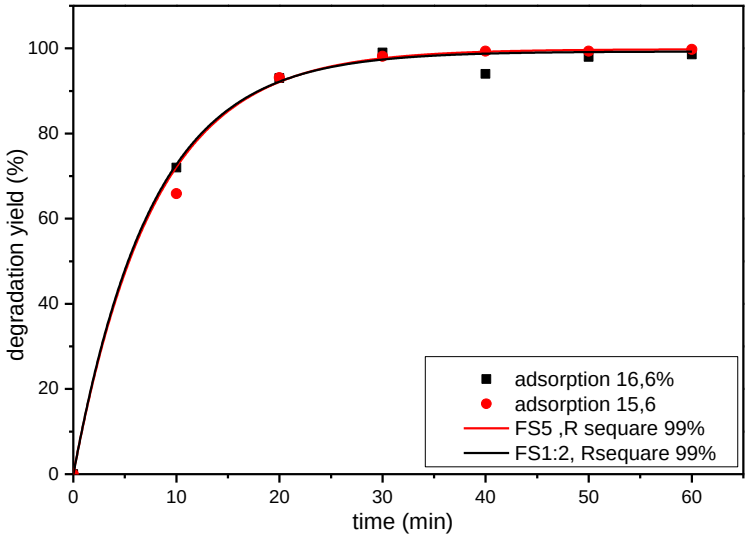

Figure.V.10: adsorption plot

From figure V.10, it is noted that both catalysts have the same catalytic performance.

V.7.Photocatalysis

Table.IV.6: Experimental conditions for the Red Congo adsorption process

Echantillon	pH_i	pH_f	T_i (C°)	T_f (C°)	m_{cat} (g/100ml)	m_{CR} (mg/ ml)	V_{H2O2} (µl)
FS5	7	5.01	22.5	24	0.0504	7.2/250	/
FS12	7	4.98	22.5	25	0.0500	7.2/250	/

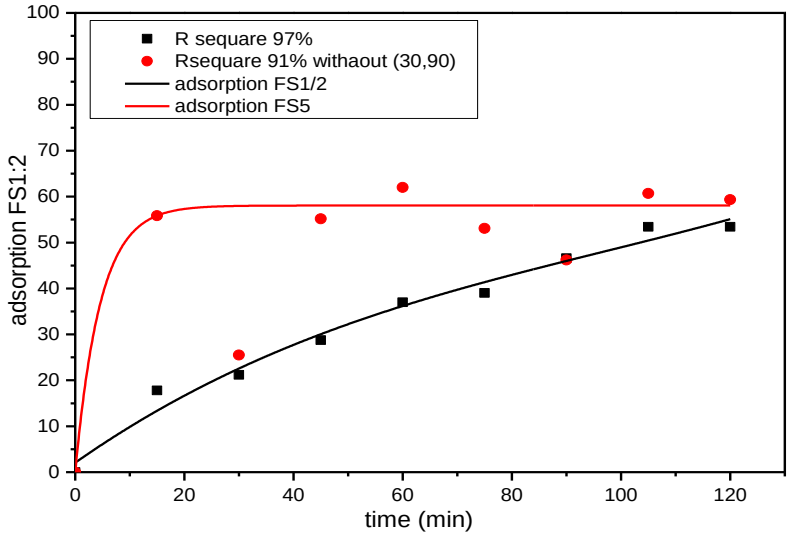

Figure.V.11: Comparaison ofthetwo cat FS5 et FS12.

From both figures and it is noted that the adsorption test is in-significant for the catalyst FS1/2, since the equilibrium time is probably reached at 90 min with an adsorption capacity of 50%, unlike the FS5 catalyst which has an equilibrium time after only 15 minutes with an adsorption that reaches 60%.

The image you sent shows a graph of the adsorption of Red Congo dye onto the FS catalyst. The x-axis represents time in minutes, and the y-axis represents the amount of Red Congo adsorbed, expressed as a percentage of the initial dye concentration.

The graph shows that the adsorption process is rapid and efficient, with over 90% of the dye being adsorbed within 30 minutes. The adsorption rate then slows down, reaching a plateau at around 95%.

The difference in adsorption rates between samples FS5 and FS12 is likely due to the different initial pH values of the solutions. The lower initial pH of sample FS5 may have caused the dye molecules to be more protonated, making them more likely to adsorb onto the catalyst.

The increase in temperature during the adsorption process is consistent with an exothermic adsorption mechanism. The release of heat as the dye molecules adsorb onto the catalyst can cause the temperature of the solution to rise.

Figure.V.12: photos of adsorption reactions of FS1/2 and FS5.

From figure V.12 it is noted that the adsorption solution changes color from red to purple which confirms the PH lord change of adsorption, this change is probably due to the acidic nature of our catalysts,

After having degraded the Congo couge dye, to evaluate the structural stability of the two catalysts, a study by has been carried out the results are presented by the diffractogram of the figures V.13, V.14 and V.15.

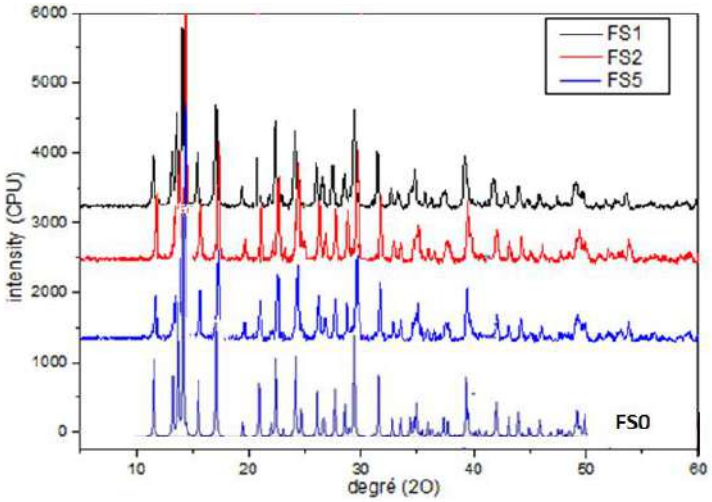

Figure.V.13: XRD patterns of FS1, FS2, FS5, FS0

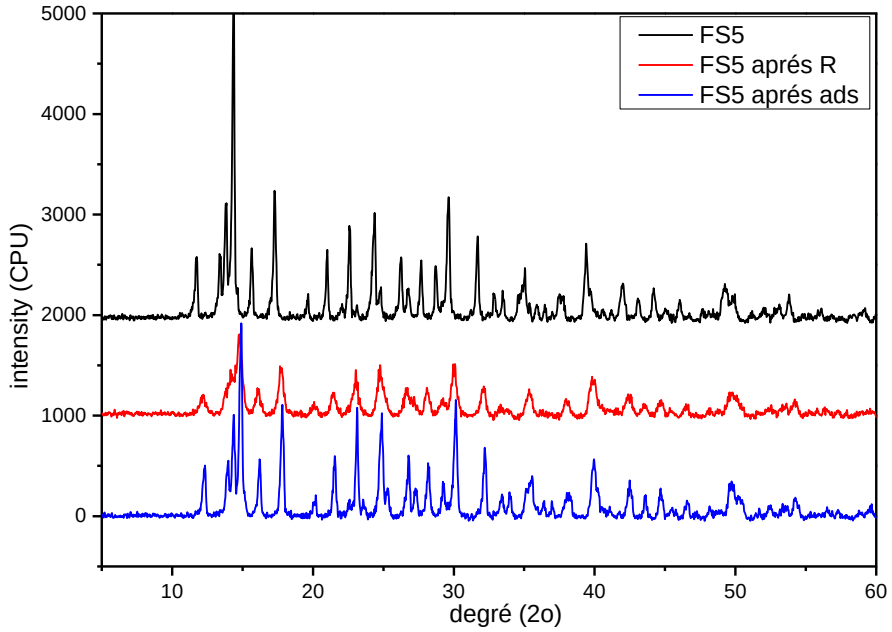

Figure.V.14:XRDpatterns of the catalysts FS5, FS5 before reaction, FS5 after reaction.

These figures presents the X diffractograms of FS recorded before and after degradation of this molecule by red congo.

The degradation of the red congo causes a change in the crystalline structure of FS. This change is characterized by a decrease in the intensity of the diffraction peaks, indicating that the crystal structure is less ordered. The degradation of red congo leads to the rupture of the bonds between the atoms of iron, oxygen, nitrogen and hydrogen of the molecule.

Congo red is an azo dye that has oxidizing properties. During the degradation of red congo, the nitrogen atoms of the dye are oxidized to nitrates. These nitrates react with the iron atoms of FS, causing the rupture of the bonds between these atoms. The rupture of these bonds leads to a decrease in order in the crystalline structure. This results in a decrease in the intensity of the diffraction peaks, as can be seen in the figure. The degradation of red congo by FS is therefore an oxidative degradation reaction that causes the breakdown of bonds in the crystal structure of the molecule.

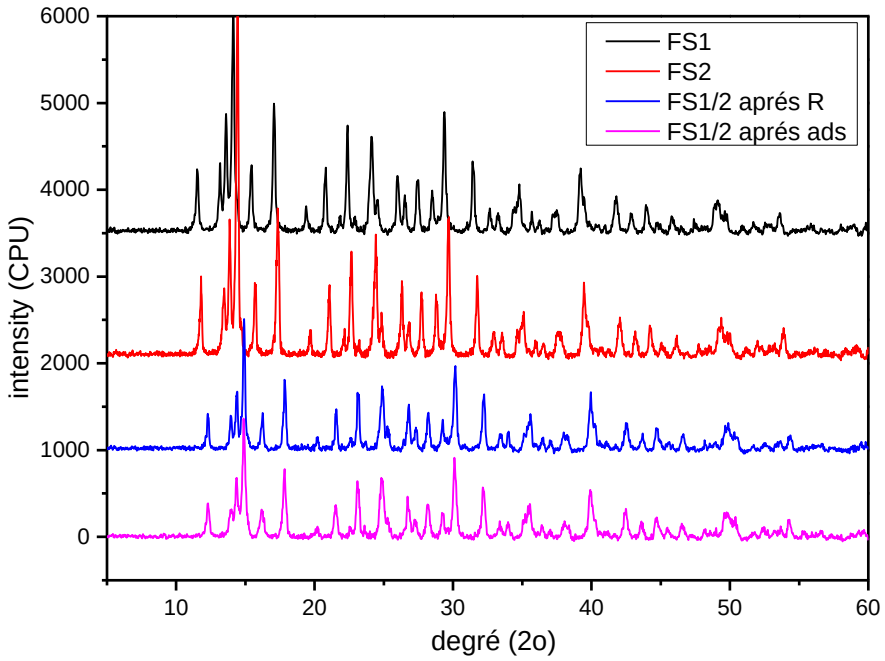

Figure.V.15:patterns of the catalysts FS1, FS2, FS1/ before adsorption, FS1/2 after adsorption.

From the figure V-13 it is noted that the 3 catalysts namely FS1, FS2, FS5 have the same characteristic pitch with the same offset towards the highest thetas for the catalysts FS2 and FS5, for this it can be said that the two catalysts FS2 and FS5 have the same product.

According to figure V-14, it is noted that the catalyst FS5 keeps their structure after adsorption and after degradation reaction but with a decrease in the intensity of the characteristic spikes and even with a shift towards the highest thetas,

According to figure V-14, the FS1/2 catalyst retains their structure after adsorption with a shift towards the highest thetas, but with decreases in the intensities of the spikes after reaction.

Possible mechanism for the degradation of Red Congo with this catalyst is as follows:

1- The Red Congo molecule adsorbs into the surface of the MOF.
2- The OH hydroxyl and water molecules in the lattice donate protons to the Red Congo molecule. This protonates the Red Congo molecule, making it more susceptible to attack by other molecules.

3- The protonated Red Congo molecule is then attacked by other molecules in the solution, such as oxygen or other organic molecules. This results in the breakdown of the Red Congo molecule into smaller, more non-toxic molecules.
4- The smaller molecules desorb from the surface of the MOF, and the reaction cycle begins again.

Another possible mechanism for the degradation of Red Congo with this catalyst is the formation of hydroxyl radicals (OH). Hydroxyl radicals are highly reactive species that can attack and degrade a wide range of organic molecules. Hydroxyl radicals can be generated on the surface of the MOF through the following reactions:

- OH + OH → H2O + O
- O + H2O → OH + OH

The hydroxyl radicals can then attack and degrade the Red Congo molecule.

The specific mechanism for the degradation of Red Congo with this catalyst will depend on the specific MOF and the reaction conditions. However, both of the mechanisms described above are possible.

Conclusion

In this chapter, we reported the preparation of the FS porous complex with physico-chemical identification, the porosity and the specific surface were first studied by the BET technique to predict its capacalytic and subsequently applied to the adsorption of red congo.

This catalyst has several advantages over other catalysts for the degradation of Red Congo. It is a porous material with a high surface area, which provides a good adsorption capacity for Red Congo molecules. The OH hydroxyl and water molecules in the lattice can act as active sites for the degradation of Red Congo. Additionally, this catalyst can be synthesized from relatively inexpensive and abundant materials.

This catalyst has the potential to be used for the treatment of wastewater and other contaminated streams containing Red Congo. It is a versatile catalyst that can be tailored to the specific requirements of the application.

[1] Corrêa, C. C.; Diniz, R.; Chagas, L. H.; Rodrigues, B. L.; Yoshida, M. I.; Teles, W. M.; Machado, F. C.; de Oliveira, L. F. C. Transition Metal Complexes with Squarate Anion and the Pyridyl-Donor Ligand 1,3-Bis(4-Pyridyl)Propane (BPP): Synthesis, Crystal Structure and Spectroscopic Investigation. *Polyhedron***2007**, *26* (5), 989–995. https://doi.org/10.1016/j.poly.2006.09.037.

[2] West, R.; Niu, H. Y. *New Aromatic Anions. VII. Complexes of Squarate1 Ion with Some Divalent and Trivalent Metals*. ACS Publications. https://doi.org/10.1021/ja00900a014.

[3] *Carranza a J,; Sletten b J,; Lloret c F,; Julve c M.Iron(III), chromium(III) and cobalt(II) complexes with squarate: Synthesis, crystal structure and magnetic properties - Inorganica Chimica Acta. 371, (1), 2011, 13-19.* https://www.sciencedirect.com/science/article/abs/pii/S0020169311002489 (accessed 2023-12-27).https://doi.org/10.1016/j.ica.2011.02.087.

[4] Long, G. J. *A Moessbauer, magnetic, and electronic structural study of two iron squarate complexes*. ACS Publications. https://doi.org/10.1021/ic50188a003.

[5] Brouca-Cabarrecq, C.; Mohanu, A.; Millet, P.; Trombe, J. C. New Binuclear Vanadium(III) and (IV) Squarate Species: Synthesis, Structure and Characterization of [V(OH)(H2O)2(C4O4)]2·2H2O and (NH4)[(VO)2(OH)(C4O4)2(H2O)3]·3H2O. *Journal of Solid State Chemistry***2004**, *177* (7), 2575–2583. https://doi.org/10.1016/S0022-4596(03)00396-7.

[6] *Binuclear Vanadium(III) Squarates with Layered and Framework Structures: Hydrothermal Synthesis and Structures of [{V(OH)(C4O4)(H2O)}2] and [{V(OH)(C4O4)}2]·4H2O - Lin - 1997 - Angewandte Chemie International Edition in English - Wiley Online Library*. https://onlinelibrary.wiley.com/doi/abs/10.1002/anie.199720761 (accessed 2023-12-27).

[7] Stalikas, C.; Pappas, A.; Karayannis, M.; Veltsistas, P. Simple and Selective Spectrophotometric Method for the Determination of Iron (III) and Total Iron Content, Based on the Reaction of Fe(III) with 1,2-Dihydroxy-3,4-Diketocyclo-Butene (Squaric Acid). *Microchimica Acta***2003**, *142*, 43–48. https://doi.org/10.1007/s00604-002-0950-4.

[8] Goswami, S.; Adhikary, A.; Jena, H. S.; Biswas, S.; Konar, S. A 3D Iron(II)-Based MOF with Squashed Cuboctahedral Nanoscopic Cages Showing Spin-Canted Long-Range Antiferromagnetic Ordering. *Inorg. Chem.***2013**, *52* (20), 12064–12069. https://doi.org/10.1021/ic401886f.

[9] Goswami, S.; Jena, H. S.; Konar, S. Study of Heterogeneous Catalysis by Iron-Squarate Based 3D Metal Organic Framework for the Transformation of Tetrazines to Oxadiazole Derivatives. *Inorg. Chem.***2014**, *53* (14), 7071–7073. https://doi.org/10.1021/ic5003258.

CHAPTER SIX :

(Illite , Kaolinite, SiO_2) CLAY

DBO, COD, SS and turbidity parameters: Key indicators of wastewater pollution

Introduction

Urban wastewater is a significant cause of pollution. Techniques for purifying wastewater are critical for environmental conservation. At the moment, wastewater purification concerns focus primarily with cost and efficiency. This prompted us to investigate utilizing a low-cost natural substance in collecting and preparing it for use in wastewater treatment in aOuargla region by enhancing the absorption capacity of clay through the application of chemical activation and thermal activation of clay to remove organic contaminants. Slurry efficiency is determined by the factors (COD), (BOD5), (TSS), and turbidity.

VI.1. Clay (CM)samplepreparation

The clay sample was prepared to obtain grains measuring less than 2 micrometers by following the method detailed in the work of D.Atia [1]. It was obtained from El M'Guer municipality in El Oued province (46.73° N, 33.42° E), as shown in Figure. The granulometric analysis revealed that the raw soil contains 42% clay, with the remainder being silt and sand. Preliminary purification of organic compounds and calcite was carried out to obtain particles with a diameter of less than 2 μm. The physicochemical description of the clay was performed using a standardized method based on the principles established by the International Congress of Agriculture, primarily utilizing Stokes' law."

VI.2.Waste water

The ONA (Office National de l'Assainissement) station is a place of purification of OUARGLA CITY urban wastewater by lagoon. ONA implemented technical solutions consisting of the construction of a wastewater treatment plant by aerated lagoon, the renovation and extension of the urban sewerage network, the improvement of drainage conditions in the various palm groves of the basin through the construction of new drains or the improvement of the existing drainage system, and the construction of a channel for the discharge of sewage and drainage water to a new outlet sufficiently far from the agglomeration. This solution aims to ensure sustainable sanitation of the Ouargla basin.

Figure.VI.1: Location of ONA by google earth

This chapter work consists of two main processes for a sample of water taken from this station: activating the clay and treating the wastewater.

VI.3. Activation of clay:

The clay was activated according to the protocol of a previous study conducted on other types of clay by Soh, N. H. [2]. Activation helps improve the physical and chemical properties of clay. Acid processing removes impurities from the surface of the clay, while heat treatment changes the structure of the clay molecules. This process can be used to produce a variety of activated clay with different characteristics, which can be used in a variety of applications. Activated slurry properties depend on the type of slurry used, acid processing conditions and heat treatment conditions. Activated clay can have a variety of characteristics, including: high surface area, high porosity, high cation exchange ability, high adsorption ability and high catalytic activity

VI.3.1.Chemical activation

The acid treatment is typically carried out using a dilute solution of a strong acid, such as sulfuric acid or hydrochloric acid. The clay is suspended in the acid solution for a period of time. The acid dissolves the impurities on the clay surface.

a. Activation with hydrochloric acid (HCl)

The activation with hydrochloric acid was carried by removing of 5 g of purified clay to be mixed with 50 ml of hydrochloric acid at the following concentrations: (0.134 N, 0.335N, 0.671N, 006 N, 1.342N). Vibration was set 200 rpm at 60 ° C for one hour. After one hour, the mixture was removed and add distilled water to stop the reaction, then leave to stagnate. The clay obtained was washed with distilled water by centrifugation until we make sure that it is completely free of chloride ions, and we deduce that by testing the filtrate with a solution of silver nitrate ($AgNO_3$) with chlorinated acid and repeat the process until the white precipitate disappears from the filtrate to which the silver nitrate is added. silver nitrate

b. Activation with sulfuric acid (H_2SO_4):

We carried out the same previous process with the following acid concentrations: (0.1 N, 0.25N, 0.5N, 0.75N, 1N). We deduce sulfur ions without clay by filtering with a solution of $BaCl_2$ with sulfuric acid

VI.3.2.Thermal activation:

Thermal activation of clay is a process of heating clay to a high temperature in order to improve its physical and chemical properties. The heat treatment changes the structure of the clay particles, making them more porous and reactive. This process can be used to produce a variety of activated clays with different properties, which can be used in a variety of applications.

The thermal activation process typically involves heating the clay to a temperature of 400-800 degrees Celsius for a period of several hours. The specific temperature and heating time will vary depending on the type of clay and the desired properties of the activated clay.

The thermal activation process can have a number of effects on the properties of clay, including:

- Increased surface area: The heat treatment can increase the surface area of the clay particles. This makes the clay more reactive and capable of adsorbing more pollutants or other substances.

- Increased porosity: The heat treatment can also increase the porosity of the clay particles. This makes the clay more effective at filtering and removing pollutants from liquids and gases.

- Changed chemical composition: The heat treatment can also change the chemical composition of the clay particles. This can make the clay more effective at catalyzing certain reactions or removing certain types of pollutants.

The thermal activation of the raw studied clay is carried out according to a previous study [2], by burning the clay in an Amovel oven (High Therm VMK 39, over a temperature range of 100 to 500 ° C. 2 g the chemically activated clay were taken in a crucible, then this amount was placed in a removable oven, and the oven temperature was adjusted to the desired temperature, after 5 days, the samples were heated for one hour, then these samples were cooled in the dryer for 15 minutes.

VI.4.Processing step for wastewater treatment

The samples were collected from the Ouargla city wastewater treatment plant, which is located in the Said Otba neighborhood.

Throughout all treatment processes, a fixed volume of 600 ml of water was used to ensure the measurement of all treated water properties by studying the effect of chemical stimulation using a sulfuric acid concentration (H_2SO_4) from (1N 0.1-N) and relative to acid chlorine (HCl) from (1.342 N - 0.134N). We measured the required qualities after soaking 2 g of treated clay in 600 ml of water for two hours and stirring for two hours.

VI.4.1.The effect of chemical activation:

VI.4.1.1.The effect of the chemical activation of clay on the change of the value of the pH for -wastewater

Through the results obtained for the values of pH in polluted water ranging between (7.4-7,63) with an average value estimated at 7.51, while we distinguish according to Figure.VI.2 a slight increase in the values of water treated with raw clay (8,20).), and in general, we notice a decrease in the pH values after the activation process to be estimated at (7.55) 7.48 (7.53) for sulfuric acid and 8.15 (8.33 - 8.01) for hydrochloric acid, and this decrease explains The effect of acid on the crystalline structure of clay by substituting replaceable cations by protons [3], which leads to a change in the physical and chemical

properties of clay such as improving surface area, ketone exchange capacity and surface acidity, thus providing the required properties of the adsorbent influencer[4].

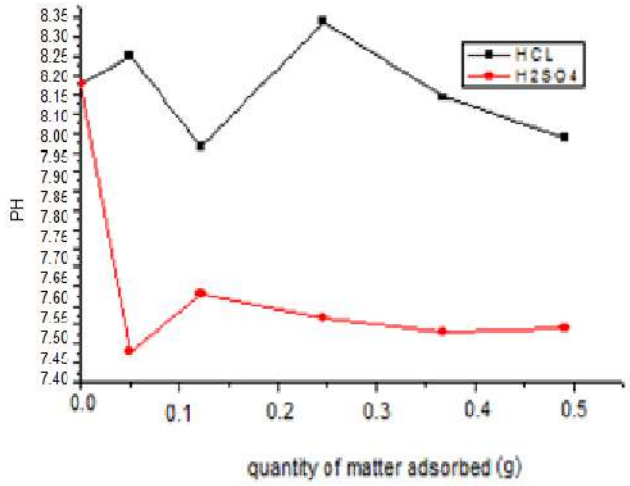

Figure.VI.2: pH changes of wastewater treated with chemically activated clay

VI.4.1.2.The effect of the chemical activation of clay on the change of the value of the Temperature for wastewater

Through the results obtained, the temperature values in polluted water ranged between (20.4 °C-19.7 °C) with an estimated average value of 20.05 °C, while we distinguish according to Figure.VI.3the temperature increased to Water treated with raw clay (25.6°C), and as is the case after the activation process with sulfuric acid and hydrochloric acid, respectively, to be estimated at (22.2 °C, 21.3 °C, -23,4 °C and 23.6 °C) (24°C– 23.3 °C), and this increase is generally explained by the fact that the adsorption process (solid-liquid) is an exothermic reaction [5].

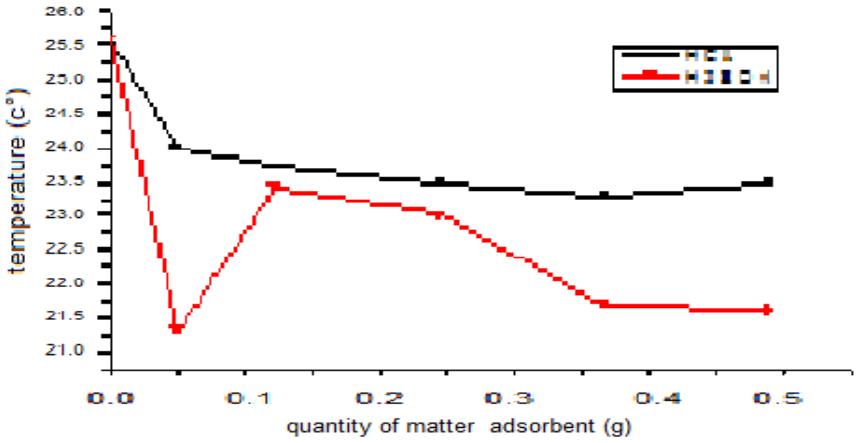

Figure.VI.3: Temperature changes of wastewater treated with chemically activated clay

VI.4.1.3.The effect of the chemical activation of clay on the change of the value of the EC for wastewater

Through the results obtained for electrical conductivity values (EC) in polluted water, we find that they range between (36-35.1ms/cm) with an average value estimated at 35.55ms/cm, while we distinguish according to Figure.VI.4 (confirmation of conduction values) The electrolysis of water treated with raw clay (44.9 ms/cm), as is the case after the activation process, is estimated at 33.26 ms/cm 31.6 ms/cm - (33.9ms/cm for sulfuric acid and 35.92ms/cm). cm (36,1ms/cm- 35.7ms/cm) for hydrochloric acid.

In general, the electrical conductivity values are very large, due to the mixing of the waste water coming to the station with the horizontal drainage water, the surface layer experienced by the region, to be affected by the high value of salinity in the water.

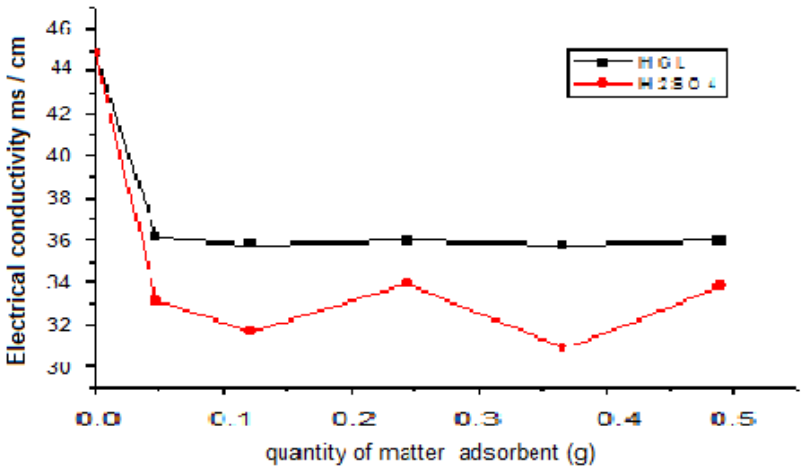

Figure.VI.4: Electrical conductivity values changes of wastewater treated with chemically activated clay

VI.4.1.4.The effect of the chemical activation of clay on the change of the value of the turbidity for wastewater

From Figure VI.4, we note that there is a high efficiency in removing turbidity from polluted water, as the raw clay achieved an average turbidity removal efficiency of 55.25% (75% - 35.5%), to notice an increase in that The ratios after enhancing the clay's ability by chemical activation process, where we obtained an average removal of 76.60% (76.60% - 90,74% - 61.52%) with sulfuric acid. As for the clay treated with hydrochloric acid, the removal rate ranged between (65.57% - 26.39%), with an average of 46.97%.

In order to compare which of the two acids is better for the activation process, we found that the best percentage of turbidity removal was at 90.75% for the amount of adsorbent (0.36 g/g), which corresponds to the concentration of N) (0.75 for sulfuric acid, as for hydrochloric acid). , the best percentage of turbidity removal was at 65,57 % for the amount of adsorbent (0.49 g / g), which corresponds to the concentration of N) (0,134). And through the obtained ratios, we conclude that sulfuric acid has a greater ability to further enhance the ability of the slurry to remove Compared to hydrochloric acid

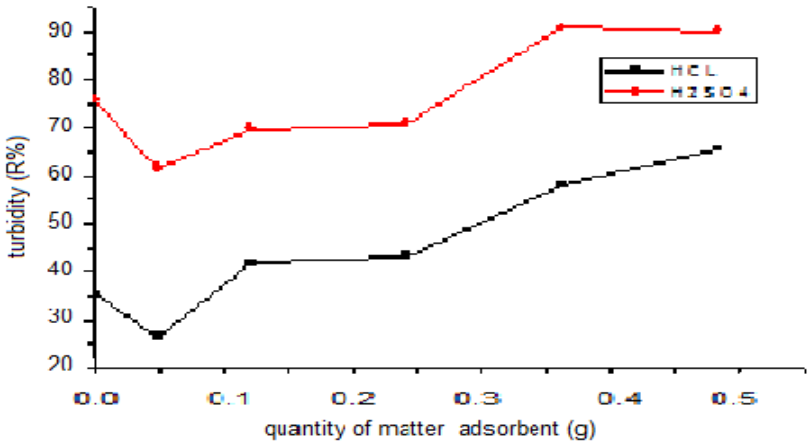

Figure.VI.5: Turbidity values changes of wastewater treated with chemically activated clay

VI.4.1.5.The effect of the chemical activation of clay on the change of the value of the suspended material(TSS) from wastewater

From Figure VI.5, we note that there is a high efficiency in removing suspended materials from polluted water, as the clay achieved a removal rate of 79.27%, which shows the effectiveness of the removal process with raw clay. To note the increase of that percentage after enhancing the clay's ability by chemical activation process, where we obtained an average removal of 84.09% (93.33% - 77.89%) with sulfuric acid. As for the mud treated with hydrochloric acid, the removal rate ranged between (79.26% to 94.31%), with an average of 89.37%.

In order to compare which of the two acids is better for the activation process, we found that the best percentage of suspended matter removal was at 93.33% for the amount of adsorbent (0.36 g/g), which corresponds to the concentration of N) (0.75 for sulfuric acid, while for chlorine acid In water, the best percentage of removal was at 94.31% for the amount of adsorbent (0.49 g / g), which corresponds to the concentration of N) (0,134). And through

the obtained ratios, we conclude that the two acids have a capacity that is considered close in order to further enhance the ability of the clay for removal.

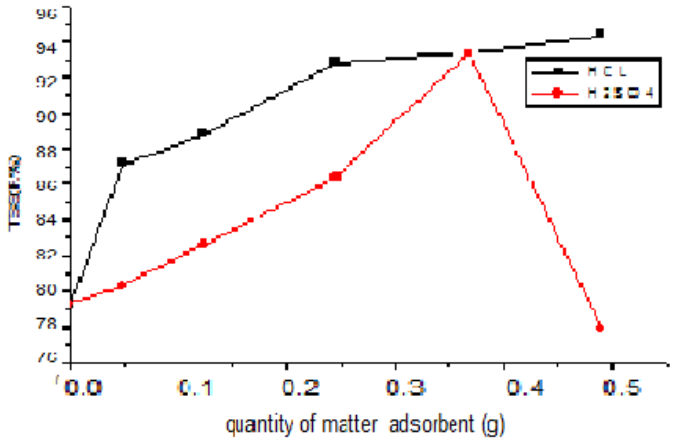

Figure.VI.6: Changes in the value of suspended matter (TSS) of wastewater treated with chemically activated clay

VI.4.1.6.The effect of the chemical activation of clay on the change of the value of the biochemical demand for oxygen (BOD_5) from wastewater

Figure VI.6 shows that there is a high efficiency in removing the biochemical oxygen demand (BOD5) from polluted water, as the clay achieved an average removal rate of 57,04%, which shows the effectiveness of the removal process with raw mud. To note the increase of those percentages after enhancing the clay's ability by chemical activation process, where we obtained an average removal of 85.68% (90.74% - 72.22%) with sulfuric acid. As for the mud treated with hydrochloric acid, the removal percentage ranged between (60.92% - 38.94%), with an average of 52.6%.

In order to compare which of the two acids is better for the activation process, we found that the best percentage of biochemical oxygen demand removal was at 90.74% for the amount of adsorbent (0.36 g/g), which corresponds to the concentration of N) (0.75 for sulfuric acid, as for sulfuric acid, as for the Water chlorine, the best percentage of removal was at 60.92 % for the amount of adsorbent (0.49 g/g), which corresponds to the concentration of N) (0,134). And through the results obtained, we conclude that sulfuric acid has a greater ability to further enhance the ability of clay to remove compared to hydrochloric acid.

The obtained results show a high efficiency of activated clay, especially with sulfuric acid (90.74%) to remove the biochemical oxygen demand compared to the activated carbon method, where a return of 87.55% was recorded [5].

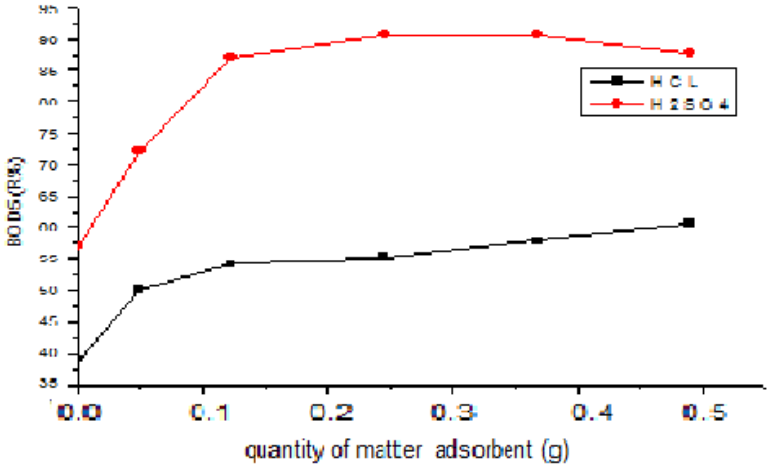

Figure.VI.7: Changes in the value of the biochemical demand for oxygen (BOD_5) of wastewater treated with chemically activated clay

VI.4-1.7.The effect of the chemical activation of clay on the change of the value of the chemical demand for oxygen (COD) from wastewater

The results obtained in Figure VI.7, show that there is a high efficiency in removing chemical oxygen demand (COD) from polluted water, as the mud achieved a removal rate of 71%, which indicates the effectiveness of the removal process with raw clay. To note the increase of that percentage after enhancing the clay's ability by chemical activation process, where we obtained an average removal of 75.02% (80.16% - 72.6%) with sulfuric acid. As for the clay treated with hydrochloric acid, the removal percentage ranged between (73% - 69%), with an average of 71%.

In order to compare which of the two acids is better for the activation process, we found that the best percentage of suspended matter removal was at 80.16% for the amount of adsorbent (0.36 g/g), which corresponds to the concentration of N) (0.75 for sulfuric acid, while for chlorine acid In water, the best removal rate was at 73% for the amount of adsorbent (0.49 g/g), which corresponds to a concentration of N) (0,134). And through the results obtained, we conclude that sulfuric acid has a greater ability to enhance the ability of clay to remove compared to chloridric acid. On the other hand, the activated carbon method recorded

a yield of 86.90%(higher for removing chemical oxygen demand compared to activated clay, especially with sulfuric acid (80,16%) [5].

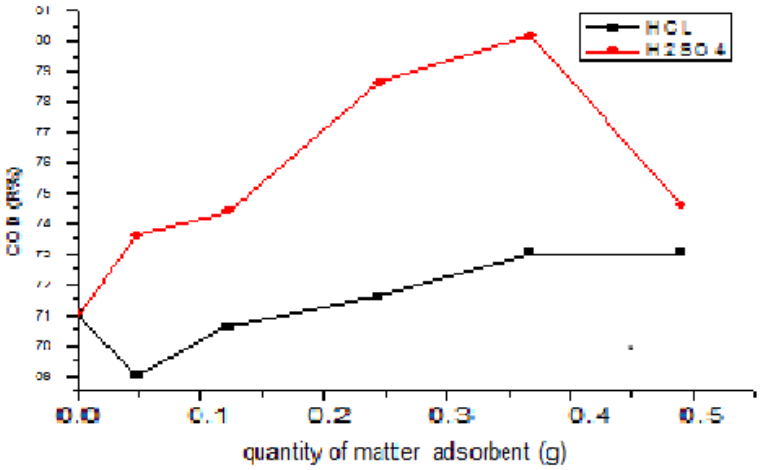

Figure.VI.8: Changes in the value of the chemical demand for oxygen (COD) of wastewater treated with chemically activated clay

VI.4.2.The effect of thermal activation:

The optimum conditions for chemical activation were determined, from sulfuric acid with a concentration of (0,75N), and on this basis, we performed a heat treatment process according to those conditions.

VI.4.2.1.Effect of activated clay with sulfuric acid and heat on the efficiency of changing physical properties (pH, T, EC)

From Figure VI.8, we note that the values of the physical properties of (pH, T, EC) remained constant at all temperatures from (500 °C -100 °C) for water treated with chemically activated and thermally activated clay, and this indicates that the activation Thermal temperature does not change the physical properties, the change is only related to particle size and heating system [6]

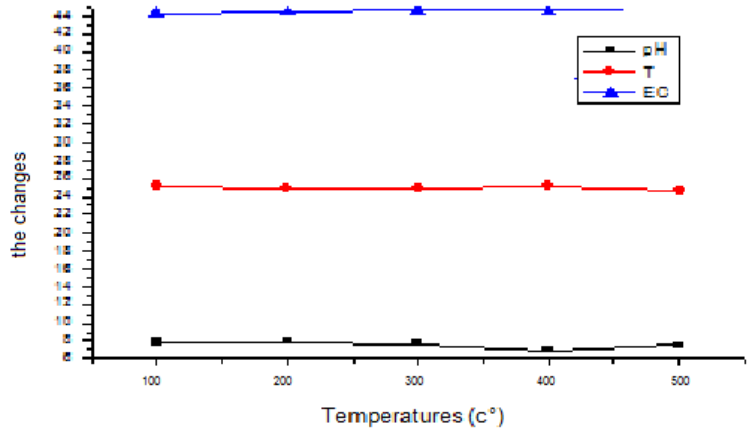

Figure.VI.9: Changes of physical properties (pH, T, EC) of wastewater treated with chemically and thermally activated clay

VI.4.2.2.Efficiency of sulfuric acid and heat activated clay in removing organic pollutants.

Figure VI.9 shows. The effectiveness of chemical and thermal activation in removing organic pollutants, as it is noted that the removal rate increases with increasing temperature until it reaches 400 °C, so the removal percentage of COD, BOD5, TTS and Turb, respectively, becomes 82%, 65%, 89.56%, 78.65 % . Then the removal rate begins to decrease after 400°C, due to the decrease in the surface area due to the damage to the clay structure by collapsing its interspaces, which makes the particles closer to each other [7].

Similar results were obtained by [7], where they examined the thermal activation of bentonite in the temperature range from 100°C to 1300°C and observed that the surface area increased with increasing temperature and then decreased at a temperature of more than 400°C.

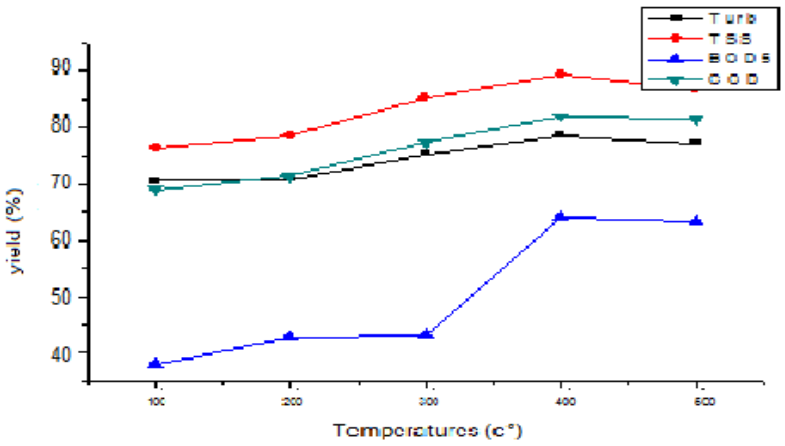

Figure.VI.10: Efficiency of sulfuric acid and heat activated clay in removing organic pollutants.

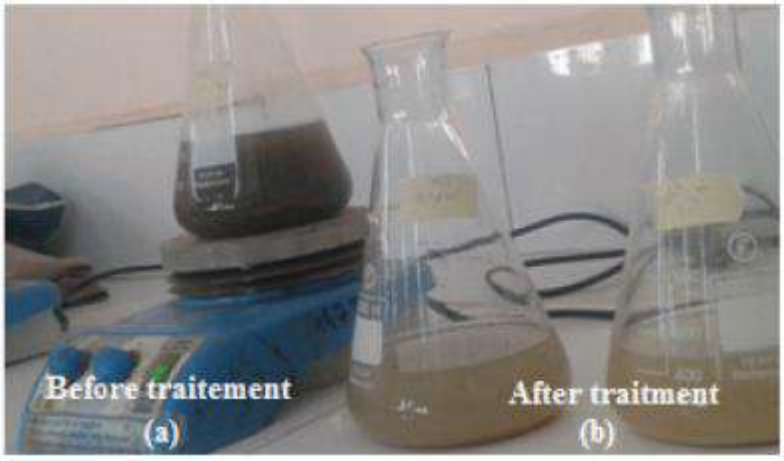

Here we show the picture taken of the sample before and after our processing process. This picture shows the effectiveness and success of our purification process. Where we note the big difference between the original vaginal sample and the final sample.

CONCLUSIONS

This chapter studies the adsorption capacity enhanced it thermally and chemically activating with sulfuric acid and hydrochloric acid to remove organic pollutants from wastewater in the Ouargla region (Said Otba) and also specifying the best experimental conditions for chemical and thermal activation.The results of the wastewater analyses showed good efficiency due to the use of raw clay by eliminating pollutants. Sulphuric acid activated clay showed increased efficiency in removing pollutants from wastewater more than hydrochloric acid.

Reference

[1] Atia, D.; Bebba, A. A.; Haddad, L.; Zobeidi, A. Elimination of Organic Pollutants from Urban Wastewater by Illite-Kaolinite Local Clay from South-East of Algeria. *Cienc Tecn Vitivinic***2018**, *33*, 17–28.

[2] Ndé, H. S.; Tamfuh, P. A.; Clet, G.; Vieillard, J.; Mbognou, M. T.; Woumfo, E. D. Comparison of HCl and H2SO4 for the Acid Activation of a Cameroonian Smectite Soil Clay: Palm Oil Discolouration and Landfill Leachate Treatment. *Heliyon***2019**, *5* (12), e02926. https://doi.org/10.1016/j.heliyon.2019.e02926.

[3] Steudel, A.; Batenburg, L.; Fischer, H.; Weidler, P.; Emmerich, K. Alteration of Swelling Clay Minerals by Acid Activation. *Appl. Clay Sci. - APPL CLAY SCI***2009**, *44*, 105–115. https://doi.org/10.1016/j.clay.2009.02.002.

[4] Doulia, D.; Leodopoulos, C.; Gimouhopoulos, K.; Rigas, F. Adsorption of Humic Acid on Acid-Activated Greek Bentonite. *J. Colloid Interface Sci.***2009**, *340*, 131–141. https://doi.org/10.1016/j.jcis.2009.07.028.

[5] Douadi, A.; Kamarchou, A.; Bebba, A. A. Elimination of Phosphorus by Activated Carbon Prepared from Algerian Dates Stones. *Res. J. Pharm. Biol. Chem. Sci.***2015**, *6*, 1271–1278.

[6] *Handbook of Clay Science, Volume 1 - 1st Edition*. https://shop.elsevier.com/books/handbook-of-clay-science/bergaya/978-0-08-044183-2 (accessed 2023-12-30).

[7] Önal, M.; Sarıkaya, Y. Preparation and Characterization of Acid-Activated Bentonite Powders. *Powder Technol.***2007**, *172* (1), 14–18. https://doi.org/10.1016/j.powtec.2006.10.034.

CHAPTER SEVEN :

Kornerupine Clay

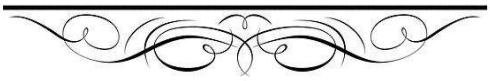

Introduction

The study carried out in this chap the identification of the mineralogical composition of a clay sample from the south-east of Ouargla "Oued N'sa", in Algeria. Mineralogical identification was performed using scanning electron microscope, infrared spectroscopy (IR) and x-ray diffraction (XRD).The majority composition in this variety of clay is found Kornerupine.

The chemical formula of kornerupine, a complex mineral, can change as a result of compositional changes and substitutions[1,2].. The key elements found in the structure of kornerupine are represented by the principal chemical formula $(Mg,Fe^{2+}).4(Al,Fe^{3+}).6(SiO_4,BO_4)5(O,OH)_2$, which is composed of magnesium (Mg), iron (Fe), aluminum (Al), silicon (Si), boron (B), oxygen (O), and hydroxide (OH).

However, due to elemental substitutions within its structure, there may be very tiny differences in the chemical composition. The proportion of magnesium, iron, aluminum, and boron in different kornerupine specimens may change, changing the chemical formula while preserving the species' general structure and characteristics.

Although the previously given formula depicts the general composition of kornerupine, some modifications and deviations may happen depending on the particular mineral sample. These differences represent the inherent variety frequently seen in mineral compositions rather than altering the fundamental nature of the mineral. In 2009, Mark A. Cooper et al, developed a procedure for obtaining complete chemical formula and chemical composition of a kornerrupin sample from data acquired with an electron microprobe and reticular parameters. it was able to express the content of atoms by a linear function of the mesh parameters and the Al_2O_3 and FeO contents (in %, weight) [3].

The adsorption behavior of the anionic dye (Congo Red) from aqueous solutions onto the natural clay studiedisexamined here by the mean of Fenton process, photocatalysis process, photo-Fenton process.

VII.1.Samples

Clay sample was collected from "Oued N'sa" regions (figure VII.1) in Algeria. As shown in figure VII.2. Pieces of brown mud and rough texture were reaped and formed by irregular, broken pieces with small to medium pieces size.

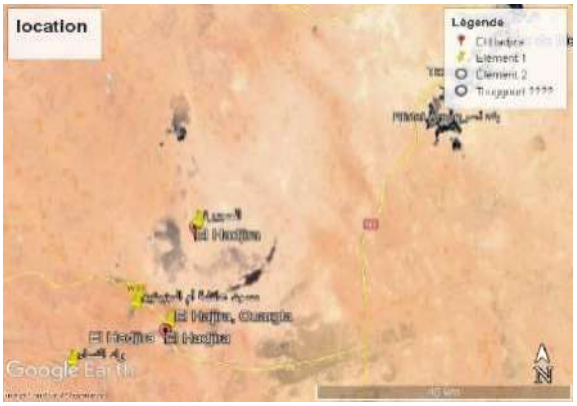

Figure.VII.1: The Google Earth-captured location of the sample collection region

Figure.VII.2: the clay sample

VII.2.Simple preparation

A successful identification of the physico-chemical properties of clay is an essential step in the development of technological applications[4].Before preparing the sample for both the physiochemical characterization and application in the field of water pollution removal, a very important process was carried out, namely granular analysis

VII.2.1.Granulometry analysis

Granulometry analysis is fundamental in the first step of preparing a clay sample because it helps to determine the size distribution of the clay particles. The conditions for preparing the sample for analysis are presented in Table VII.1

Table.VII.1: Conditions for preparing clay

sample preparation	
Total weight before washing	350
Total weight after washing	72,9
Drying temperature	65°C

Table.VII.2 summariz the results of a granulometric analysis of the sample. The table lists the mesh size (mm) of each sieve used, the weight of the material retained on each sieve, the cumulative weight retained on all finer sieves, and the percentage of material retained on each sieve. The simple contains a wide range of particle sizes.

Table.VII.2: Granulometric analysis of the sample results

Sieve (mm)	Weight	Cumulative weight	% refusal	% sieve
100	0		0,00	**100**

50	0	0	0,00	**100**
40	0	0	0,00	**100**
31,5	0	0	0,00	**100**
25	0	0	0,00	**100**
20	0	0	0,00	**100**
16	0	0	0,00	**100**
12,5	0	0	0,00	**100**
10	0	0	0,00	**100**
5	0	0	0,00	**100**
2	4	4	1,14	**99**
1	2,8	6,8	1,94	**98**
0,4	4,3	11,1	3,17	**97**
0,2	10,4	21,5	6,14	**94**
0,08	43,2	64,7	18,49	**82**

Table VII.2 shows the weight and percentage of particles that passed through each sieve, as well as the corresponding weight and percentage of particles that were retained on the sieve mesh. We conclude that the sample contains a high percentage of micrograins. 94% of the sample weight is granules with a size below 0.4 mm. This indicates that the clay is sticky and formable, and has low permeability. This makes it suitable for different applications.

- **Micrograin ratio 94%:** This ratio indicates that the sample contains a high percentage of granules less than 0.4 mm in size. These granules are too precise to be seen with the naked eye.
- **Coarse granule ratio 6%:** This ratio indicates that the sample contains a low percentage of granules with a size greater than 0.4 mm. These granules are larger than micrograins and can be seen with the naked eye.
- **Dominant granule diameter 0.08mm**: This diameter indicates that the most common diameter of granules in the sample is 0.08mm. This means that most granules in the sample are about the same size.

From these data results,wich indicate that the clay sample contains a large amount of small particles. This shows that the clay sample has low permeability, making it acceptable for diverse use. In order to learn more about the grain measurement in the nanoscale field, since granular analysis included only the micrometric field, we resorted to the automated sifting method as follows.

VII.2.2.Grain separation

The clay was purificated using the wet approach, which involved three steps, which can be summarized as follows:

1. First, we separate the impurities and the coarse clay grains by placed clay in water until it was completely dissolved, then it was sifted in the vibratory sieve shakers

(Retsch. AS 200) through 5 sieves of different porosities (125, 100, 63, 50,40 µm) in order from top to bottom (Figure VII.3), after which it was dried under the sun.

Figure VI.3. Vibratory sieve shakers (Retsch. AS 200)

2. Once more dissolved, the clay in water is then passed through a fitting that has a 5 µmand dried in the sun and then, the clay is additionally dried at 80 C° in the oven to remove moisture(Figure VII.4).

FigureVII.4: Experimental setup used in clay purification.

3. In order to obtain clay minerals with a size of 2µm, a sieve with a porosity of 2 µm was used at this point. However, the process failed due to a hole in the sieve, which was caused by the vacuum pump's pulling force, so we had to change the procedure and use another method. We used the sedimentation method, where we took 10 g of the clay obtained from stage 2 and put it in a liter of distilled water and shook it for two hours (Figure.VII.5). It was placed in a graduated tube of 1 liter for 24 hours

(Figure.VII.6), after which 2/3 of its volume was withdrawn and dried in the oven at a temperature of 105 degrees.

Figure.VII.5: The shaking process.

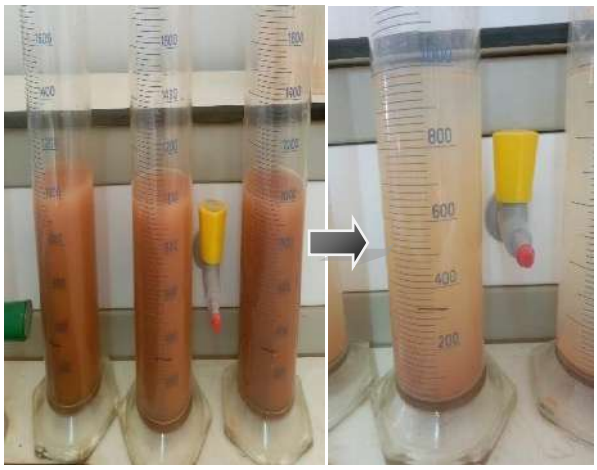

Figure.VII.6: A picture of the clay before and after 24 h

VII.3. Sample caracterization

VII.3.1.Clay microstructure using SEM-EDX

The physical microstructure of the sample was analysed on the basis of the SEM-EDX. Figure VII.7shows the individual grains that make up the clay. As shown by the magnification (x5.00), the presence of pores is evident, different pore sizes averaging 1 µm to 2,5 µm, are observed.

The results of the elemental analysis, in terms of weight and atomic percentage, are listed in Table VII.3. The major elements are silicon (Si), aluminum (Al), and sodium (Na). The minor elements are potassium (K), calcium (Ca), magnesium (Mg), iron (Fe). The Si and Al atoms are the main components of the clay minerals. The Fe atoms are also present in some clay minerals. The K, Ca, Mg, Fe, Mn atoms are typically present in smaller amounts in clay minerals.

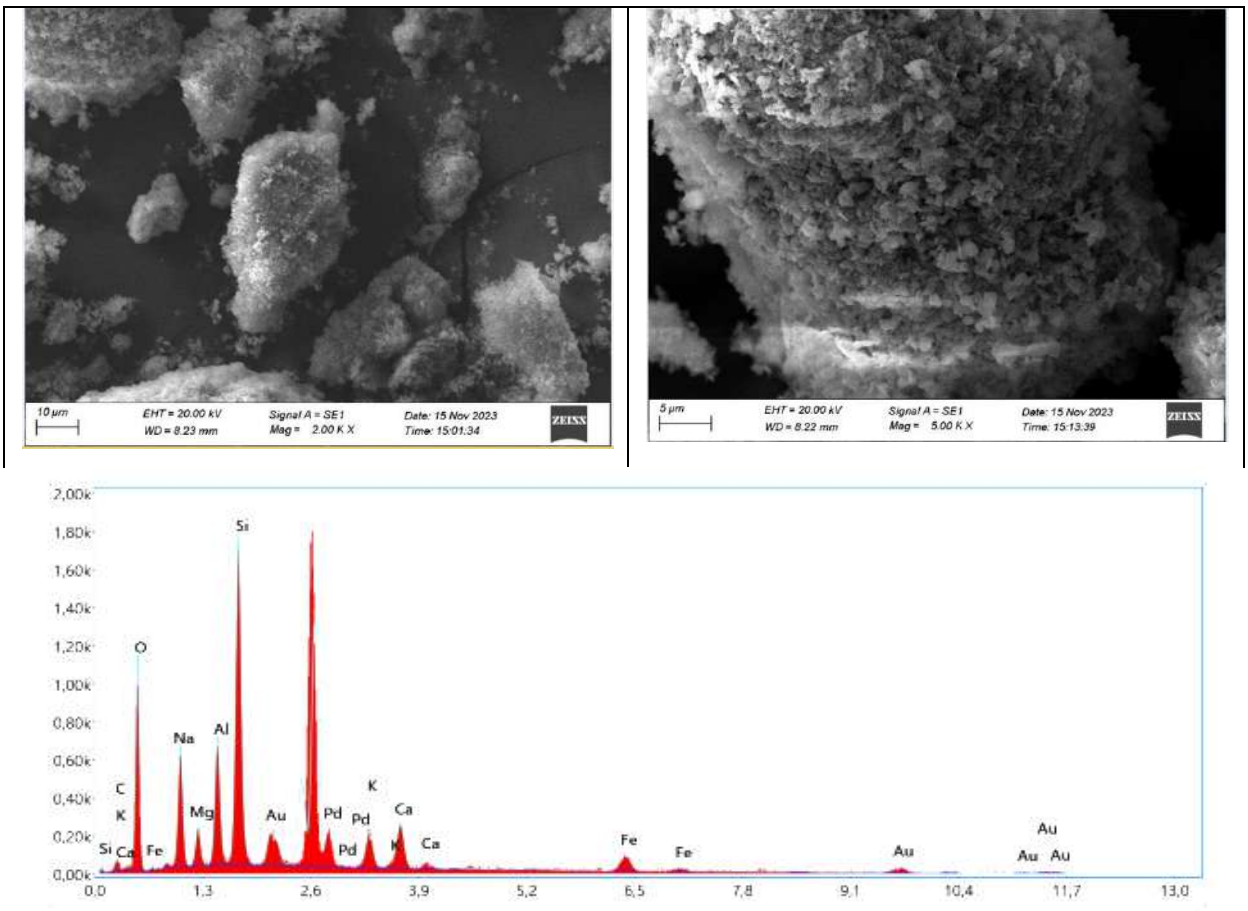

Figure.VII.7: Scanning electron microscopic images of clay materials

Table.VII.3: Quantitafsresultof clay EDX

element	% of mass	% atomic	Intensity total	Error %	Kratio	Z	A	F
C K	0.37	0.83	0.41	99.99	0.0007	1.1925	0.1695	1.0000
O K	27.20	46.35	73.64	10.09	0.0726	1.1462	0.2330	1.0000
NaK	11.51	13.65	48.30	9.32	0.0454	1.0460	0.3772	1.0006
MgK	2.65	2.98	16.28	10.42	0.0126	1.0653	0.4443	1.0013
AlK	7.53	7.61	56.17	7.32	0.0433	1.0271	0.5579	1.0021
SiK	17.78	17.26	152.75	5.71	0.1171	1.0508	0.6252	1.0024
PdL	7.94	2.03	26.54	3.82	0.0566	0.7868	0.9055	1.0009
K K	2.86	1.99	17.15	12.55	0.0229	0.9788	0.8097	1.0109
CaK	5.17	3.52	27.21	7.39	0.0434	0.9975	0.8318	1.0123
FeK	4.06	1.98	13.69	9.40	0.0377	0.8940	0.9699	1.0717
AuL	12.92	1.79	6.02	25.81	0.0809	0.6042	1.0335	1.0027

VII.3.2.Clay identification using FT-IR

The absorption at roughly 1650 cm^{-1}, which corresponds to the H–O–H angular deformation, confirms the presence of H2O [5].The presence of this peak indicates that the clay minerals in the sample have a large surface area and are capable of adsorption of water.The vibrational bandat 1950 $cm^{-1}$is attributed to the CO stretching, which confirms the presence of calcite [6]. The vibration bands of valence at 3400 - 3600 cm^{-1} are characteristic of the vibration of the hydroxyl function of the water of hydration of the clay [6].As , we can found in the same interval vibrations of the bonding of an atom of aluminum and a magnesium atom (3582 cm^{-1}) or two aluminum atoms (3431 cm^{-1}. The bands between 800 and 750 cm^{-1} , from the Si–O–Al bond, also give way to a band around 778.4 cm−1 . The bands observed at 798 cm−1 are attributable to the Si–O–Al stretching vibrations and the hydroxyls perpendicular to the surface (translational OH). The band at 660 cm−1 is characteristic of the deformation vibrations of hydroxyls in trioctaedric clay minerals in general. Nevertheless, the absorption bands at 797 and 779 cm−1 can correspond to Quartz [24,34,35].The Si-O group band, intense at around 1100, 550 cm^{-1} are ascribed to binding valence vibration in clay minerals.

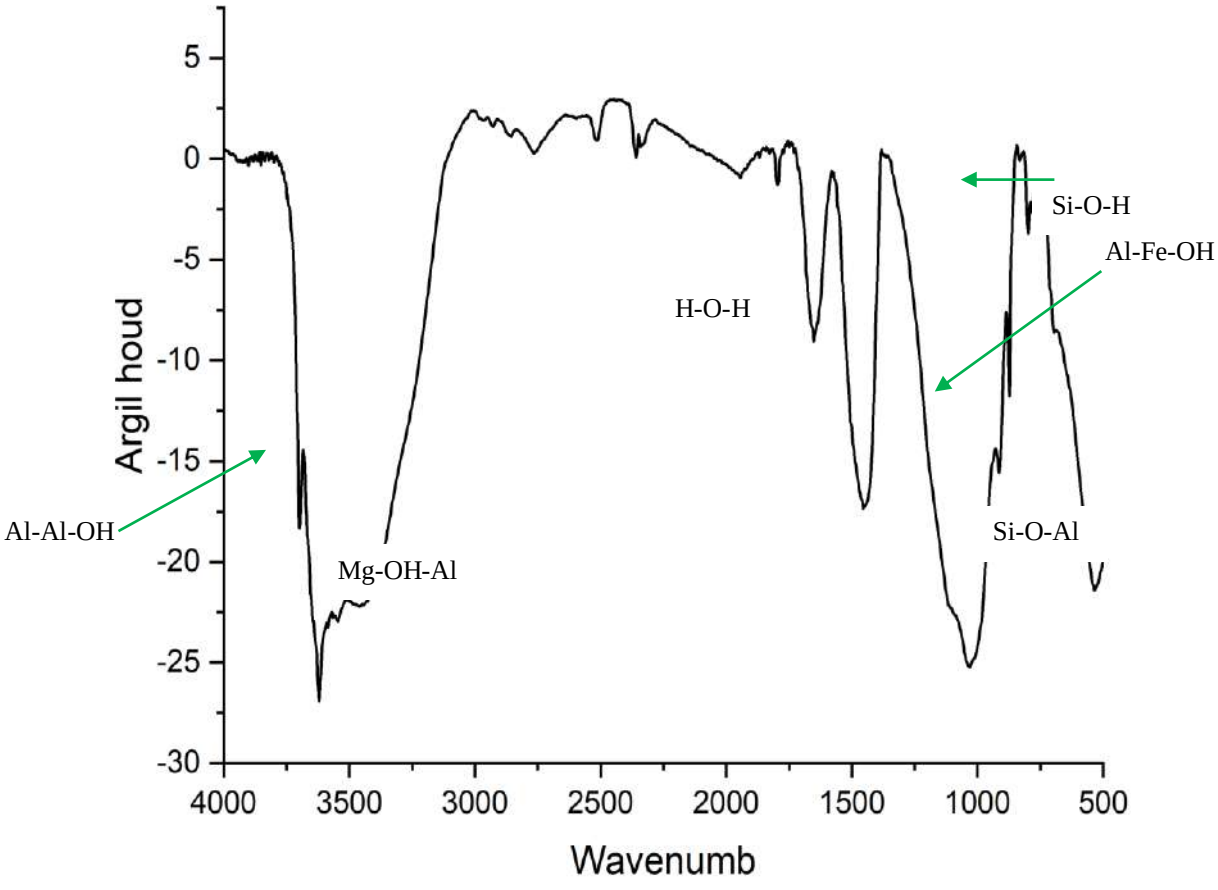

Figure.VII.8:FTIR spectrum of clay sample

VII.3.3. X-Rays Analysis

Figure VII.9 shows the meusurement profil of the clay. The diffractogramenregistred suggests that the clay sample is relatively impure, with minimal amounts of other minerals present. Based on the diffractogram of figure VII.9, and the phase identification the clay sample usingPDXL2 Program (figure.VII.9) shows that the simplecontains Kornerrupine ($Mg_3Al_6(Si_8Al_2)_5O_{21}(OH)$) [1], $MgSiO_3$(Enstatite)[7], silica and calcite as listed in the table VII.4 quantitative analysis of the clay. Kornerupineis the most abundant phase, with a figure of merit of 3.340.Enstatite and quartz are less abundant, with figures of merit of 3.340 and 3.207, respectively.

The diffractogramme also shows the presence of quartz, as indicated by peak at around $2\theta = 26{,}6°$. Quartz is a common mineral that is often found in association with clay minerals [8].

The presence of enstatite and quartz suggests that the sample may have been subjected to high-temperature conditions. Enstatite is a high-temperature mineral found in igneous and metamorphic rocks, while quartz is a common mineral that can form in a wide range of geological settings.

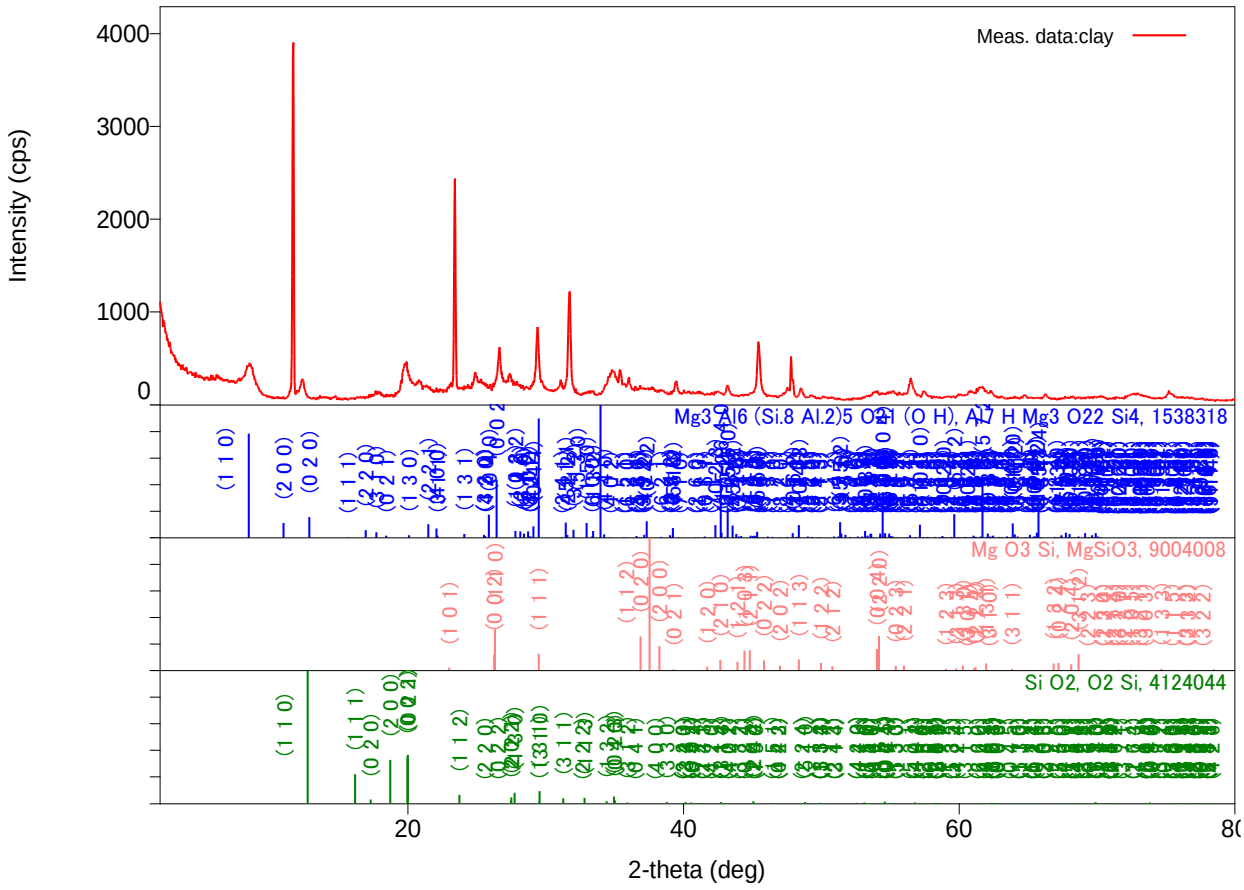

Figure.VII.9: Xrays patter of the clay

Table.VII.4: Qualitative analysis results of the clay

Phase name	Formula	Figure of merit	Phase reg. detail	DB card N°	Space group
Mg3 Al6 (Si.8 Al.2)5 O21 (O H)	Al7 H Mg3 O22 Si4	3.340	User (COD)	1538318	63 : Cmcm
Mg O3 Si	MgSiO3	3.340	User (COD)	9004008	62 : Pbnm
Si O2	O2 Si	3.207	User (COD)	4124044	63 : Cmcm

Table.VII.5: Cell parameters of the clay phases

Phase name	a(A)	b(A)	c(A)	α(deg)	β(deg)	ϒ(deg)	V(A^3)
Mg3 Al6 (Si.8 Al.2)5 O21 (O H)	15.631615	14.109659	6.709678	90	90	90	1479.86486
	16.1	13.76	6.735	90	90	90	1492.8
Mg O3 Si	4.618691	4.909397	6.644185	90	90	90	150.656801
	4.701	4.87	6.782	90	90	90	155.266
Si O2	9.768989	10.312022	8.981858	90	90	90	904.814684
	9.475	10.244	8.888	90	90	90	862.873

VII.3.3.1.Crystallite size and lattice strain

Crystallite size and lattice strain, As previously presented are calculed using Williamson-Hall method. Table VII.6 repport the calculated crystallite sizes and the slopes of the regression lines indicate the lattice strain for each phase.

Table.VII.6: Crystallite size and lattice strain

Phase name	Crystallite size(A)	Strain(%)
Mg3Al6 (Si.8 Al.2)5 O21 (O H)	206.59(6)	0.22(3)
MgO3Si	9486(171)	0.3803(10)
SiO2	440.54(4)	0.111(4)

Enstatite has the largest crystallite size, followed by kornerupine and then quartz. This order may be related to the formation conditions of the minerals, with enstatite potentially forming in higher temperature environments compared to the other two.

Kornerupine has the highest lattice strain, followed by enstatite and then quartz. This suggests that the Kornerupine lattice is more distorted compared to the other two minerals. This could be due to various factors, such as substitutions within the crystal structure or internal defects.

VII.3.3.2.Quantitative analysis result

The quantitative analysis in table VII.7 provides information about the relative abundances of the different phases.

Table.VII.7:abundances of the different phases in the clay sample

Phase name	Content (%)
Mg3 Al6 (Si.8 Al.2)5 O21	94(19)
Mg O3 Si	2(2)
Si O2	4(2)

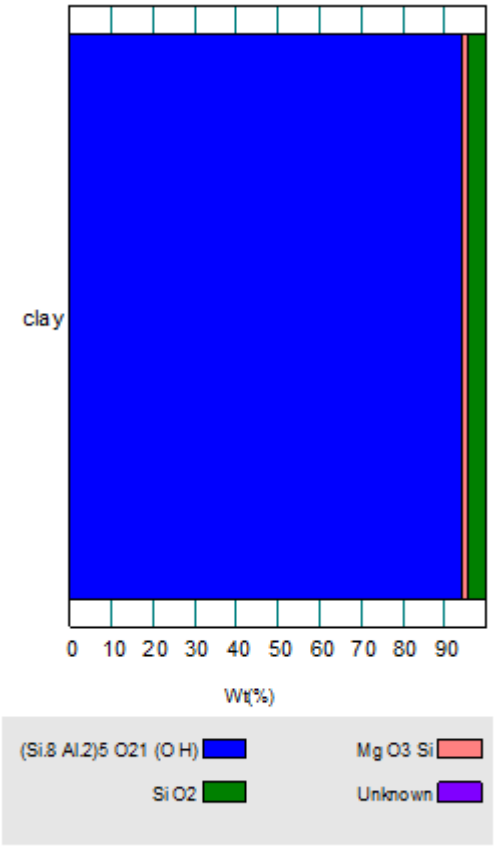

Figure.VII.10: Quantitative analysis of the clay

Since kornerupine is the chemical phase that is most prevalent in the sample, we will present his crystal structure based on earlier research because he will be accountable for this sort of clay's efficacy. In order to comprehend the crystal structural structure's content. Clay assymetric unit .

VII.4.Crystal structure description

First, using mercury programm, we visualis the asymetric unit and the molecule (figure. VII.11), then the package to show the lattice (figure.VII.12).

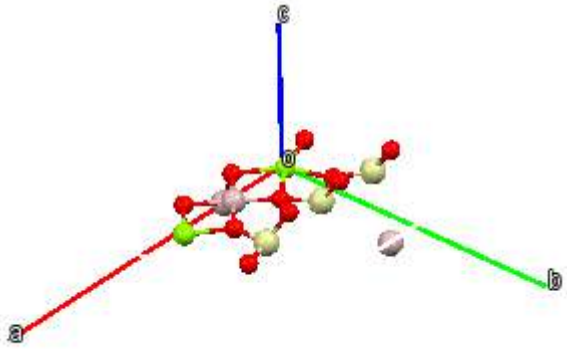

Figure.VII.11:asymetric unit

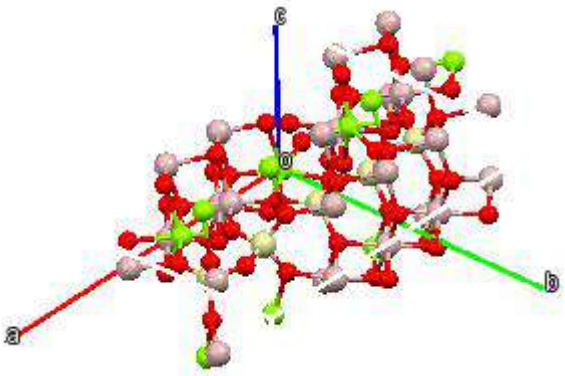

Figure.VII.12: the molecule

The crystal structure consists of chains of alternating Mg-O and Al-O octahedra bonded to the walls by further edge-sharing to form dense slabs, and walls made of Al-O edge- and corner-sharing octahedra. Corner-sharing tetrahedral pairs [Si2O7] and corner-sharing tetrahedral triplets [(Al,Si)2SiO10] hold these slabs together.

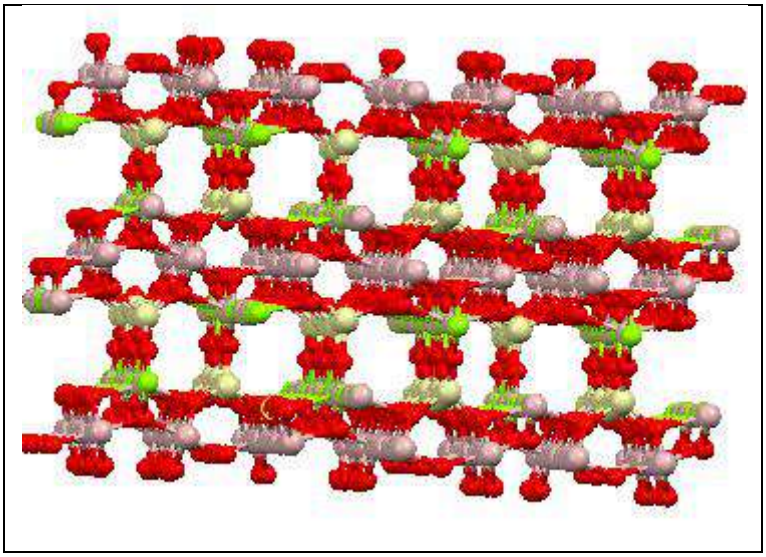

Figure.VII.13: arrangement in kornerupine lattice

VII.5. Removal of congo red dye by Clay

VII.5.Remove of congo red dye byclay

VII.5.1.Adsorption

For adsorption, the 0.05g catalyst (Clay) was dispersed in an aqueous solution of Rouge Congo (CR) in a beaker, with samples taken 15 minutes apart for a period of 120 minutes

under vigorous agitation. The samples were centrifuged at 6000 rpm for 5 minutes, and the supernatant was analyzed by UV-Visible spectrophotometry

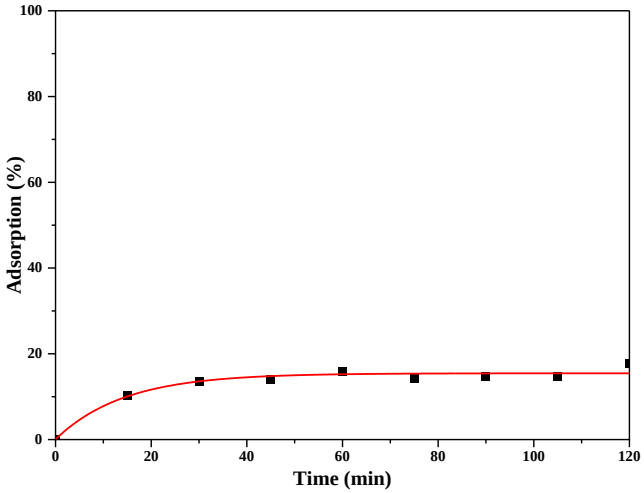

Figure.VII.14: The kineticsof coloran CR adsorption

VII.5.2.Fenton

For the Fenton degradation process, was performed in the dark at room temperature. 0.05 g of clay was first dispersed in 100 ml of CR solution[24.5 mg/L] for 60 minutes. When adsorption equilibrium was reached, the reaction was started by adding 52 µl of hydrogen peroxide (30%) (H_2O_2), and finally samples were taken at 10-minute intervals for a total of 120 minutes for analysis by UV and visible spectrophotometry.

VII.5.3.Photodegradation

The photodegradation activity of the clay was evaluated using 0.05 g of material in 100 mL of CR solution. Following 60 minutes of stirring to achieve adsorption equilibrium, the suspension was irradiated with UV light (λ = 254 nm, 10 W). Samples were withdrawn at 10-minute intervals for UV-vis analysis to monitor the dye degradation progress.

VII.5.4.Photo-Fenton

Building upon the photocatalysis setup, Photo-Fenton experiments employed identical conditions with the addition of 52 µL of H_2O_2 introduced at 30 minutes along with the initiation of UV irradiation.

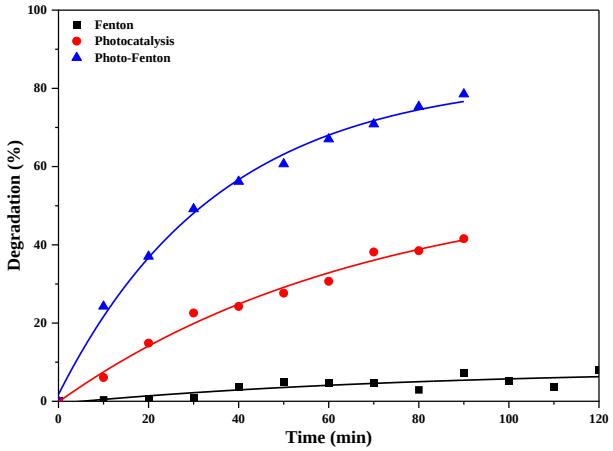

Figure.VII.15:CR degradation by fenton, photocatalysisand photofenton.

Test results show that the photofentone method is the most effective in degrading Congo Red dye, as the degradation rate reached 77%. Followed by the photocatalytic method at a rate of 40%, then the Fenton method at a rate of 7%.

In fonton method, hydrogen peroxide is added in the dark to form free hydroxyl radicals, which react with Congo Red dye molecules and destroy them.The results obtained can be explained as The main reason may be that the amount of hydrogen peroxide you added is insufficient to create enough free hydroxyl radicals.or The reason may be that the room temperature was too low, which slowed down the rate of formation of free hydroxyl radicals.and also The reason may be that there are some impurities in the clay or in Congo Red dye that prevent the formation of free hydroxyl radicals.

Photodegradation method relies on the use of ultraviolet (UV) light to stimulate redox reactions on the clay surface. This reaction breaks down Congo Red dye molecules into smaller, less stable compounds, facilitating the degradation process.

Photo-fonton method relies on the use of ultraviolet light and the addition of hydrogen peroxide (H_2O_2) to the medium. The reaction of hydrogen peroxide with ultraviolet light produces free hydroxyl radicals (OH), which are highly reactive molecules that can react with and destroy Congo red dye molecules.

Socio-Economic Study

Evaluation of the efficiency and cost of the degradation of red Congo by hybrid chemical complexes and natural clay.

Introduction

Congo Red is a synthetic dye used in many industrial products, including textiles, cosmetics and inks. It is also used in paints, varnishes and plastics. Red Congo is an environmental pollutant and a threat to human health. It is classified as a possible carcinogen by the International Agency for Research on Cancer (CIRC).

The results obtained in the work of this thesis as we pointed out in chapters (III and V) led to the synthesis of the two compounds FS and CD. Those were concerned by the cathalytic study against the degradation of red congo. In chapter (IV) for clay of the H'jira region.

The cost of producing hybrid chemical complexes

Table 1 lists the purchase costs of precursers in Algerian dinard and euro. Note that we will neglect the costs of solvent (distilled water), heating energy and thermal agitation.

According to the results of Table 2, in order to produce 0.43 g of FS, 5.269 € must be supplied, and 0.52 g of FS must be supplied 0.383 €. This means that the production of one kilogram of FS is 12253.48 € and the production of one kilogram of CD is 736,53 €. These results show that the production of 1 kg of FS equals 16 the production cost of CD.

Table 1: Cost of purchasing the main starting products.

	Chemical formula	Name		DZA	Euro
1	$FeCl_3.6H_2O$	iron(III) chloride	5 g	5301,83	36
2	$H_2C_4O_4$	squaric acid	5 g	13004,22	88.3
3	$CdCl_2.H_2O$	Cadmium chloride hydrated	50g	13122,04	89.10
4	$C_2H_8N_2O_4.H_2O$	Ammonium oxalat	1000 g	18846,13	176.38

And table 2, gives the costs of the quantities used for an experimental preparation for a given chemical synthesis and the quantities obtained.

Table 2: Cost of quantity used in chemical synthesis and quantity obtained

	Chemical formula	quantité	DZA	Euro	Total (Euro)	Quantité obtenu
1	$FeCl_3.6H_2O$	0.11 g	11664,026	0.792	5.269	0.43 g
2	$H_2C_4O_4$	0.2705 g	7.352.83	4.777		
3	$CdCl_2.H_2O$	0.20132 g	5283,458	0.358	0.383	0.52 g
4	$C_2H_8N_2O_4.H_2O$	0.14212 g	267841199-	0.025		

The cost of producing natural clay.

Clay is a natural material that is found in many places on earth. It is usually extracted by mining methods, such as open pit or underground mining. The cost of clay extraction depends on several factors, including the quality of the clay, the depth of the extraction and the distance to which the clay must be transported.

In general, the cost of clay extraction is relatively low. For example, the cost of extracting bentonite clay in Algeria is estimated at about 100 Algerian dinars (0.75 euro) per tonne.

The cost of clay production in our study may be consdered as negligible. It was extracted from the by flying persons. In addition, clay is a renewable resource, meaning it can be extracted and used without depleting reserves.

The cost of implementation the degradation technique.

The cost of implementing photocathalysis depends on several factors, including the size of the facility and the complexity of the system.

For hybrid chemical complexes, the cost of implementing photocathalysis includes:

1. The cost of materials: hybrid chemical complexes are synthetic products that can be expensive. The cost of materials depends on the composition of the complexes and the amount needed.

2. Equipment cost: photocathalysis requires specific equipment including UV or lamps. The cost of the equipment depends on the power of the lamps and the size of the installation.

3. Energy cost: photocathalysis requires energy to power UV or LED lamps. The cost of energy depends on the power of the lamps and the operating time of the installation.

For natural clay, the cost of implementing photocathalysis includes the following:

The cost of materials: clay is a natural material that is relatively inexpensive. The cost of clay depends on the quality of the clay and the amount needed.

1. Equipment cost: photocathalysis requires specific equipment including UV or LED lamps. The cost of the equipment depends on the power of the lamps and the size of the installation.
2. Energy cost: photocathalysis requires energy to power UV or LED lamps. The cost of energy depends on the power of the lamps and the operating time of the installation.

It can be concluded that the cost of implementing photocathalysis for hybrid chemical complexes is higher than for natural clay.

- The cost of UV or LED lamps can vary from a few hundred euros to several thousand euros per unit.
- The energy cost may vary depending on the power of the lamps and the operating time of the installation

Table 3 : Percentage of Congo red degradation in the three compound using the three process.

Degradation						
CLAY (**Figure. VII-5)**		FS (**Figure. V-10)**		CD (**Figure. III-18)**		
%	Time	%	Time	%	Time	
6	120	99	60	25	120	Fonton
44	90			25	90	Phonodegradation
80	90			77	90	Photo-fonton

The table 3 shows the percentage of Congo red degradation in three different compounds (CLAY, FS, and CD) using three different processes (Fenton, photodegradation, and photo-Fenton).

As we can see, the Fenton process was the most effective for degrading Congo red in FS, with 99% degradation achieved in just 60 minutes. Photodegradation was not effective for

FS or CD, but it did achieve some degradation (44%) of CLAY. Photo-Fenton was effectivefor CLAY and CD, but not for FS.

Cost of 1 kilogram of each material

Compound	**FS**	**CD**	**Clay**
Cost of 1 kg (Euro)	**12253.4**	**736.5**	**0**

Considering both degradation effectiveness and cost, Fenton treatment using CLAY appears to be the most suitable option.

Effectiveness: CLAY achieved 80% degradation with Fenton treatment within 90 minutes, which is lower than FS (99% in 60 minutes) but significantly higher than CD (25% in 120 minutes).

Cost: CLAY is the cheapest catalyst by far, at only €0 per kg, compared to €12253.4 for FS and €736.5 per kg, mentioned for CD.

Therefore, using CLAY with Fenton treatment offers a good balance between effectiveness and cost. While FS might achieve slightly higher degradation rates, the significantly higher cost makes it less favorable. CD might be even cheaper than CLAY, but its much lower degradation efficiency makes it a less attractive option.

Finally, economically and industrially, we can argue that if the priority is the quickest possible decline, regardless of expense, Fenton treatment with FS may be the greatest option. If cost was the most important consideration and a slight drop in degrading efficiency was acceptable, CLAY, which was already cheaper than CD, might be worth considering.

Conclusion

Hybrid chemical complexes are a promising solution for the degradation of red Congo. They are more effective and cost effective than natural clay.The degradation of red Congo helps reduce its presence in the environment and protect human health. The environmental benefits of Congo Red degradation include:

- Reducing water pollution: Congo red can be released into the environment by businesses, households and communities. It can be found in wastewater, runoff and groundwater. The degradation of red Congo reduces its concentration in water, which helps protect water quality.
- Reducing air pollution: Congo Red can also be released into the air by industries and vehicles. It can end up in the atmosphere, where it can harm human health and the

environment. The degradation of red Congo reduces its concentration in the air, which helps protect air quality.

- Reducing soil pollution: Congo red can also be found in soils, where it can harm plants and animals. The degradation of red Congo reduces its concentration in soils, which helps protect biodiversity.

The environmental benefits of Congo Red degradation are:

- Protecting the Algerian environment: Algeria is a country with a rich natural heritage. The degradation of red Congo helps protect the Algerian environment from the harmful effects of this pollutant.
- Promoting sustainable development: The degradation of the Congo red is a sustainable solution for waste management. It reduces the amount of red Congo released into the environment and protects human health.

The degradation of red Congo is an effective solution to reduce environmental pollution and protect human health. It has significant environmental benefits.

GeneralConclusion

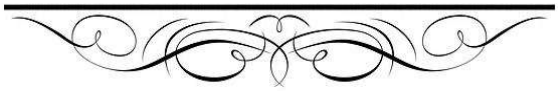

GeneralConclusion

The aim of this thesis is to provide new solutions for water pollution and improve the performance of traditional techniques by removing some organic pollutants from water, such as those found in urban wastewater (Congo red), and ionic pollutants (nitrate), using organic-inorganic hybrid materials synthesized by co-precipitation method in soft chemistry process at room temperature. These materials are based on metals (cadmium, copper, and iron), acids (squaric acid and malic acid), amides (acetanilide, ammonium oxalate), in addition to two types of natural clay, one of which was chemically and thermally treated, while the other was used as it was obtained from nature.These materials were characterized using Fourier-transform infrared spectroscopy (FTIR), X-ray diffraction (XRD), scanning electron microscopy (SEM/EDS), and surface area analysis (BET) method. Cristalline structures identification were found using HighScore Plus softward, While Mercury softward was utilized in structures visualization and FullProf programs in aterns indexation. The titles comounds efficiency in removing pollutants from water was then tested using photo-Fenton and photo-Fenton photocatalysis methods.

We prepared 3 compounds by synthesis by co-precipitation method at room temperature. First, the CD compound, which is a new member of the NH3[Ti(C2O4)2H2O] family, performed unsatisfactorily when tested for its effectiveness in removing nitrates and Congo red from water. Second, the identical CMA compound of [fluorenlithium-2-ethylenediamine], which we were unable to reproduce, preventing us from studying its effectiveness. Finally, the FS compound gave very satisfactory results in removing Congolese red color from water.

Concerning the clay samples, we obtained good results in removing organic matter from the urban wastewater of Ouargla using modified clay after chemical and thermal activation, while results in removing Congo Red from the water using natural clay from the Nissa Valley were not satisfactory.

As a future prospect, we are looking forward to improving the quality of the materials we manufacture and natural clayby:

- Carry out modification of natural clay and test its effectiveness in removing heavy metals from water.
- Test the effectiveness of CMA to eliminate CR from water.
- Modification of the CD manufacturing conditions to improve its performance.

- Experiment with the combination of hybrid compounds with clay to modify the clay.

It's important to note that the specific mechanisms and intermediates involved in the degradation of Congo Red using $NH_3[Cd(C_2O_4)_2].2H_2O$ as a catalyst in the photo-Fenton process might vary and could be further elucidated through detailed experimental studies and analysis, including spectroscopic techniques and kinetic investigations. Additionally, the conditions of the reaction (pH, concentration of reactants, irradiation time, etc.) will significantly influence the efficiency and pathways of the degradation process.

Annexes

Annexe1

Apparetus used in caracterisation of matters

Figure 1 : FTIR-7600 Fourier-Transform Infrared spectrometer

Figure 3 : ZEISS EVA 15 SEM/EDS apparitus

Figure 4 :Holder

Image 7 : TG, DSC LINSEIS TGA PT 1000 thermobalence.

Image 6: Micromeritics 3Flex 5.00) device

Figure 8 : D 8 Diffractometer

Annex 2

X-Rays diffractometer measurement conditions

X-Ray	40 kV , 15 mA	Scan speed / Duration time	5.0000 deg/min
Goniometer	MiniFlex 300/600	Step width	0.0200 deg
Attachment	Standard	Scan axis	Theta/2-Theta
Filter	None	Scan range	2.0100 - 79.9900 deg
CBO selection slit	-	Incident slit	1.250deg
Diffrected beam mono.	Bent	Length limiting slit	10.0mm
Detector	SC-70	Receiving slit #1	1.250deg
Scan mode	CONTINUOUS	Receiving slit #2	0.3mm

Annex 3

CD

Peak list

No.	2-theta(deg)	d(ang.)	Height(cps)	FWHM(deg)	Int. I(cps deg)	Int. W(deg)	Asym. factor
1	9.088(3)	9.723(4)	7521(177)	0.104(3)	1007(14)	0.134(5)	0.60(9)
2	11.257(13)	7.854(9)	230(31)	0.214(12)	64(2)	0.28(5)	1.6(4)
3	12.39(3)	7.140(18)	94(20)	0.10(3)	13.9(16)	0.15(5)	0.7(10)
4	13.0300(15)	6.7889(8)	10136(206)	0.1065(10)	1184(11)	0.117(3)	1.03(5)
5	13.988(3)	6.3261(14)	5664(154)	0.124(2)	877(10)	0.155(6)	1.34(12)
6	15.591(10)	5.679(4)	1712(84)	0.318(12)	600(26)	0.35(3)	2(2)
7	15.724(6)	5.631(2)	2109(94)	0.120(7)	279(26)	0.133(18)	0.45(13)
8	16.887(10)	5.246(3)	538(47)	0.138(8)	81(3)	0.15(2)	4.2(19)
9	17.652(19)	5.020(5)	137(24)	0.215(17)	31(2)	0.23(6)	0.58(19)
10	18.101(18)	4.897(5)	147(25)	0.196(15)	31(2)	0.21(5)	0.6(2)
11	19.140(8)	4.6333(18)	687(53)	0.190(6)	143(4)	0.21(2)	3.8(9)
12	19.885(6)	4.4614(12)	1811(87)	0.155(4)	344(6)	0.190(12)	1.6(2)
13	20.473(14)	4.335(3)	250(32)	0.081(16)	28(4)	0.11(3)	0.5(2)
14	21.85(3)	4.065(5)	125(23)	0.12(4)	20(3)	0.16(5)	2(3)
15	22.542(9)	3.9411(15)	595(50)	0.161(10)	122(4)	0.20(2)	4.1(16)
16	22.821(15)	3.894(3)	206(29)	0.10(2)	28(3)	0.13(3)	1.2(7)
17	23.547(15)	3.775(2)	251(32)	0.265(18)	84(5)	0.33(6)	1.0(2)
18	24.149(8)	3.6825(12)	1139(69)	0.218(12)	296(23)	0.26(4)	2.2(5)
19	24.388(3)	3.6468(4)	1092(67)	0.142(17)	179(20)	0.16(3)	4.3(16)
20	24.748(5)	3.5946(7)	776(57)	0.096(6)	108(3)	0.139(14)	0.58(15)
21	26.146(4)	3.4055(6)	340(38)	0.234(10)	97(3)	0.28(4)	3.4(16)
22	27.622(11)	3.2268(12)	494(45)	0.140(12)	88(4)	0.18(3)	1.0(3)
23	28.023(4)	3.1815(4)	4025(130)	0.114(3)	584(8)	0.145(7)	1.41(19)
24	29.22(2)	3.054(2)	284(34)	0.413(16)	127(5)	0.45(7)	2.5(5)
25	31.191(10)	2.8653(9)	761(56)	0.145(8)	127(4)	0.166(18)	1.0(2)
26	31.708(7)	2.8196(6)	972(64)	0.167(7)	187(5)	0.193(18)	3.0(6)
27	32.762(12)	2.7313(10)	572(49)	0.197(13)	123(7)	0.22(3)	1.2(3)
28	33.075(9)	2.7062(7)	808(58)	0.148(11)	130(5)	0.161(18)	1.7(4)
29	33.363(10)	2.6835(8)	470(44)	0.127(11)	65(3)	0.139(19)	0.9(3)
30	33.909(3)	2.6415(2)	6772(168)	0.109(3)	958(12)	0.141(5)	1.14(13)
31	35.948(14)	2.4962(10)	140(24)	0.23(5)	55(6)	0.39(11)	4(5)
32	36.303(3)	2.4726(2)	434(43)	0.093(11)	52(3)	0.119(19)	0.3(2)
33	37.98(3)	2.3673(17)	136(24)	0.30(3)	44(3)	0.33(8)	3.2(15)
34	38.47(3)	2.3383(16)	169(27)	0.23(3)	43(4)	0.26(7)	0.7(3)
35	39.099(17)	2.3020(9)	296(35)	0.26(2)	84(5)	0.28(5)	3.7(14)
36	39.912(16)	2.2570(9)	218(30)	0.234(17)	55(2)	0.25(5)	3.1(10)
37	40.255(8)	2.2385(4)	464(44)	0.125(9)	62(3)	0.135(19)	1.2(3)
38	40.474(10)	2.2269(5)	296(35)	0.119(12)	38(2)	0.13(2)	0.9(3)
39	40.86(3)	2.2068(17)	88(19)	0.24(6)	23(4)	0.26(10)	0.3(2)
40	41.279(8)	2.1853(4)	339(38)	0.127(12)	46(4)	0.14(3)	2.0(5)
41	42.459(4)	2.1273(2)	1376(76)	0.132(5)	216(7)	0.157(14)	0.74(10)
42	42.774(11)	2.1123(5)	203(29)	0.13(2)	32(5)	0.16(5)	2.2(10)
43	43.261(6)	2.0897(3)	151(25)	0.113(16)	22.3(19)	0.15(4)	0.7(4)
44	44.024(13)	2.0552(6)	360(39)	0.173(13)	66(3)	0.18(3)	1.7(5)
45	44.305(11)	2.0428(5)	359(39)	0.142(14)	54(3)	0.15(2)	1.0(3)

46	44.617(5)	2.0293(2)	332(37)	0.172(14)	61(3)	0.18(3)	0.8(2)
47	45.80(2)	1.9794(9)	171(27)	0.17(2)	31(3)	0.18(5)	2.3(13)
48	46.007(12)	1.9712(5)	478(45)	0.162(16)	82(5)	0.17(3)	0.8(2)
49	46.390(16)	1.9557(6)	170(27)	0.16(4)	30(4)	0.18(5)	4(3)
50	46.697(17)	1.9436(7)	460(44)	0.238(12)	117(4)	0.25(3)	0.9(2)
51	47.507(15)	1.9123(5)	253(32)	0.150(16)	40(3)	0.16(3)	1.8(7)
52	47.99(3)	1.8942(12)	150(25)	0.18(5)	28(5)	0.19(7)	0.8(6)
53	48.33(2)	1.8818(9)	257(33)	0.19(3)	52(6)	0.20(5)	1.4(7)
54	49.56(2)	1.8377(8)	260(33)	0.26(7)	76(15)	0.29(9)	0.39(19)
55	49.864(15)	1.8273(5)	191(28)	0.09(3)	19(11)	0.10(7)	2(2)
56	50.185(8)	1.8164(3)	564(48)	0.120(12)	75(13)	0.13(3)	0.9(3)
57	50.45(3)	1.8076(11)	228(31)	0.21(7)	53(15)	0.23(10)	1.7(16)
58	50.68(3)	1.7996(10)	135(24)	0.16(7)	24(10)	0.18(10)	1.4(15)
59	51.011(18)	1.7889(6)	192(28)	0.14(2)	29(3)	0.15(4)	1.3(6)
60	51.361(10)	1.7775(3)	325(37)	0.116(10)	42(3)	0.13(2)	0.9(3)
61	52.859(12)	1.7306(4)	158(26)	0.113(16)	30(3)	0.19(5)	0.7(3)
62	53.368(7)	1.7153(2)	346(38)	0.130(7)	48(2)	0.14(2)	0.77(17)
63	54.108(11)	1.6936(3)	168(26)	0.113(10)	20.1(19)	0.12(3)	0.7(3)
64	55.377(17)	1.6577(5)	156(26)	0.15(2)	44(3)	0.28(6)	1.8(12)
65	55.997(7)	1.64085(19)	584(49)	0.152(9)	108(6)	0.19(3)	0.98(19)
66	56.281(19)	1.6333(5)	163(26)	0.17(3)	34(4)	0.21(6)	0.8(3)
67	57.036(9)	1.6134(2)	264(33)	0.110(16)	54(3)	0.21(4)	3.0(14)
68	57.367(9)	1.6049(2)	297(35)	0.096(14)	44(4)	0.15(3)	2.2(8)
69	57.86(4)	1.5924(9)	103(21)	0.33(7)	54(8)	0.53(18)	1.8(7)
70	58.349(7)	1.58020(16)	434(43)	0.094(11)	65(6)	0.15(3)	1.6(5)
71	60.758(9)	1.5232(2)	218(30)	0.102(15)	30(3)	0.14(3)	0.4(2)
72	61.860(16)	1.4987(4)	211(30)	0.32(4)	97(6)	0.46(9)	1.9(8)
73	62.908(19)	1.4762(4)	149(25)	0.102(16)	16(2)	0.11(3)	1.7(13)
74	63.40(3)	1.4660(6)	172(27)	0.22(3)	40(4)	0.23(6)	1.2(6)
75	64.18(3)	1.4500(5)	117(22)	0.11(3)	17(3)	0.15(5)	1.1(13)
76	65.219(15)	1.4294(3)	190(28)	0.09(2)	20(3)	0.11(3)	0.4(4)
77	66.297(14)	1.4087(3)	82(18)	0.23(4)	36(4)	0.44(15)	5(6)
78	66.853(6)	1.39834(11)	189(28)	0.124(17)	27(3)	0.14(4)	0.3(3)
79	69.093(16)	1.3584(3)	169(27)	0.160(16)	29(2)	0.17(4)	1.1(5)
80	69.70(4)	1.3480(7)	116(22)	0.27(4)	34(3)	0.29(8)	0.8(4)
81	71.117(16)	1.3246(3)	203(29)	0.171(16)	37(3)	0.18(4)	2.4(12)
82	72.093(15)	1.3090(2)	112(22)	0.21(5)	31(5)	0.27(10)	0.3(4)

Annex 4

CMA

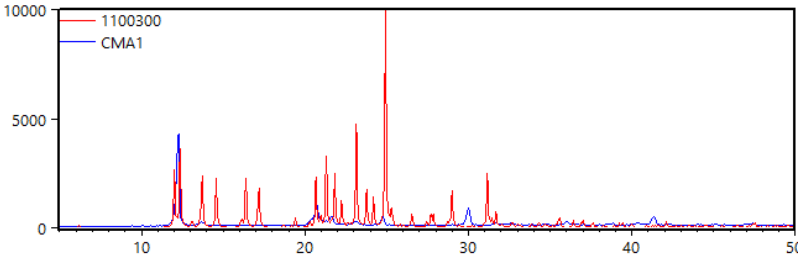

Powder X-ray diffraction pattern, the bleu of the title compoud and the red of [fluorenyllithium .2 ethylenediamine]

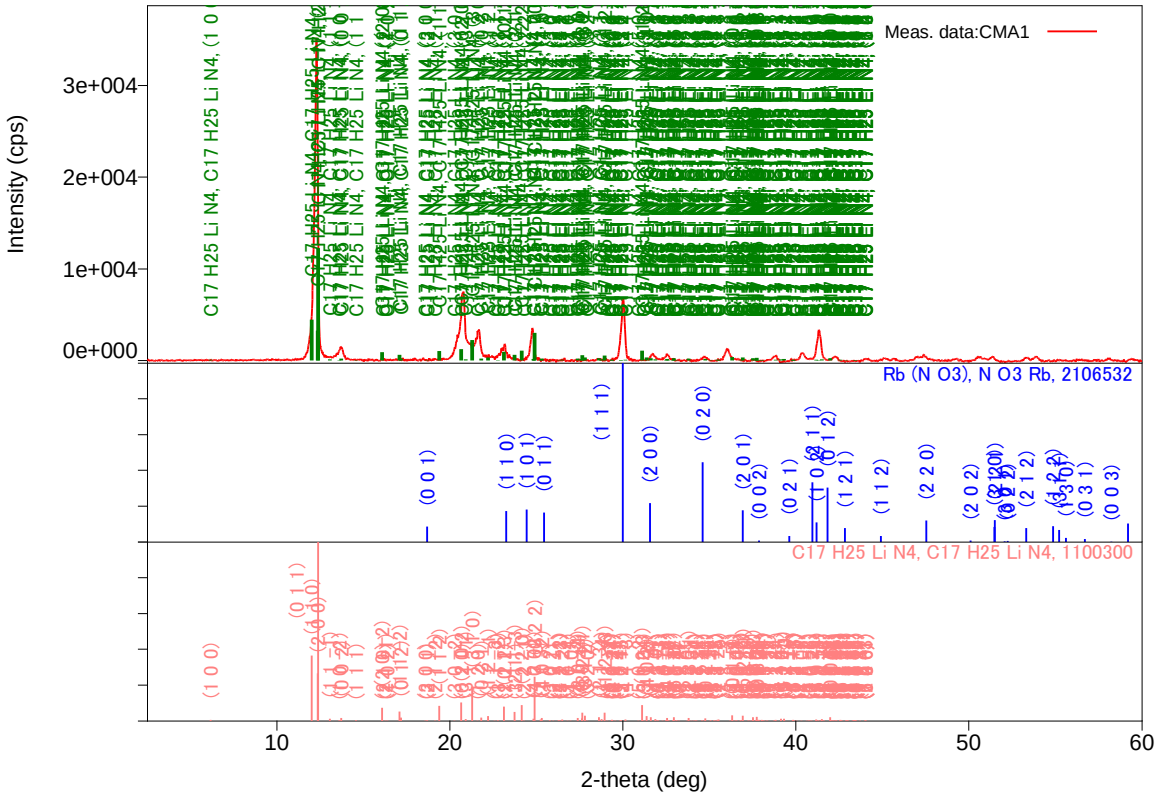

Peack list

No.	2-theta(deg)	d(ang.)	Height(cps)	FWHM(deg)	Int. I(cps deg)	Int. W(deg)	Asym. factor
1	12.313(5)	7.183(3)	22358(432)	0.228(4)	6326(67)	0.283(8)	3.3(4)
2	13.72(3)	6.451(16)	950(89)	0.34(5)	567(28)	0.60(9)	1.9(13)
3	20.762(7)	4.2747(15)	4466(193)	0.367(12)	2463(54)	0.55(4)	2.16(19)
4	21.673(10)	4.0971(19)	1894(126)	0.38(2)	1049(49)	0.55(6)	3.6(5)
5	23.154(15)	3.838(3)	1016(92)	0.35(4)	615(24)	0.61(8)	2.5(5)
6	24.775(11)	3.5908(16)	2377(141)	0.199(9)	622(15)	0.26(2)	2.2(7)
7	30.017(7)	2.9745(7)	4808(200)	0.214(5)	1256(18)	0.261(15)	2.2(3)
8	31.701(18)	2.8202(16)	465(62)	0.31(3)	201(10)	0.43(8)	1.1(3)
9	32.569(15)	2.7470(12)	452(61)	0.22(2)	133(10)	0.29(6)	2.1(6)
10	34.6353	2.58776	49.0167	0.266654	66.455	1.355761	1.8989
11	36.008(16)	2.4922(11)	923(88)	0.27(3)	359(17)	0.39(6)	1.1(3)
12	38.8796	2.31448	450.935	0.266654	150.062	0.332779	1.8989

13	40.34(3)	2.2340(15)	626(72)	0.23(2)	196(11)	0.31(5)	0.9(4)
14	41.332(6)	2.1826(3)	2528(145)	0.222(5)	723(9)	0.29(2)	1.7(2)
15	42.220(12)	2.1387(6)	324(52)	0.22(4)	79(12)	0.24(8)	0.8(8)
16	47.24(7)	1.923(3)	290(49)	0.68(5)	210(22)	0.7(2)	1.0(4)
17	50.59(4)	1.8029(14)	176(38)	0.83(13)	155(31)	0.9(4)	0.4(3)
18	53.3304	1.71644	614.101	0.266654	136.224	0.221827	1.10792
19	53.8862	1.70004	266.463	0.266654	107.697	0.404172	1.10792

Parameters used for WF

Rofile parameters

Common parameter	Background	Data	CMA1
		Function name	B-spline
		param0	307.79444945198219
		param1	323.29015251783056
		param2	793.98315992215635
		param3	909.03446968893343
		param4	1132.568183953774
		param5	1005.8681879354236
		param6	894.79871186664741
		param7	1096.1060186203636
		param8	713.21458703527605
		param9	1080.5580662750478
		node0	2.5
		node1	15.26
		node2	26.440000000000001
		node3	37.619999999999997
		node4	45.079999999999998
		node5	50.039999999999999
		node6	55
		node7	60
Common parameter	Peak shift		
		Function name	Shift axial displacement
		param0	0
		param1	0
		param2	0
Rb (N O3)	Scale factor	s	6.1(16)
	FWHM	U	0.0000
		V	0.0000
		W	0.0508
	Asym. Factor	A0	1.4699
		A1	2.9717
	Decay rate factor	etaL0/mL0	0.4517
		etaL1/mL1	0.0000
		etaL2/mL2	0.0000
		etaH0/mH0	0.6912
		etaH1/mH1	0.0000
		etaH2/mH2	0.0000
	Preferred orientationMarch-Dollase	h	0
		k	0
		l	0
		March coefficient	1.000000
C17 H25 Li N4	Scale factor	s	53.1(16)
	FWHM	U	0.0000

		V	-0.0264
		W	0.0633
	Asym. Factor	A0	1.4606
		A1	3.1029
	Decay rate factor	etaL0/mL0	0.6773
		etaL1/mL1	-0.3770
		etaL2/mL2	0.0000
		etaH0/mH0	1.0812
		etaH1/mH1	-0.5262
		etaH2/mH2	0.0000
	Preferred orientationMarch-Dollase	h	0
		k	0
		l	0
		March coefficient	1.000000

Structure parameters

Data set name	Phase Name	Element	x	y	z	Occupancy	Temperature factor
CMA1	Rb (N O3)	Rb	0.000000	0.500000	0.600000	1.000	0.500
CMA1	Rb (N O3)	O	0.000000	0.000000	0.260000	1.000	0.500
CMA1	Rb (N O3)	O	0.190000	0.000000	-	1.000	0.500
CMA1	Rb (N O3)	N	0.000000	0.000000	0.000000	1.000	0.500
CMA1	C17 H25 Li	N	0.203700	0.137400	0.346700	1.000	0.500
CMA1	C17 H25 Li	N	0.295100	0.339400	0.133300	1.000	0.500
CMA1	C17 H25 Li	N	0.126200	-	0.509400	1.000	0.500
CMA1	C17 H25 Li	N	0.373200	-	0.485500	1.000	0.500
CMA1	C17 H25 Li	C	0.272200	0.199800	0.291500	1.000	0.500
CMA1	C17 H25 Li	C	0.227500	0.266200	0.184800	1.000	0.500
CMA1	C17 H25 Li	C	0.042400	0.031900	0.483100	1.000	0.500
CMA1	C17 H25 Li	C	0.455800	0.035700	0.509800	1.000	0.500
CMA1	C17 H25 Li	Li	0.248300	0.040100	0.493000	1.000	0.500
CMA1	C17 H25 Li	H	0.175000	0.045000	0.312000	1.000	0.500
CMA1	C17 H25 Li	H	0.161000	0.214000	0.343000	1.000	0.500
CMA1	C17 H25 Li	H	0.324000	0.427000	0.168000	1.000	0.500
CMA1	C17 H25 Li	H	0.340000	0.264000	0.134000	1.000	0.500
CMA1	C17 H25 Li	H	0.140000	-	0.573000	1.000	0.500
CMA1	C17 H25 Li	H	0.112000	-	0.477000	1.000	0.500
CMA1	C17 H25 Li	H	0.388000	-	0.522000	1.000	0.500
CMA1	C17 H25 Li	H	0.361000	-	0.421000	1.000	0.500
CMA1	C17 H25 Li	H	0.315000	0.291000	0.339000	1.000	0.500
CMA1	C17 H25 Li	H	0.314000	0.105000	0.287000	1.000	0.500
CMA1	C17 H25 Li	H	0.191000	0.177000	0.140000	1.000	0.500
CMA1	C17 H25 Li	H	0.185000	0.355000	0.190000	1.000	0.500
CMA1	C17 H25 Li	H	0.440000	0.146000	0.474000	1.000	0.500
CMA1	C17 H25 Li	H	0.472000	0.062000	0.586000	1.000	0.500
CMA1	C17 H25 Li	H	0.058000	0.142000	0.510000	1.000	0.500
CMA1	C17 H25 Li	H	0.020000	0.045000	0.403000	1.000	0.500
CMA1	C17 H25 Li	C	0.193000	0.794700	0.214500	1.000	0.500
CMA1	C17 H25 Li	C	0.287500	0.752100	0.239400	1.000	0.500
CMA1	C17 H25 Li	C	0.364200	0.797900	0.198200	1.000	0.500
CMA1	C17 H25 Li	C	0.450200	0.734300	0.237700	1.000	0.500
CMA1	C17 H25 Li	C	0.467100	0.626000	0.318100	1.000	0.500
CMA1	C17 H25 Li	C	0.394300	0.579300	0.362100	1.000	0.500
CMA1	C17 H25 Li	C	0.305600	0.640400	0.323000	1.000	0.500

CMA1	C17 H25 Li	C	0.217400	0.614500	0.348300	1.000	0.500
CMA1	C17 H25 Li	C	0.190700	0.515500	0.421200	1.000	0.500
CMA1	C17 H25 Li	C	0.097800	0.509200	0.423700	1.000	0.500
CMA1	C17 H25 Li	C	0.030700	0.601100	0.357600	1.000	0.500
CMA1	C17 H25 Li	C	0.054300	0.701600	0.287300	1.000	0.500
CMA1	C17 H25 Li	C	0.148700	0.708600	0.280900	1.000	0.500
CMA1	C17 H25 Li	H	0.158000	0.862000	0.160000	1.000	0.500
CMA1	C17 H25 Li	H	0.353000	0.879000	0.143000	1.000	0.500
CMA1	C17 H25 Li	H	0.498000	0.775000	0.214000	1.000	0.500
CMA1	C17 H25 Li	H	0.530000	0.585000	0.346000	1.000	0.500
CMA1	C17 H25 Li	H	0.411000	0.492000	0.429000	1.000	0.500
CMA1	C17 H25 Li	H	0.242000	0.454000	0.466000	1.000	0.500
CMA1	C17 H25 Li	H	0.080000	0.436000	0.468000	1.000	0.500
CMA1	C17 H25 Li	H	-	0.597000	0.355000	1.000	0.500
CMA1	C17 H25 Li	H	0.005000	0.775000	0.241000	1.000	0.500
CMA1	C17 H25 Li	Li	0.248300	0.459900	-	1.000	0.500
CMA1	C17 H25 Li	N	0.295100	0.160600	0.633300	1.000	0.500
CMA1	C17 H25 Li	C	-	-	0.516900	1.000	0.500
CMA1	C17 H25 Li	C	0.544200	-	0.490200	1.000	0.500
CMA1	C17 H25 Li	N	0.203700	0.362600	-	1.000	0.500
CMA1	C17 H25 Li	N	0.126200	0.566600	0.009400	1.000	0.500
CMA1	C17 H25 Li	N	0.373200	0.565200	-	1.000	0.500
CMA1	C17 H25 Li	C	0.227500	0.233800	0.684800	1.000	0.500
CMA1	C17 H25 Li	H	0.324000	0.073000	0.668000	1.000	0.500
CMA1	C17 H25 Li	H	0.340000	0.236000	0.634000	1.000	0.500
CMA1	C17 H25 Li	N	-	0.066600	0.490600	1.000	0.500
CMA1	C17 H25 Li	H	-	-	0.490000	1.000	0.500
CMA1	C17 H25 Li	H	-	-	0.597000	1.000	0.500
CMA1	C17 H25 Li	N	0.626800	0.065200	0.514500	1.000	0.500
CMA1	C17 H25 Li	H	0.560000	-	0.526000	1.000	0.500
CMA1	C17 H25 Li	H	0.528000	-	0.414000	1.000	0.500
CMA1	C17 H25 Li	C	0.272200	0.300200	-	1.000	0.500
CMA1	C17 H25 Li	H	0.175000	0.455000	-	1.000	0.500
CMA1	C17 H25 Li	H	0.161000	0.286000	-	1.000	0.500
CMA1	C17 H25 Li	C	0.042400	0.468100	-	1.000	0.500
CMA1	C17 H25 Li	H	0.140000	0.601000	0.073000	1.000	0.500
CMA1	C17 H25 Li	H	0.112000	0.665000	-	1.000	0.500
CMA1	C17 H25 Li	C	0.455800	0.464300	0.009800	1.000	0.500
CMA1	C17 H25 Li	H	0.388000	0.655000	0.022000	1.000	0.500
CMA1	C17 H25 Li	H	0.361000	0.605000	-	1.000	0.500
CMA1	C17 H25 Li	C	0.272200	0.300200	0.791500	1.000	0.500
CMA1	C17 H25 Li	H	0.191000	0.323000	0.640000	1.000	0.500
CMA1	C17 H25 Li	H	0.185000	0.145000	0.690000	1.000	0.500
CMA1	C17 H25 Li	Li	-	-	0.507000	1.000	0.500
CMA1	C17 H25 Li	H	-	0.101000	0.427000	1.000	0.500
CMA1	C17 H25 Li	H	-	0.165000	0.523000	1.000	0.500
CMA1	C17 H25 Li	Li	0.751700	-	0.507000	1.000	0.500
CMA1	C17 H25 Li	H	0.612000	0.155000	0.478000	1.000	0.500
CMA1	C17 H25 Li	H	0.639000	0.105000	0.579000	1.000	0.500
CMA1	C17 H25 Li	C	0.227500	0.233800	-	1.000	0.500
CMA1	C17 H25 Li	H	0.315000	0.209000	-	1.000	0.500
CMA1	C17 H25 Li	H	0.314000	0.395000	-	1.000	0.500
CMA1	C17 H25 Li	C	-	0.531900	0.016900	1.000	0.500
CMA1	C17 H25 Li	H	0.058000	0.358000	0.010000	1.000	0.500
CMA1	C17 H25 Li	H	0.020000	0.455000	-	1.000	0.500
CMA1	C17 H25 Li	C	0.544200	0.535700	-	1.000	0.500

CMA1	C17 H25 Li	H	0.440000	0.354000	-	1.000	0.500
CMA1	C17 H25 Li	H	0.472000	0.438000	0.086000	1.000	0.500
CMA1	C17 H25 Li	N	-	-	0.653300	1.000	0.500
CMA1	C17 H25 Li	N	-	-	0.366700	1.000	0.500
CMA1	C17 H25 Li	N	-	0.065200	0.514500	1.000	0.500
CMA1	C17 H25 Li	N	-	0.433400	-	1.000	0.500
CMA1	C17 H25 Li	H	-	0.642000	-	1.000	0.500
CMA1	C17 H25 Li	H	-	0.545000	0.097000	1.000	0.500
CMA1	C17 H25 Li	N	0.626800	0.434800	0.014500	1.000	0.500
CMA1	C17 H25 Li	H	0.560000	0.646000	0.026000	1.000	0.500
CMA1	C17 H25 Li	H	0.528000	0.562000	-	1.000	0.500
CMA1	C17 H25 Li	C	-	-	0.708500	1.000	0.500
CMA1	C17 H25 Li	H	-	-	0.688000	1.000	0.500
CMA1	C17 H25 Li	H	-	-	0.657000	1.000	0.500
CMA1	C17 H25 Li	C	-	-	0.315200	1.000	0.500
CMA1	C17 H25 Li	H	-	-	0.332000	1.000	0.500
CMA1	C17 H25 Li	H	-	-	0.366000	1.000	0.500
CMA1	C17 H25 Li	Li	-	0.540100	0.007000	1.000	0.500
CMA1	C17 H25 Li	H	-	0.399000	-	1.000	0.500
CMA1	C17 H25 Li	H	-	0.335000	0.023000	1.000	0.500
CMA1	C17 H25 Li	Li	0.751700	0.540100	0.007000	1.000	0.500
CMA1	C17 H25 Li	H	0.612000	0.345000	-	1.000	0.500
CMA1	C17 H25 Li	H	0.639000	0.395000	0.079000	1.000	0.500
CMA1	C17 H25 Li	C	-	-	0.815200	1.000	0.500
CMA1	C17 H25 Li	H	-	-	0.661000	1.000	0.500
CMA1	C17 H25 Li	H	-	-	0.713000	1.000	0.500
CMA1	C17 H25 Li	C	-	-	0.208500	1.000	0.500
CMA1	C17 H25 Li	H	-	-	0.360000	1.000	0.500
CMA1	C17 H25 Li	H	-	-	0.310000	1.000	0.500
CMA1	C17 H25 Li	N	-	0.637400	0.153300	1.000	0.500
CMA1	C17 H25 Li	N	-	0.660600	-	1.000	0.500
CMA1	C17 H25 Li	N	-	0.434800	0.014500	1.000	0.500
CMA1	C17 H25 Li	N	-	-	0.866700	1.000	0.500
CMA1	C17 H25 Li	H	-	-	0.860000	1.000	0.500
CMA1	C17 H25 Li	H	-	-	0.810000	1.000	0.500
CMA1	C17 H25 Li	N	-	-	0.153300	1.000	0.500
CMA1	C17 H25 Li	H	-	-	0.161000	1.000	0.500
CMA1	C17 H25 Li	H	-	-	0.213000	1.000	0.500
CMA1	C17 H25 Li	C	-	0.699800	0.208500	1.000	0.500
CMA1	C17 H25 Li	H	-	0.545000	0.188000	1.000	0.500
CMA1	C17 H25 Li	H	-	0.714000	0.157000	1.000	0.500
CMA1	C17 H25 Li	C	-	0.733800	-	1.000	0.500
CMA1	C17 H25 Li	H	-	0.573000	-	1.000	0.500
CMA1	C17 H25 Li	H	-	0.736000	-	1.000	0.500

Pattern indexation using FullProf

M O N O C L I N I C S Y S T E M

DIRECT PARAMETERS : A=14.5499 B= 8.1467 C=13.0358 BETA= 102.91

STANDARD DEVIATIONS: .0051 .0024 .0036 .032

REFINED ZERO-POINT SHIFT :-0.0304 deg. 2-theta

REDUCED CELL : A=13.0358 B= 8.1467 C=14.5499 BETA= 102.91

H	K	L	DOBS	DCAL	DOBS-DCAL	2TH.OBS	2TH.CAL	DIF.2TH.
2	0	0	7.19625	7.20424	-0.00799	12.290	12.276	0.014
0	0	2	6.45887	6.45621	0.00266	13.699	13.705	-0.006
1	0	-3	4.27641	4.27064	0.00577	20.754	20.783	-0.028
3	0	-2	4.10024	4.10094	-0.00070	21.657	21.653	0.004
1	1	-1	3.83790	3.84022	-0.00231	23.157	23.143	0.014
2	1	0	3.59183	3.59172	0.00012	24.767	24.768	-0.001
4	0	-1		3.58754	0.00429	24.797		-0.030
1	1	-3	2.97496	2.97414	0.00082	30.013	30.021	-0.008
2	0	4	2.82269	2.82561	-0.00293	31.673	31.639	0.034
5	0	1	2.74843	2.74743	0.00100	32.552	32.564	-0.012
0	0	5	2.58681	2.58600	0.00081	34.648	34.660	-0.011
1	0	5	2.49442	2.49396	0.00046	35.975	35.982	-0.007
6	0	1	2.31569	2.31539	0.00029	38.858	38.864	-0.005
4	0	-5	2.23195	2.23325	-0.00131	40.379	40.354	0.025
4	1	-4	2.18235	2.18178	0.00057	41.338	41.349	-0.011

* NUMBER OF LINES

.- LINES INPUT = 14

.- LINES INDEXED = 14

.- LINES CALCULATED = 105

* MEAN ABSOLUTE DISCREPANCIES

<Q> =0.9144E-04

<DELTA(2-THETA)> =0.1284E-01

MAX. ERROR ACCEPTED (DEG. 2-THETA) =0.4500E-01

* FIGURES OF MERIT

1.- M(14) = 10.9

2.- F(14) = 10.4(0.0128, 105)

Annex 4

FS

Peak list

No.	2-theta(deg)	d(ang.)	Height(cps)	FWHM(deg)	Int. I(cps deg)	Int. W(deg)	Asym. factor
1	11.833(4)	7.473(2)	484(63)	0.211(9)	126(4)	0.26(4)	4(2)
2	13.452(14)	6.577(7)	442(61)	0.234(15)	138(8)	0.31(6)	1.4(4)
3	13.868(9)	6.381(4)	904(87)	0.186(11)	225(9)	0.25(3)	1.3(3)
4	14.448(6)	6.126(2)	2814(153)	0.195(5)	706(14)	0.251(19)	2.7(5)
5	15.749(5)	5.6224(19)	531(67)	0.197(12)	119(7)	0.22(4)	5(4)
6	17.357(9)	5.105(3)	1095(96)	0.218(7)	282(7)	0.26(3)	2.0(3)
7	19.70(3)	4.503(6)	171(38)	0.19(2)	38(3)	0.22(7)	2(2)
8	21.068(13)	4.213(3)	455(62)	0.222(9)	108(5)	0.24(4)	1.7(4)
9	22.10(4)	4.018(8)	114(31)	0.26(5)	37(8)	0.33(15)	1.1(7)
10	22.681(17)	3.917(3)	807(82)	0.193(16)	181(11)	0.22(4)	3.4(18)
11	24.413(18)	3.643(3)	755(79)	0.302(14)	245(11)	0.32(5)	1.8(4)
12	24.80(3)	3.587(5)	251(46)	0.23(3)	63(6)	0.25(7)	0.9(5)
13	26.333(12)	3.3818(15)	485(64)	0.220(12)	126(6)	0.26(5)	3.6(8)
14	26.814(17)	3.322(2)	237(44)	0.18(2)	54(5)	0.23(6)	2.4(8)
15	27.710(15)	3.2168(17)	452(61)	0.212(10)	104(5)	0.23(4)	1.2(3)
16	28.761(8)	3.1015(8)	532(67)	0.133(19)	123(5)	0.23(4)	0.47(11)
17	29.615(5)	3.0140(5)	1159(98)	0.178(6)	290(7)	0.25(3)	0.39(3)
18	31.771(12)	2.8142(11)	619(72)	0.194(11)	137(5)	0.22(3)	3.5(12)
19	32.90(3)	2.720(2)	157(36)	0.26(2)	44(3)	0.28(9)	0.9(3)
20	33.53(3)	2.671(2)	153(36)	0.21(2)	33(3)	0.22(7)	1.6(9)
21	35.034(12)	2.5592(8)	262(47)	0.46(3)	144(8)	0.55(13)	2.3(12)
22	35.9996	2.49276	22.7502	0.248901	25.5153	1.121543	0.931621
23	36.5048	2.45941	137.194	0.248901	26.4504	0.192795	0.931621
24	37.631(14)	2.3884(8)	180(39)	0.43(3)	82(7)	0.45(14)	0.9(4)
25	39.475(11)	2.2809(6)	517(66)	0.284(13)	222(7)	0.43(7)	1.37(14)
26	40.7491	2.2125	86.4008	0.26404	11.5658	0.133862	0.931621
27	41.1028	2.19428	2.79867	0.26404	7.20866	2.575741	0.931621
28	41.995(8)	2.1497(4)	263(47)	0.308(13)	86(3)	0.33(7)	0.83(7)
29	43.133(8)	2.0956(4)	175(38)	0.22(2)	42(3)	0.24(7)	0.9(4)
30	44.21(2)	2.0471(9)	247(45)	0.19(3)	63(5)	0.25(7)	0.9(4)
31	45.0945	2.00888	47.1816	0.26404	25.5698	0.541943	0.931621
32	46.09(8)	1.968(3)	105(30)	0.25(5)	28(5)	0.26(13)	1.0(3)
33	47.7219	1.90423	9.17334	0.26404	14.6117	1.592842	0.931621
34	49.25(6)	1.849(2)	215(42)	0.42(10)	104(41)	0.5(3)	0.8(7)
35	49.98(8)	1.823(3)	137(34)	0.5(3)	83(44)	0.6(5)	3(4)
36	51.1577	1.78411	36.2462	0.26404	15.9419	0.439823	0.931621
37	52.00(2)	1.7572(8)	66(24)	0.43(6)	31(4)	0.5(2)	0.6(5)
38	52.93(13)	1.728(4)	46(20)	0.61(11)	30(4)	0.7(4)	0.5(5)
39	53.819(10)	1.7020(3)	197(40)	0.25(3)	52(4)	0.26(7)	1.0(6)
40	59.141	1.5609	31.8171	0.26404	19.983	0.628058	0.931621

Parameters used for WPPF

Profile parameters

Common parameter	Background	Data	FS2
		Function name	B-spline
		param0	39.582275754355784
		param1	36.259448480960934
		param2	30.036854155428369
		param3	25.533980370812685
		param4	38.139134070313609
		param5	37.712109140845349
		param6	53.97451842920659
		param7	58.782131544421915
		param8	44.419946643567577
		param9	101.66421308357646
		param10	52.818350721283991
		param11	90.217267666949738
		param12	69.063774299114883
		param13	100.99910810334204
		param14	51.140676595671231
		param15	103.44839198225236
		node0	2.5
		node1	7.8799999999999999
		node2	11.640000000000001
		node3	15.4
		node4	19.16
		node5	22.960000000000001
		node6	27.280000000000001
		node7	31.600000000000001
		node8	35.979999999999997
		node9	41.979999999999997
		node10	47.979999999999997
		node11	51.979999999999997
		node12	55.979999999999997
		node13	60
Common parameter	Peak shift		
		Function name	Shift axial
		param0	0
		param1	0
		param2	0
((V(OH)(H2O)2)(C4O4))2(H2O)	Scale factor	s	7.9(3)
	FWHM	U	0.2389
		V	-0.0609
		W	0.0450
	Asym. factor	A0	0.1458
		A1	1.7596
	Decay rate factor	etaL0/mL0	0.4632
		etaL1/mL1	-0.3849
		etaL2/mL2	0.0000
		etaH0/mH0	0.7286
		etaH1/mH1	-0.3849
		etaH2/mH2	0.0000
	Preferred orientationMarch-	h	0

	k	0
	l	0
	March	1.000000

Structure parameters

Data set name	Phase Name	Element	x	y	z	Occupancy	T
FS2	((V (O H) (H2 O)2) (C4 O4))2 (H2 O)2	O	0.725380	0.505930	0.849980	1.000	0
FS2	((V (O H) (H2 O)2) (C4 O4))2 (H2 O)2	O	0.676640	0.810800	0.097130	1.000	0
FS2	((V (O H) (H2 O)2) (C4 O4))2 (H2 O)2	C	0.747360	0.931180	0.254800	1.000	0
FS2	((V (O H) (H2 O)2) (C4 O4))2 (H2 O)2	O	0.778540	0.386640	0.135300	1.000	0
FS2	((V (O H) (H2 O)2) (C4 O4))2 (H2 O)2	C	0.673640	0.923310	0.412010	1.000	0
FS2	((V (O H) (H2 O)2) (C4 O4))2 (H2 O)2	H	0.919200	0.146000	0.858300	1.000	0
FS2	((V (O H) (H2 O)2) (C4 O4))2 (H2 O)2	C	0.854260	0.117300	0.516020	1.000	0
FS2	((V (O H) (H2 O)2) (C4 O4))2 (H2 O)2	H	0.869700	0.494300	0.195800	1.000	0
FS2	((V (O H) (H2 O)2) (C4 O4))2 (H2 O)2	V	0.808240	0.806300	0.894960	1.000	0
FS2	((V (O H) (H2 O)2) (C4 O4))2 (H2 O)2	H	0.538200	0.759100	0.651000	1.000	0
FS2	((V (O H) (H2 O)2) (C4 O4))2 (H2 O)2	O	0.925800	0.111000	-0.044330	1.000	0
FS2	((V (O H) (H2 O)2) (C4 O4))2 (H2 O)2	H	0.653100	0.410400	0.757800	1.000	0
FS2	((V (O H) (H2 O)2) (C4 O4))2 (H2 O)2	H	0.821700	0.298600	0.097600	1.000	0
FS2	((V (O H) (H2 O)2) (C4 O4))2 (H2 O)2	C	0.927170	0.117880	0.356160	1.000	0
FS2	((V (O H) (H2 O)2) (C4 O4))2 (H2 O)2	O	0.523680	0.796570	0.442770	1.000	0
FS2	((V (O H) (H2 O)2) (C4 O4))2 (H2 O)2	O	0.551580	0.752150	0.752030	1.000	0
FS2	((V (O H) (H2 O)2) (C4 O4))2 (H2 O)2	O	0.921310	0.228280	0.672510	1.000	0
FS2	((V (O H) (H2 O)2) (C4 O4))2 (H2 O)2	O	0.089630	0.231800	0.326510	1.000	0
FS2	((V (O H) (H2 O)2) (C4 O4))2 (H2 O)2	H	0.450200	0.707900	0.784300	1.000	0
FS2	((V (O H) (H2 O)2) (C4 O4))2 (H2 O)2	H	0.712600	0.452300	-0.074000	1.000	0

Annex 7

Clay H'jira

peak list

No.	2-theta(deg)	d(ang.)	Height(cps)	FWHM(deg)	Int. I(cps deg)	Int. W(deg)	Asym. factor
1	8.47(3)	10.43(4)	189(14)	0.98(4)	285(10)	1.51(17)	1.04(11)
2	11.672(2)	7.5755(14)	2875(57)	0.1006(15)	328(4)	0.114(4)	1.43(11)
3	12.36(2)	7.157(13)	123(12)	0.44(2)	61(3)	0.50(7)	1.4(3)
4	19.79(3)	4.481(6)	206(15)	0.63(4)	213(8)	1.03(12)	0.69(15)
5	23.398(4)	3.7989(6)	1833(45)	0.096(3)	198(4)	0.108(5)	0.98(14)
6	24.84(5)	3.582(7)	73(9)	0.50(5)	43(5)	0.58(14)	0.29(16)
7	26.669(6)	3.3399(8)	259(17)	0.223(16)	71(4)	0.28(3)	2.9(17)
8	27.37(10)	3.256(12)	53(8)	0.94(10)	56(6)	1.0(3)	1.4(6)
9	29.386(11)	3.0370(11)	498(24)	0.184(15)	149(3)	0.30(2)	0.8(2)
10	31.094(10)	2.8739(9)	92(10)	0.119(14)	23.3(17)	0.25(5)	1.9(5)
11	31.717(11)	2.8189(10)	838(31)	0.173(8)	189(4)	0.226(13)	1.2(3)
12	34.76(5)	2.579(3)	132(12)	1.17(7)	219(8)	1.7(2)	0.39(9)
13	39.415(12)	2.2842(7)	102(11)	0.160(19)	18.3(15)	0.18(3)	0.59(18)
14	43.16(2)	2.0942(11)	81(9)	0.16(2)	15.4(15)	0.19(4)	0.5(3)
15	45.436(7)	1.9946(3)	480(23)	0.174(9)	124.5(18)	0.260(16)	1.2(2)
16	47.842(13)	1.8997(5)	294(18)	0.13(3)	72(5)	0.25(3)	3.1(13)
17	48.487(6)	1.8760(2)	95(10)	0.162(19)	25.5(10)	0.27(4)	0.41(7)
18	49.18(12)	1.851(4)	19(5)	0.7(2)	26(4)	1.3(5)	0.21(8)
19	53.91(5)	1.6994(14)	23(5)	2.1(2)	51(5)	2.2(7)	0.20(9)
20	56.45(3)	1.6288(8)	117(11)	0.32(2)	39(2)	0.34(5)	0.7(2)
21	57.43(3)	1.6032(8)	52(8)	0.16(3)	9.1(11)	0.18(5)	0.7(5)
22	61.62(7)	1.5040(16)	59(8)	1.65(6)	104(5)	1.8(3)	1.5(3)
23	66.204(18)	1.4105(3)	38(6)	0.14(5)	6.8(17)	0.18(8)	0.4(8)
24	72.51(8)	1.3026(13)	30(6)	0.96(7)	32(2)	1.1(3)	0.34(15)
25	75.21(6)	1.2623(9)	43(7)	0.42(5)	20.0(15)	0.47(11)	0.7(4)

Table 2: Profil parameters used for WPPF

Common parameter	Background	Data	clay
		Function name	B-spline
		param0	726.1040421640497
		param1	157.02984641866797
		param2	48.774946093269527
		param3	74.755161631079318
		param4	154.36607854006866
		param5	228.28203828257071
		param6	92.696047564700848
		param7	161.17421585968327
		param8	112.33746833657882
		param9	103.22457095425507
		param10	31.981299454998069
		param11	110.53087910570881
		param12	78.212446384174044
		param13	72.590394941449389
		param14	71.472002377152236
		param15	82.790785486950398

		param16	40.05079785314593
		node0	2
		node1	11.18
		node2	18.050000000000001
		node3	22.43
		node4	26.809999999999999
		node5	31.190000000000001
		node6	35.600000000000001
		node7	40.939999999999998
		node8	46.340000000000003
		node9	50.57
		node10	54.799999999999997
		node11	59.030000000000001
		node12	63.350000000000001
		node13	69.109999999999999
		node14	80
Common parameter	Peak shift		
		Function name	Shift axial displacement
		param0	0
		param1	0
		param2	0
Mg3 Al6 (Si.8 Al.2)5 O21 (O H)	Scale factor	s	1.97(17)
	FWHM	U	0.0000
		V	0.0000
		W	0.0957
	Asym. factor	A0	0.0529
		A1	1.5429
	Decay rate factor	etaL0/mL0	0.8518
		etaL1/mL1	-0.4250
		etaL2/mL2	0.0000
		etaH0/mH0	0.8255
		etaH1/mH1	-0.2900
		etaH2/mH2	0.0000
	Preferred orientationMarch-Dollase	h	0
		k	0
		l	0
		March coefficient	1.000000
Mg O3 Si	Scale factor	s	0.04(6)
	FWHM	U	0.5075
		V	0.0000
		W	0.0001
	Asym. factor	A0	0.4201
		A1	1.8648
	Decay rate factor	etaL0/mL0	0.5434
		etaL1/mL1	-0.1783
		etaL2/mL2	0.0000
		etaH0/mH0	0.5388
		etaH1/mH1	-0.0746
		etaH2/mH2	0.0000
	Preferred orientationMarch-Dollase	h	0
		k	0
		l	0
		March coefficient	1.000000
Si O2	Scale factor	s	0.27(12)
	FWHM	U	0.1326
		V	0.0000

		W	0.0247
	Asym. factor	A0	0.0367
		A1	1.8204
	Decay rate factor	etaL0/mL0	0.4882
		etaL1/mL1	-0.0729
		etaL2/mL2	0.0000
		etaH0/mH0	0.7895
		etaH1/mH1	-0.3930
		etaH2/mH2	0.0000
	Preferred orientationMarch-Dollase	h	0
		k	0
		l	0
		March coefficient	1.000000

Table 3: Structure parameters used for WPPF

Data set name	Phase Name	Element	x	y	z	Occupancy	T f
clay	Mg3 Al6 (Si.8 Al.2)5 O21 (O H)	O	0.403200	0.235400	0.250000	1.000	0.5
clay	Mg3 Al6 (Si.8 Al.2)5 O21 (O H)	Al	0.314600	0.140700	0.250000	1.000	0.5
clay	Mg3 Al6 (Si.8 Al.2)5 O21 (O H)	Si	0.401800	0.353000	0.250000	1.000	0.5
clay	Mg3 Al6 (Si.8 Al.2)5 O21 (O H)	Al	0.179400	0.333000	0.250000	0.500	0.5
clay	Mg3 Al6 (Si.8 Al.2)5 O21 (O H)	Mg	0.122600	0.140200	0.250000	1.000	0.5
clay	Mg3 Al6 (Si.8 Al.2)5 O21 (O H)	O	0.234600	0.235600	0.250000	1.000	0.5
clay	Mg3 Al6 (Si.8 Al.2)5 O21 (O H)	O	0.500000	0.087800	-0.050500	1.000	0.5
clay	Mg3 Al6 (Si.8 Al.2)5 O21 (O H)	O	0.084200	0.279400	0.250000	1.000	0.5
clay	Mg3 Al6 (Si.8 Al.2)5 O21 (O H)	O	0.500000	0.387500	0.250000	1.000	0.5
clay	Mg3 Al6 (Si.8 Al.2)5 O21 (O H)	Si	0.000000	0.342500	0.250000	1.000	0.5
clay	Mg3 Al6 (Si.8 Al.2)5 O21 (O H)	Si	0.179400	0.333000	0.250000	0.500	0.5
clay	Mg3 Al6 (Si.8 Al.2)5 O21 (O H)	O	0.224200	0.043900	0.250000	1.000	0.5
clay	Mg3 Al6 (Si.8 Al.2)5 O21 (O H)	Al	0.214700	0.000000	0.000000	1.000	0.5
clay	Mg3 Al6 (Si.8 Al.2)5 O21 (O H)	Mg	0.500000	0.146400	0.250000	1.000	0.5
clay	Mg3 Al6 (Si.8 Al.2)5 O21 (O H)	O	0.316200	0.094200	-0.044800	1.000	0.5
clay	Mg3 Al6 (Si.8 Al.2)5 O21 (O H)	O	0.000000	0.088200	0.250000	1.000	0.5
clay	Mg3 Al6 (Si.8 Al.2)5 O21 (O H)	O	0.403200	0.045700	0.250000	1.000	0.5
clay	Mg3 Al6 (Si.8 Al.2)5 O21 (O H)	O	0.138100	0.100800	-0.052000	1.000	0.5
clay	Mg3 Al6 (Si.8 Al.2)5 O21 (O H)	Al	0.092800	0.500000	0.000000	1.000	0.5
clay	Mg O3 Si	Mg	0.519600	0.559000	0.250000	1.000	0.3
clay	Mg O3 Si	Si	0.500000	0.000000	0.500000	1.000	0.2
clay	Mg O3 Si	O	0.104600	0.467900	0.250000	1.000	0.4
clay	Mg O3 Si	O	0.193300	0.200300	0.553600	1.000	0.3
clay	Si O2	Si	0.664280	0.634800	0.425090	1.000	0.5
clay	Si O2	O	0.500000	0.339290	0.545230	1.000	0.5
clay	Si O2	O	0.299500	0.372240	0.750000	1.000	0.5
clay	Si O2	O	0.750000	0.750000	0.500000	1.000	0.5
clay	Si O2	O	0.713110	0.500000	0.500000	1.000	0.5